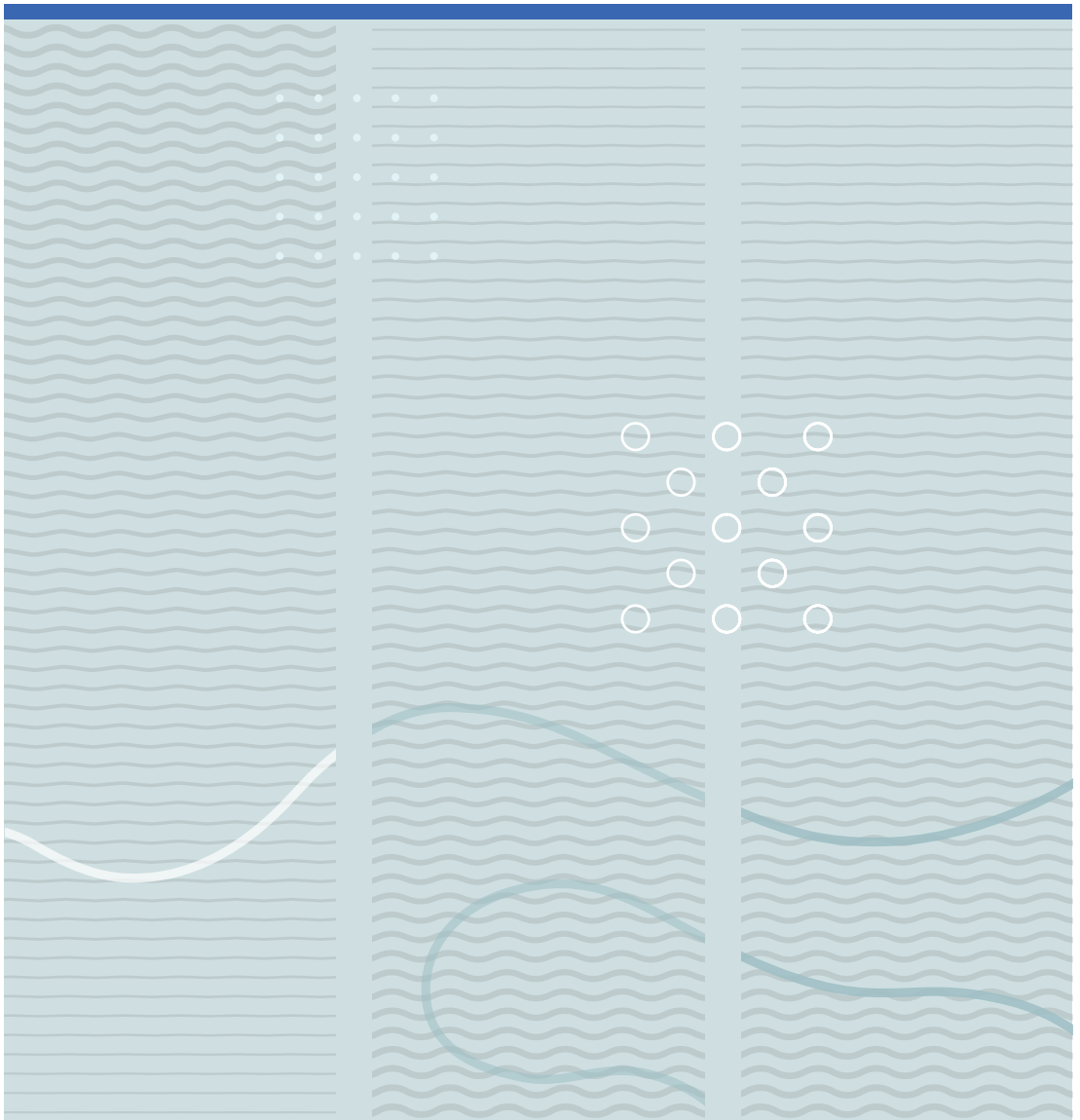


Ellen Sagaas Røed

# Impact of single crystal properties on underwater transducer designs





Ellen Sagaas Røed

**Impact of single crystal properties on underwater  
transducer designs**

A PhD dissertation in  
**Applied micro- and nanosystems**

© Ellen Sagaas Røed, 2023

Faculty of Technology, Natural Sciences and Maritime Studies  
University of South-Eastern Norway  
Horten, 2023

**Doctoral dissertations at the University of South-Eastern Norway no. 154**

ISSN 2535-5244 (print)

ISSN 2535-5252 (online)

ISBN 978-82-7206-746-4 (print)

ISBN 978-82-7206-745-7 (online)



This publication is licensed with a Creative Commons license. You may copy and redistribute the material in any medium or format. You must give appropriate credit, provide a link to the license, and indicate if changes were made. Complete license

terms at <https://creativecommons.org/licenses/by-nc-sa/4.0/deed.en>

Print: University of South-Eastern Norway

## Preface

This thesis has been submitted to the Faculty of Technology, Natural Sciences and Maritime Studies at the University of South-Eastern Norway as part of the requirements for the Ph.D. degree in Applied Micro- and Nanosystems. The work was carried out in the Ultrasound Group at the Department of Microsystems, and it was supervised by Professor Lars Hoff. The thesis is the result of an industrial Ph.D.-project, funded by The Research Council of Norway (project: 290462) and by Kongsberg Maritime AS. The work was co-supervised by Kongsberg designers Martin Bring, Ph.D. and Frank Tichy, Ph.D., and the experimental work was carried out using Kongsberg facilities.

I have been working as a transducer designer at Kongsberg Maritime since 2002. We make piezoelectric underwater transducers for oceanic science, fishery, seabed mapping, naval applications, positioning and communication. The active material of underwater transducers is usually lead zirconate titanate (PZT) polycrystalline ceramics. For medical transducers, on the other hand, relaxor-based single crystals have become widely used since the discovery of ultrahigh electromechanical coupling in certain domain engineered compositions. The single crystals have been considered too expensive for use in commercial underwater applications. Now there is a robotic revolution going on in oceanic science, requiring the underwater transducers to be compact and to collect a wide range of data. Use of single crystals can help us meet these new requirements, but to what extent? That is the research question of this Ph.D.-project, in its most general form. Additional motivation for the project is given by the ongoing development of textured ceramics, promised to provide single crystal-like properties at a lower cost.



## Acknowledgements

I would like to start by thanking my supervisors Lars Hoff, Martin Bring and Frank Tichy, and my mentor Else-Marie Åsjord. Having Lars as my main supervisors has been very reassuring. His experience, knowledge and analytical mind has been very important to me throughout the project, and his review of my work has greatly enhanced my learning and the resulting quality. Working with Martin is always very inspiring. I feel lucky to work with someone as intelligent as he is. He has been a kind and encouraging supervisor. Franks experience and system knowledge has also been of great value. He has provided some very good advice and has been very supportive. I really appreciate that he has made this project possible to implement. Else is a transducer design expert and shares enthusiastically knowledge, ideas, and program code. She makes the transducer department an exciting place to work. Her analytical skills have been of high importance for the articles. The quality of the project has also been greatly enhanced by cooperation with a mechanical designer. All credit for successful fabrication of prototypes should go to mechanical designer Andreas Henriksen and a highly skilled team of manufacturing operators. Thanks to Andreas for dedication and innovation. One of the things I love the most about my job is that I get to work with experts in so many different fields: Thanks to Roy Henriksen and Anel Habibovic for careful machining, to Stig Harefallet, Kenneth Andreassen and the rest of the team for lending their expertise to the composite fabrication, to Tor Edvin Kolstad for inspection and to Trine Ressem for high precision assembly. Thanks also to my Kongsberg colleagues Hermann Sundklakk, Sveinung Skjervheim and Are Johansen. It has also been a pleasure to work with the Ultrasound Group at USN (The University of South-Eastern Norway). A special thanks to Martijn Frijlink who is always enthusiastic and provides helpful questions and comments, and to Tonni Franke Johansen, Amirfereydoon Mansoori and Kenneth Kirkeng Andersen for giving me a flying start with their excellent MatLab code.

Although I enjoy working with transducers at Kongsberg and USN, my favorite team will always be Magne, Marie and Ole. Thanks for being incredible patient and supportive!



## Abstract

The ongoing robotic revolution in oceanic science puts new requirements on underwater transducers. Small platforms require compact multi-purpose transducers, and there is limited space available for the electronics. Introducing single crystal ferroelectrics as the active material can be one way of meeting the new requirements. Compared to lead zirconate titanate (PZT) polycrystalline ceramics, single crystals provide higher electromechanical coupling, higher strain per electric field and higher elastic compliance. A higher electromechanical coupling coefficient,  $k$ , enables an increase in frequency bandwidth. With more frequencies available, more tasks can be covered using only one type of transducer, saving space on the small platforms. Higher elastic compliance reduces the thickness of the transducer element, and larger strain per electric field enables reduction of the voltage source. The object of this Ph.D.-project was to investigate the impact of the single crystal properties on underwater transducer designs, keeping in mind the current development of textured ceramics promised to provide single crystal-like properties at a lower cost.

For many underwater transmitters, the usable frequency band is restricted by both the transmitted acoustic power and the reactive electrical power. Single crystals have the potential to double the usable band compared to PZT, but the acoustic matching required for this can be difficult to obtain in practice. We investigated this for a 1-3 piezocomposite plate and for a tonpilz. The composite plate had air backing for high efficiency. Tonpilz transducers are common for resonance frequencies below 50 kHz, while piezocomposites are widely used for higher frequencies. We started by exploring simple 1D models for a plate, using real, frequency independent acoustic loading, and we observed that an increase in  $k$  has a larger bandwidth impact on the electrical power factor than on the acoustic power.

For piezocomposite plates, acoustic matching to water is achieved by adding matching layers. These matching layers are frequency dependent, and when optimized for a maximally flat passband, the matching decreases rapidly outside the passband. Poor acoustic matching prevents the bandwidth of the electrical power factor from reaching its potential. For many underwater applications, the diversity provided by a selection of narrow-band pulses at a variety of frequencies is more important than a flat acoustic response. We proposed to extend



the passband by separating the resonances of the complex system constituted by the piezocomposite plate and the matching layers. Using this strategy, we modelled and fabricated a single crystal 1-3 piezocomposite transducer with air backing and two matching layers, achieving reactive power below 50% in a frequency band 175 % wide relative to the resonance frequency 518 kHz. The piezocomposite had matrix material Epotek 301-2. The fabricated composite had an effective coupling coefficient of  $k = 0.83$ , in good agreement with the modelled result.

Reported single crystal underwater transducers are mainly of the tonpiliz or cylinder design. The herein presented successful fabrication of a piezocomposite transducer that can be used in the frequency range 244 kHz to 1148 kHz shows that single crystals are indeed interesting also in the high end of the frequency range applied for underwater applications. The tonpiliz and cylinder design does however have an advantage in their inherent frequency independent matching to water. Our modelling showed that a single crystal tonpiliz transducer with  $k = 0.82$  can be designed with a mechanical quality factor as large as 2 and still exhibit reactive power below 20% in a frequency band of width 150 % or below 50 % in a band of width 170%, relative to the resonance frequency.

Single crystals provide high coupling also in modes for which the electric field and the main extension are in separate directions. We investigated the 32 mode utilized in a 1-3 single crystal piezocomposite, and presented a design for which the acoustic power at a given voltage was estimated to increase by almost a factor 50 compared to a conventional PZT piezocomposite that utilizes the 33 mode. An additional benefit of the 32 mode design was almost 50 % reduction in composite thickness. We also presented a design for which a mode akin to the 31 mode was included to add an extra, usable, frequency band to a 32 mode transducer. It was concluded that the 32 mode design opens for transducers that can be operated over a wide frequency range and driven by low voltages, making it well suited for mounting on compact platforms.

*Table 1: The main results from the included papers, and their impact on underwater transducer performance.*

Main results	Impact of results
An increase of $k$ has larger bandwidth impact on the electrical power factor than on the acoustic power. (Article 1)	Potential increase of the usable frequency band is particularly large for applications limited by reactive electrical power.
Good agreement with FEM model for measured electrical impedance of fabricated 518 kHz single crystal 1-3 composite. $k = 0.83$ , close to modelled value. (Article 3)	Single crystal composites in the frequency range of underwater transducers can be fabricated without degradation of the electromechanical coupling.
The frequency dependence of the matching layers increases the power factor ripple. (Article 1)	Limits the benefit of a high $k$ when using conventional matching layer optimized for a maximally flat passband.
Electrical power factor bandwidth can be improved by separating the resonances of the system composite + matching layers. (Article 1 and 3).	Possible to achieve a large usable frequency band for piezocomposite applications for which a flat passband can be sacrificed.
Fabrication of single crystal piezocomposite transducer with reactive power below 50 % from 244 to 1148 kHz. (Article 3)	Single crystals are indeed interesting also for underwater composite transducers, commonly used in the high end of the frequency range of underwater applications.
The frequency independent acoustic matching inherent in the tonpilz design is beneficial for low power factor ripple. Modelled tonpilz with $k = 0.82$ and mechanical quality factor $\approx 2$ has power factor $> 0.8$ in 150 % bandwidth and power factor $> 0.5$ in 170 % bandwidth, relative to the resonance frequency. (Article 2)	Increase in $k$ can be utilized in a tonpilz without having to make a design with an extremely low mechanical quality factor, meaning that standard design and fabrication methods can be applied.
Modelled single crystal 32 mode 1-3 composite design provides almost 50 times more acoustic power at given voltage than a 33 mode PZT composite. Almost 50 % reduction of the thickness in the direction of main extension. (Design I, Article 4). A mode akin to the 31 mode adds an extra, usable, frequency band. Composite fabricated and measured. (Design IV, Article 4)	The 32 mode design opens for compact transducers that can be operated over a wide frequency range and driven by low voltages, making it well suited for mounting on small platforms.



## List of included papers

Papers omitted from online edition due to publisher's regulations

### Article 1

E. S. Røed, M. Bring, F. Tichy, A. Henriksen, E.-M. Åsjord and L. Hoff, "Optimization of matching layers to extend the usable frequency band for underwater single-crystal piezocomposite transducers", *IEEE Trans. Ultrason., Ferroelect., Freq. Contr.*, vol. 69, no. 2, pp. 803-811, Feb. 2022

### Article 2

E. S. Røed, M. Bring, F. Tichy, E.-M. Åsjord and L. Hoff, "Electrical power factor for a single crystal tonpilz versus a plate with matching layers", *IEEE Ultrason. Symp.*, Xi'an, China, 2021

### Article 3

E. S. Røed, M. Bring, M. Frijlink, A. Henriksen, F. Tichy, E.-M. Åsjord and L. Hoff, "Underwater single crystal piezocomposite transducer with extended usable frequency band", *Ultrasonics*, vol. 125, Sep. 2022, 106794

### Article 4

E. S. Røed, M. Bring, A. Henriksen, F. Tichy, E.-M. Åsjord and L. Hoff, "Compact and wideband underwater transducer using single crystal piezocomposite in 32 mode", submitted to *IEEE Trans. Ultrason., Ferroelect., Freq. Contr.*, Sep. 2022



## Other work presented during the Ph.D. project

The following published papers were not included in the thesis as they are covered by the reviewed Article 1:

### Article 5

E. S. Røed, K. K. Andersen, M. Bring, F. Tichy, E.-M. Åsjord and L. Hoff, “Acoustic impedance matching of PMN-PT/epoxy 1-3 composites for underwater transducers with usable bandwidth restricted by electrical power factor”, *IEEE Ultrason. Symp.*, Glasgow, UK, 2019

### Article 6

E. S. Røed, K. K. Andersen, M. Bring, F. Tichy, E.-M. Åsjord and L. Hoff, “Increased usable frequency band for underwater transducers with single crystal”, *IEEE Ultrason. Symp.*, Las Vegas, NV, USA, 2020

### Presentations at national conferences

E. S. Røed, M. Bring, F. Tichy, E.-M. Åsjord and Lars Hoff, “New active materials for sonar”, *CIUS (Centre for Innovative Ultrasound Solutions) Autumn Conference*, Horten, Norway, 2019

E. S. Røed, M. Bring, F. Tichy, E.-M. Åsjord and Lars Hoff, “New active materials in underwater transducers”, *The 43<sup>rd</sup> Scandinavian Symposium on Physical Acoustics*, Geilo, Norway, 2020

E. S. Røed, M. Bring, A. Henriksen, F. Tichy, E.-M. Åsjord and Lars Hoff “Single crystal in underwater transducers”, *The 45<sup>th</sup> Scandinavian Symposium on Physical Acoustics*, Geilo, Norway, 2022

### Other presentations

E. S. Røed, “Improving underwater pictures stone by stone”, *USN (University of South-Eastern Norway) Utforsk*, Horten, Norway, 2019



## List of figures

Figure 1-1: The Mason model .....	3
Figure 1-2: Modes, geometry .....	4
Figure 1-3: Underwater robotics .....	9
Figure 1-4: Two transducer designs .....	11
Figure 1-5: Complexity of research questions.....	13
Figure 3-1: The BVD model.....	23
Figure 3-2: Transfer fuction magnitude for various $Z_c/Z_R, f$ normalized to $f_a$ .....	25
Figure 3-3: Transfer fuction magnitude for various $Z_c/Z_R, f$ normalized to $f_r$ .....	25
Figure 3-4: Maximum bandwidth $BW_{max}$ .....	30
Figure 3-5: Parallel tuned electrical power factor for various $Z_c/Z_R$ .....	31
Figure 4-1: Frequency dependent matching layer passband.....	36
Figure 4-2: Conventional matching layers, Article 1 .....	39
Figure 4-3: Optimized matching layers, Article 1 .....	39
Figure 4-4: Tonpilz, fixed-end mass loaded bar .....	43
Figure 4-5: Mechanical quality factor for a tonpilz .....	46
Figure 4-6: Tonpilz head flexure.....	46
Figure 4-7: Comparison of performance, tonpilz and piezocomposite .....	47
Figure 5-1: Geometry of 33 mode bar and 32 mode block.....	52
Figure 5-2: Designs I, II and III, Article 4 .....	54
Figure 5-3: Design IV, Article 4 .....	55
Figure 5-4: Normalized acoustic power per area for Designs I, II and III, Article 4.....	56
Figure 5-5: Modelled electrical impedance, Design IV, Article 4 .....	57
Figure 5-6: Modelled acoustic power, Design IV, Article 4 .....	58
Figure 6-1: Schematical transducer design, Article 3.....	64
Figure 6-2: Effective composite parameters $Z_c$ and $k$ versus volume fraction .....	66
Figure 6-3: $Q_m$ versus volume fraction, for $Z_R = 1.5$ MRayl.....	67
Figure 6-4: Electrical impedance $ Z $ for different volume fractions (vf) active material. ....	68
Figure 6-5: Electrical impedance for the fabricated single crystal composite, Article 3 .....	69



Figure 6-6: Resonance peaks, single crystal composite with inner matching layer. ....	71
Figure 6-7: Single crystal composite with two matching layers, measured, Article 3 .....	73
Figure 6-8: PZT composite with two matching layers, measured, Article 3 .....	73
Figure 6-9: Transmitting voltage response for the single crystal transducer, Article 3.....	74
Figure 6-10: Electroacoustic efficiency, Article 3 .....	74
Figure 6-11: Design, fabricated composite, Article 4.....	76
Figure 6-12: Electrical impedance magnitude, fabricated composite, Article 4.....	77
Figure 7-1: Phase diagrams, PZT and PMN-PT .....	82
Figure 7-2: From rhombohedral to monoclinic phase .....	83
Figure 8-1: Schematics of the TGG process.....	89

## Symbols

$A$	Area, interface transducer/load
$A_c$	Area, driving section of tonpilz
$AR$	Aspect ratio
$b$	Total width, Article 3
$B$	Electrical susceptance
$B_r$	Electrical susceptance at resonance
$\beta_{ij}^T$	Inverse dielectric permittivity, constant stress
$\beta_{ij}^S$	Inverse dielectric permittivity, constant strain
$BW_{max}$	Maximum bandwidth
$C$	Capacitance
$C$	Cubic phase, Chapter 7
$C_0$	Clamped capacitance
$C_f$	Free capacitance
$C_m^E$	Motional capacitance
$c_{ij}^E$	Elastic stiffness coefficients, constant electric field
$c_{ij}^D$	Elastic stiffness coefficients, constant electric displacement
$c_h$	Velocity, tonpilz head ( $c$ used instead of $v$ for consistency with reference)
$d_{ij}$	Piezoelectric strain constants
$d$	Width of active area, Article 3
$D$	Electric displacement
$\Delta f$	Width of frequency band within power factor flanks
$E$	Electric field
$E_c$	Coercive field
$e_{ij}$	Piezoelectric constants
$\varepsilon_{ij}^T$	Dielectric permittivity, constant stress
$\varepsilon_{ij}^S$	Dielectric permittivity, constant strain
$f$	Frequency
$f_r$	Resonance frequency
$f_a$	Anti-resonance frequency
$f_0$	Frequency of maximum electromechanical transfer function magnitude
$g_{ij}$	Piezoelectric constants
$G$	Electrical conductance
$G_r$	Electrical conductance at resonance
$G_m$	Electrical conductance at resonance, mechanical branch
$h_{ij}$	Piezoelectric constants
$H$	Electromechanical transfer function
$I$	Electric current
$k$	Electromechanical coupling coefficient (used for general or effective value)
$k_{ij}$	Electromechanical coupling coefficient (material value for given mode)
$k_t$	Electromechanical coupling coefficient, thickness mode
$K$	Mechanical stiffness, general
$K_m^E$	Mechanical stiffness, constant electric field

$K_m^D$	Mechanical stiffness, constant electric displacement
$l$	Length
$L$	Resonator length, in the direction of main extension (can be either $t$ or $l$ )
$\lambda$	Wavelength
$M$	Effective mass
$M$	Monoclinic phase, Chapter 7
$M_c$	Mass driving section, tonpizl
$M_p$	Reference mass in Article 2, mass of plate with area $A$ and $\lambda/2$ thickness
$M_d$	Dynamic mass
$N$	Transformation ratio
$O$	Orthorhombic phase, Chapter 7
$PF$	Electrical power factor
$Q_m$	Mechanical quality factor
$Q_e$	Electrical quality factor
$Q_{opt}$	Optimum mechanical quality factor
$q_A$	Area ratio, Article 2, $A/A_c$
$\rho$	Density
$\rho_h$	Density, material of tonpizl head
$\rho_w$	Density, water
$R$	Rhombohedral phase, Chapter 7
$R$	Radiation resistance
$S$	Strain
$s_{ij}^E$	Elastic compliance coefficient, constant electric field
$s_{ij}^D$	Elastic compliance coefficient, constant electric displacement
$\sigma$	Poisson's ratio
$\sigma_{ij}$	Stress tensor coefficients
$T$	Stress
$T$	Tetragonal phase, Chapter 7
$T_c$	Curie temperature
$T_{RT}$	Phase transition temperature, Rhombohedral to tetragonal
$t$	Thickness, between the electrodes
$\theta$	Electrical impedance phase
$\theta_r$	Electrical impedance phase, at resonance
$u$	Normal velocity at the face of the transducer
$v$	Velocity, Mason model
$v_w$	Velocity, water
$V$	Electrical voltage
$vf$	Volume fraction active material
$w$	Width
$Z_c$	Acoustic impedance, open circuit
$Z_a$	Impedance in Mason model, the tangent-term
$Z_b$	Impedance in Mason model, the sine-term
$Z_R$	Load impedance
$Z_{ml}$	Acoustic impedance, matching layer
$Z_{mi}$	Acoustic impedance, inner matching layer

$Z_{mo}$  Acoustic impedance, outer matching layer  
 $|Z|$  Electrical impedance magnitude



## Abbreviations

1D	One dimensional
3D	Three dimensional
AUV	Autonomous underwater vehicle
BVD	Butterworth van-Dyke transducer model
BT	Barium titanate
FEM	Finite element model
IEEE	Institute of Electrical and Electronics Engineers
JASA	Journal of the Acoustic Society of America
MPT	Magnetostrictive-piezoelectric tonpilz
Mn	Manganese
MPB	Morphotropic phase boundary
NDT	Non-destructive testing
NUWC	Naval Undersea Warfare Center
NBT-PT	Sodium bismuth titanate – lead titanate
ONR	Office of Naval Research
PennState	Pennsylvania State University
PIN-PMN-PT	Lead indium niobate – lead magnesium niobate – lead titanate
PMN-PT	Lead magnesium niobate – lead titanate
PYN-PMN-PT	Lead yttrium niobate - lead magnesium niobate – lead titanate
PZT	Lead zirconate titanate
PZN-PT	Lead zirconate niobate – lead titanate
RVS	Receiving voltage sensitivity
RTGG	Reactive templated grain growth
TGG	Templated grain growth
TVR	Transmitting voltage sensitivity
SrTiO <sub>3</sub>	Strontium titanate



## Table of contents

<b>1 Material properties, motivation, and outline .....</b>	<b>1</b>
1.1 Material properties of importance for transducer performance .....	1
1.2 Materials .....	4
1.3 Inspiration and new requirements.....	5
1.4 Research questions and structure of thesis .....	9
1.5 Two types of transmitter design .....	11
1.6 Complexity of research questions.....	12
<b>2 State of the art for single crystal underwater transducers .....</b>	<b>15</b>
2.1 Method.....	15
2.2 Results .....	15
<b>3 Impact of the electromechanical coupling coefficient on the usable frequency band .....</b>	<b>21</b>
3.1 The impact of $k$ on the transfer function bandwidth.....	21
3.1.1 Theory .....	21
3.1.2 Method.....	24
3.1.3 Results .....	24
3.1.4 Discussion.....	26
3.2 Impact of $k$ on the electrical power factor.....	27
3.2.1 Theory .....	27
3.2.2 Method.....	31
3.2.3 Result.....	32
3.2.4 Discussion.....	32
3.3 Conclusion .....	33
<b>4 Maximizing the usable frequency band for selected underwater transducer designs .....</b>	<b>35</b>
4.1 Piezocomposite with matching layers .....	35
4.1.1 Theory .....	35
4.1.2 Method.....	36
4.1.3 Results .....	38
4.1.4 Discussion.....	38
4.2 Tonpilz transducer.....	41



4.2.1	Theory .....	42
4.2.2	Method, sub question 1: What does it take to reduce $Q_m$ to $Q_{opt}$ ?.....	43
4.2.3	Results, sub question 1: What does it take to reduce $Q_m$ to $Q_{opt}$ ?.....	45
4.2.4	Discussion, sub question 1: What does it take to reduce $Q_m$ to $Q_{opt}$ ?.....	45
4.2.5	Method, sub question 2: Comparison of performance .....	47
4.2.6	Results, sub question 2: Comparison of performance .....	47
4.2.7	Discussion, sub question 2: Comparison of performance .....	48
4.3	Discussion and conclusion.....	48
<b>5 Compactness of selected underwater designs .....</b>		<b>51</b>
5.1	Piezocomposite .....	51
5.1.1	Theory .....	51
5.1.2	Method.....	53
5.1.3	Results.....	56
5.1.4	Discussion.....	58
5.2	Tonpilz .....	61
5.3	Conclusion .....	62
<b>6 Performance of fabricated piezocomposites .....</b>		<b>63</b>
6.1	The 33 mode piezocomposite .....	64
6.1.1	Design choice: Composite materials.....	65
6.1.2	Design choice: Pillar aspect ratio .....	65
6.1.3	Design choice: Volume fraction active material .....	66
6.1.4	Result: Measured electrical impedance for the single crystal composite.....	69
6.1.5	Design choice: Use of FEM model for optimization of matching layers.....	70
6.1.6	Results: Measurements of final transducers .....	71
6.1.7	Conclusion:.....	75
6.2	The 32 mode 1-3 piezocomposite.....	75
6.2.1	Conclusion.....	78
<b>7 Literature study: Changes in properties due to temperature, stress, or electric field .....</b>		<b>79</b>
7.1	Theory, phase transitions.....	80
7.2	Parameter variation reported in literature .....	83

<b>8 Literature study: State of the art for textured ceramics .....</b>	<b>87</b>
8.1 Theory, texturing.....	87
8.2 State of the art .....	88
8.3 Commercially available textured ceramics .....	90
<b>9 Thesis conclusion.....</b>	<b>93</b>
9.1 Future work.....	96



# 1 Material properties, motivation, and outline

High coupling between electrical and mechanical energy makes the single crystals interesting for transducer designers. The coupling has impact on piezoelectric, dielectric, and elastic properties.

## 1.1 Material properties of importance for transducer performance

For a piezoelectric material, the governing equations that determine the relationship between strain,  $\mathbf{S}$ , stress,  $\mathbf{T}$ , electric field,  $\mathbf{E}$ , and electric displacement,  $\mathbf{D}$ , are given by:

$$\mathbf{S} = \mathbf{s}^E \mathbf{T} + \mathbf{d} \mathbf{E} \quad (1)$$

$$\mathbf{D} = \mathbf{d} \mathbf{T} + \boldsymbol{\varepsilon}^T \mathbf{E} \quad (2)$$

The elastic compliance coefficient matrix,  $\mathbf{s}$ , is a 6x6 matrix. The superscript  $E$  means that the elasticity is measured under constant electric field. The  $\mathbf{d}$  represents the piezoelectric strain constants and is a 3x6 matrix. The dielectric permittivity,  $\boldsymbol{\varepsilon}$ , is a 3x3 matrix, and the superscript  $T$  means that the permittivity is measured under constant stress. Other forms of the governing equations are:

$$\mathbf{T} = \mathbf{c}^E \mathbf{S} - \mathbf{e} \mathbf{E} \quad (3)$$

$$\mathbf{D} = \mathbf{e} \mathbf{S} + \boldsymbol{\varepsilon}^S \mathbf{E} \quad (4)$$

$$\mathbf{S} = \mathbf{s}^D \mathbf{T} + \mathbf{g} \mathbf{D} \quad (5)$$

$$\mathbf{E} = -\mathbf{g} \mathbf{T} + \boldsymbol{\beta}^T \mathbf{D} \quad (6)$$

$$\mathbf{T} = \mathbf{c}^D \mathbf{S} - \mathbf{h} \mathbf{D} \quad (7)$$

$$\mathbf{E} = -\mathbf{h} \mathbf{S} + \boldsymbol{\beta}^S \mathbf{D} \quad (8)$$

where  $\mathbf{e}$ ,  $\mathbf{h}$ , and  $\mathbf{g}$  are alternative formulations of the piezoelectric matrix,  $\mathbf{c}$  is the matrix with the elastic stiffness coefficients and  $\boldsymbol{\beta}$  is the inverse permittivity matrix.

The Mason model is a one-dimensional model that can be used to predict the behaviour of piezoelectric resonators, given that their shape and loading are compatible with wave motion in a specific mode. Mason models corresponding to the thickness extensional, length extensional and length thickness extensional modes are shown in Figure 1-1. The length thickness extensional mode is also called the transversely poled length extensional mode. Geometry and poling for common modes used for material characterization are shown in Figure 1-2.

Dependent on the mode, either the short circuit resonance frequency,  $f_r$ , or the open circuit anti-resonance frequency,  $f_a$ , can be found from a simple expression containing the resonator length, the material's density,  $\rho$ , and the elastic coefficient, see Figure 1-1.

- The higher the elastic compliance coefficient  $s_{ij}$ , the shorter the resonator length is needed for a given resonance frequency.
- The piezoelectric constants  $d_{ij}$  determines the strain per electric field. A high  $d_{ij}$  provides high transmitted acoustic power per electric field for the relevant mode. Note that the power is proportional to squared transducer face velocity.
- The electrical impedance of the resonator is dependent on the permittivity,  $\epsilon_{ij}$ . The higher the permittivity, the lower the electrical impedance.
- The coupling between electrical and mechanical energy causes changes in elastic stiffness and dielectric permittivity when the electrical or mechanical boundary conditions are changed [1]. The distance between the short circuit resonance frequency and the open circuit anti-resonance frequency is dependent on the size of the coupling. In Article 1, we explain why this results in an increase in bandwidth for an increase in coupling. Expressions for the electromechanical coupling coefficient,  $k$ , of the different modes are listed in Figure 1-1. For the length extensional mode, the 33 mode,  $k_{33}$  is given by  $d_{33}$ ,  $s_{33}^E$  and  $\epsilon_{33}^T$ .

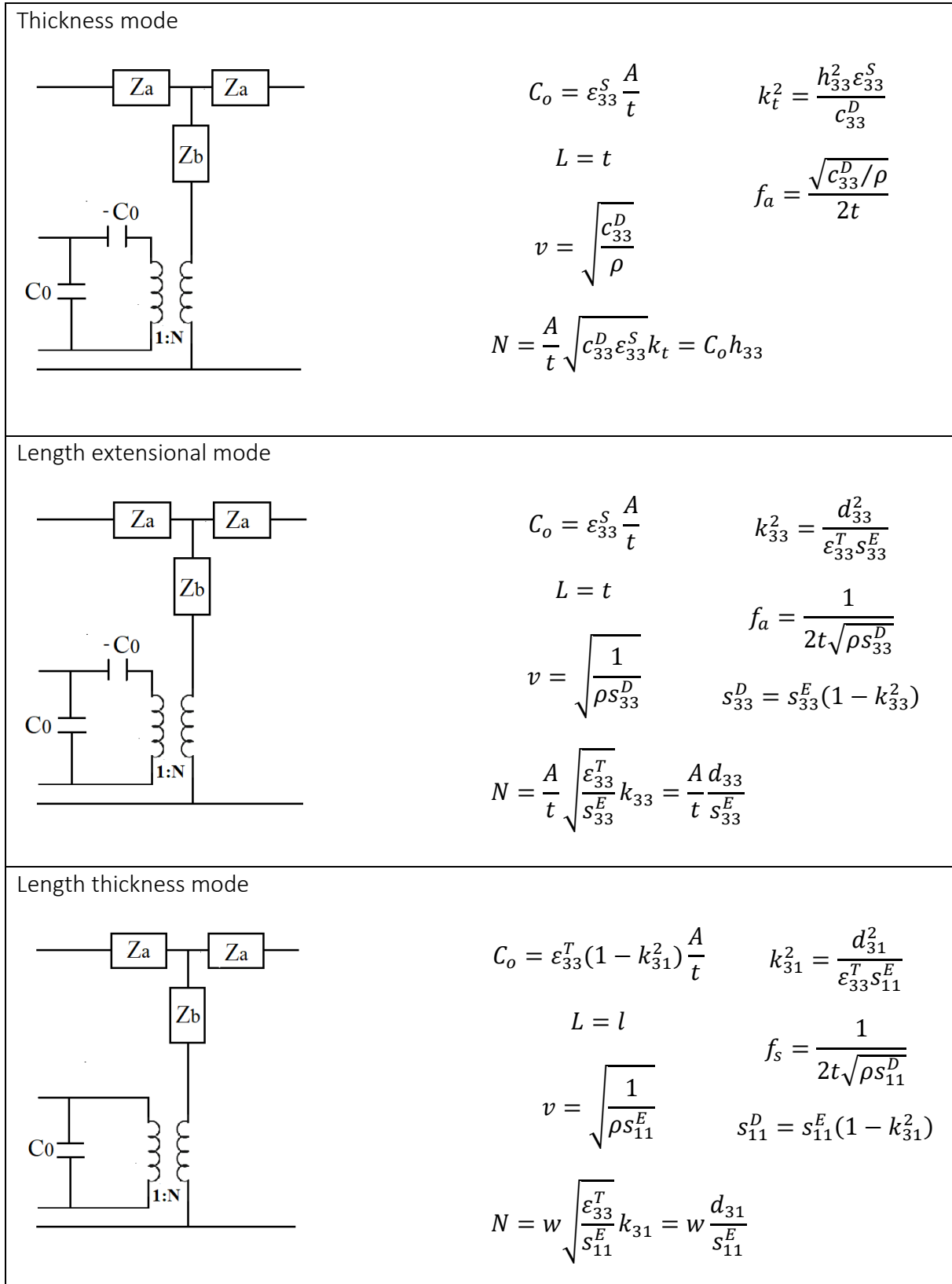


Figure 1-1 [2][3]. Mason model for different modes, see Figure 1-2.  $A$  is the area of each electrode,  $t$  is the thickness between the electrodes,  $L$  is the resonator length,  $\rho$  is density,  $v$  is velocity,  $\lambda$  is wavelength,  $Z_c = A\rho v$ ,  $Z_a = jZ_c \tan(2\pi L/2\lambda)$  and  $Z_b = -jZ_c / \sin(2\pi L/\lambda)$ .

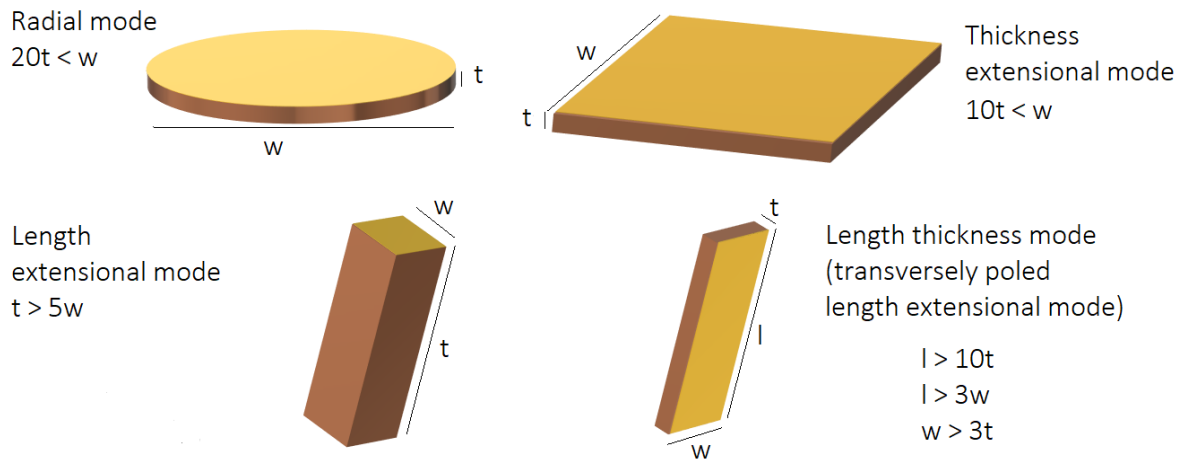


Figure 1-2: Geometrical shape and electrodes (yellow) for different modes. Adapted from Sherrit and Mukherjee [4].

## 1.2 Materials

High piezoelectricity was found in lead zirconate titanate  $\text{Pb}(\text{Zr}_x\text{Ti}_{1-x})\text{O}_3$ , abbreviated PZT, in the early 1950s and PZT ceramics were the most successful piezoelectric materials in practical applications for 50 years. Important factors for the technical dominance of PZT are high longitudinal electromechanical coupling  $k_{33}$  and high piezoelectric coefficient  $d_{33}$ . The discovery of ultrahigh  $k_{33}$  and  $d_{33}$  for lead zinc niobate-lead titanate  $\text{Pb}(\text{Zn}_{1/3}\text{Nb}_{2/3})\text{O}_3$ -% $\text{PbTiO}_3$  (PZN-%PT) and lead magnesium niobate-lead titanate  $\text{Pb}(\text{Mg}_{1/3}\text{Nb}_{2/3})\text{O}_3$ -% $\text{PbTiO}_3$  (PMN-%PT) relaxor ferroelectric single crystals represents an important advancement in ferroelectric materials [5]. The last decade, the single crystals have become the preferred choice for high-end medical transducers, but high material cost per volume has limited the use of single crystals in commercial underwater transducers. The resonance frequency for underwater transducers is typically one decade lower than for medical transducers, and thus the volume active material is typically  $10^3$  times larger. Single crystals have lower fracture toughness [6] than polycrystalline ceramics, and they are limited in size, geometry, and compositional range. Recent research shows that textured ceramics can provide single crystal-like properties as well as mechanical reliability and compositional versatility. Single crystals are expensive and time-consuming to grow, whereas textured ceramics can be fabricated at a lower cost, using

standard ceramic powder processing techniques [7]. The promising results from the research on textured ceramics motivates an evaluation of how much the performance of underwater transducers could be improved by use of active materials with electromechanical coupling in the range provide by the single crystals.

In Table II, material parameters for soft and hard polycrystalline PZT ceramics are compared to material parameters for generation I (PMN-PT) and generation II (PIN-PMN-PT) single crystals. Generation II was developed to increase the temperature stability and coercive field of the single crystals.

### 1.3 Inspiration and new requirements

Although reported only for very few commercial underwater transducers, use of single crystals is widely investigated for naval applications, mainly by researchers affiliated with the US Office of Naval Research (ONR). This research was an important inspiration for the Ph.D.-project. Amin, McLaughlin, Robinson and Ewart [8] summarize the benefits of single crystals in the following wording:

*“Compared to standard PZT8 projector material, single crystals offer nearly triple the bandwidth and an order of magnitude higher acoustic power because of their substantially higher coupling factor and piezoelectric coefficient. Additionally, their small Young’s modulus allows for a compact acoustic source design for a given frequency”*.

A comparison of the material parameters of the commercially available materials in Table II shows that:

- the largest single crystal piezoelectric strain constant  $d_{33}$  is 1620 pC/N, which is a factor 2.5 larger than the 640 pC/N of soft type VI pz21 and a factor 5 larger than the 328 pC/N of hard pz26.



Table II: Material parameters for PZT (blue columns) and single crystal (green columns) materials. PZT-data from Meggitt [9]. The material pz21 is similar to PZT5H1, pz26 is similar to PZT4 and pz28 is similar to PZT8. Single crystal data from CTS [10] and [11]. PMN28 is short for PMN-28%PT. PIN24 is short for PIN24%-PMN-PT. Numbers in brackets denote polarization direction (crystal direction). For symbols  $E_c$ ,  $T_c$  and  $T_{R,T}$ , see Chapter 7.

Meggitt and CTS's brand names	PZT			Single crystals		[001]	[011]
	pz21	pz26	pz28	PMN28	PMN32	PIN24	PIN24
Type	Soft VI	Hard I	Hard III	Gen I	Gen I	Gen II	Gen II
Density $\rho$ (kg/m <sup>3</sup> )	7780	7700	7700	<b>8100</b>	8100	8122	8161
$E_c$ (kV/cm)				2.5	2.5	4.5-6	
$d_{15}$ (10 <sup>-12</sup> C/N)	616	327	403	135	192	122	<b>3122</b>
$d_{24}$ (10 <sup>-12</sup> C/N)	616	327	403	135	192	122	142
$d_{31}$ (10 <sup>-12</sup> C/N)	-259	-128	-114	-568	-760	-646	675
$d_{32}$ (10 <sup>-12</sup> C/N)	-259	-128	-114	-568	-760	-646	<b>-1693</b>
$d_{33}$ (10 <sup>-12</sup> C/N)	640	328	275	<b>1190</b>	<b>1620</b>	<b>1285</b>	1068
$g_{33}$ (10 <sup>-3</sup> Vm/N)	15.6	28	31.4	24.45	26.15	30.55	26.38
$g_{32}$ (10 <sup>-3</sup> Vm/N)	-7.4	-10.9	-13	-11.67	-12.29	-15.36	<b>-41.82</b>
$s_{11}^E$ (10 <sup>-12</sup> m <sup>2</sup> /N)	18.2	13	12.6	45.86	58.85	45.76	20.56
$s_{12}^E$ (10 <sup>-12</sup> m <sup>2</sup> /N)	-7.76	-4.35	-3.71	-28.11	-36.58	-19.60	-35.84
$s_{13}^E$ (10 <sup>-12</sup> m <sup>2</sup> /N)	-6.85	-7.05	-6.60	-15.43	-20.80	-23.16	17.96
$s_{22}^E$ (10 <sup>-12</sup> m <sup>2</sup> /N)	18.2	13	12.6	45.86	58.85	45.76	<b>87.43</b>
$s_{23}^E$ (10 <sup>-12</sup> m <sup>2</sup> /N)	-6.85	-7.05	-6.60	-15.43	-20.80	-23.16	-49.47
$s_{33}^E$ (10 <sup>-12</sup> m <sup>2</sup> /N)	18	19.6	18.3	<b>36.15</b>	<b>49.18</b>	<b>49.04</b>	35.56
$s_{44}^E$ (10 <sup>-12</sup> m <sup>2</sup> /N)	38	33.2	37.7	15.53	16.53	14.33	15.39
$s_{55}^E$ (10 <sup>-12</sup> m <sup>2</sup> /N)	38	33.2	37.7	15.53	16.53	14.33	<b>169.49</b>
$s_{66}^E$ (10 <sup>-12</sup> m <sup>2</sup> /N)	52	34.7	32.6	16.64	18.15	16.10	22.17
$s_{11}^D$ (10 <sup>-12</sup> m <sup>2</sup> /N)	16.3	11.6	11.1	39.23	49.53	35.84	9.29
$s_{22}^D$ (10 <sup>-12</sup> m <sup>2</sup> /N)	16.3	11.6	11.1	39.23	49.53	35.84	16.50
$s_{33}^D$ (10 <sup>-12</sup> m <sup>2</sup> /N)	9.39	10.5	9.65	7.06	6.82	9.78	7.39
$c_{33}^E$ (10 <sup>10</sup> N/m <sup>2</sup> )	11.1	12.3	11.8	10.71	9.68	12.45	15.54
$c_{33}^D$ (10 <sup>10</sup> N/m <sup>2</sup> )	14.2	15.8	15.2	16.66	15.77	16.49	19.49
$\epsilon_{11}^S$ ( $\epsilon_0$ )	2120	828	734	1467	1368	1611	963
$\epsilon_{22}^S$ ( $\epsilon_0$ )	2120	828	734	1467	1368	1611	1447
$\epsilon_{33}^S$ ( $\epsilon_0$ )	1980	700	510	895	700	868	684
$\epsilon_{11}^T$ ( $\epsilon_0$ )	3240	1190	1220	1600	1620	1728	<b>7459</b>
$\epsilon_{22}^T$ ( $\epsilon_0$ )	3240	1190	1220	1600	1620	1728	1596
$\epsilon_{33}^T$ ( $\epsilon_0$ )	3980	1330	990	<b>5500</b>	<b>7000</b>	<b>4753</b>	<b>4574</b>
$k_{31}$	0.323	0.327	0.332	0.43	0.44	0.46	0.74
$k_{32}$	0.323	0.327	0.332	0.43	0.44	0.46	0.9
$k_{33}$	0.691	0.684	0.687	0.9	0.93	0.89	
$k_t$	0.470	0.471	0.475	0.6	0.62	0.5	
$Q_m$	65	2700	970				
$T_c$ (°C)	220	330	330	90-100		140-170	
$T_{RT}$ (°C)				80-90		100-115	

- the largest single crystal elastic compliance coefficient  $s_{33}^E$  is  $49.18 \cdot 10^{-12} \text{ m}^2/\text{N}$ , which is a factor 2.5 larger than the approximately  $20 \cdot 10^{-12} \text{ m}^2/\text{N}$  of the various PZT ceramics.
- an additional benefit of single crystals is the opportunity for high coupling in other modes than the 33 mode. It can be seen from Table II that [011] poled 24%PIN-PMN-PT has high electromechanical coupling in the 32 mode,  $k_{32} = 0.9$ , and that the compliance coefficient  $s_{22}^E$  is  $87 \cdot 10^{-12} \text{ m}^2/\text{N}$ , which is more than 4 times larger than  $s_{33}^E$  for PZT. A 32 mode tonpilz was reported by ONR affiliated researchers Meyer and Markley [12].
- the highest single crystal coupling coefficient is  $k_{33} = 0.93$ , which is a factor 1.35 higher than the  $k_{33} = 0.691$  of pz21.

The order of magnitude higher acoustic power and the possibilities for a compact design can be conceived from Table II and Figure 1-1. The premises for a threefold increase in bandwidth are not as intuitive, and investigation of this is therefore a central part of the Ph.D. project. The amount of increase depends on how the bandwidth is defined, and this is discussed in the thesis. As the term *bandwidth* is often associated with pulse length, we have chosen to use the term *usable frequency band*. Wide usable frequency bands are demonstrated experimentally for naval single crystal transducers [6]. Moffett, Powers, Baird, and Robinson [13] explained the importance of optimum acoustic matching to achieve optimum width for a given electromechanical coupling coefficient  $k$ . Their research is important background for the investigations of the Ph.D.-project.

*A threefold increase in bandwidth, an order of magnitude higher acoustic power and a compact acoustic source design* are benefits appreciated not only by developers of naval applications. These potential improvements also fit perfectly with the new requirements emerging from the ongoing robotic revolution in oceanic science. More and more oceanic data are collected from small platforms, due to advances in robot technology, but also due to a change in the types of data requested. In a video published by the Monterey Bay Aquarium Research Institute [14], their researchers explain the value of having a constant presence in the ocean:

“*Oceanography is in the middle of a robot revolution, with platforms that can take us to places we couldn't be, at times we couldn't be there. It is really a fundamental shift in how we think about things. We have new ways of assessing fisheries, better ways of managing precious resources. We are sitting on this mountain of highly curated information, that was being mind to extract quantitative information like: Who is there? How many? How do they relate to changes in the environment? And so forth. And that gives us an incredible ability to think about these things at a grand scale, to make those connections. It is really challenging, but that is what we need to do. Just by studying anything in the ocean, you are studying climate changes. The ocean is absorbing the tremendous amount of carbon dioxide and absorbing a lot of the heat that is being produced, and the question is what does that mean for the ocean, what does it mean for the life that depends on the ocean, and what are the consequences in the future?*”

Kongsberg robotics are illustrated in Figure 1-3. Kongsberg transducers are also mounted on various small platforms designed by other companies. One such platform is the sun and wind powered robot Sailandrone (Sailandrone, Alameda, CA, US). Sailandrone's mission in the yearly Pollock survey can be used to exemplify the new transducer requirements. Due to climate changes, the pollock has moved its habitat up to 1000 km north, into the Bering sea. The researchers must follow, and it can take months to zigzag the relevant area back and forth [15]. Doing so, it is valuable to collect information on other species as well. Different species have different backscatter profiles and live at different depths, and there is therefore a need to collect data at many different frequencies. With limited space available on the small platforms, compact transducers with a large usable frequency band are of the essence.

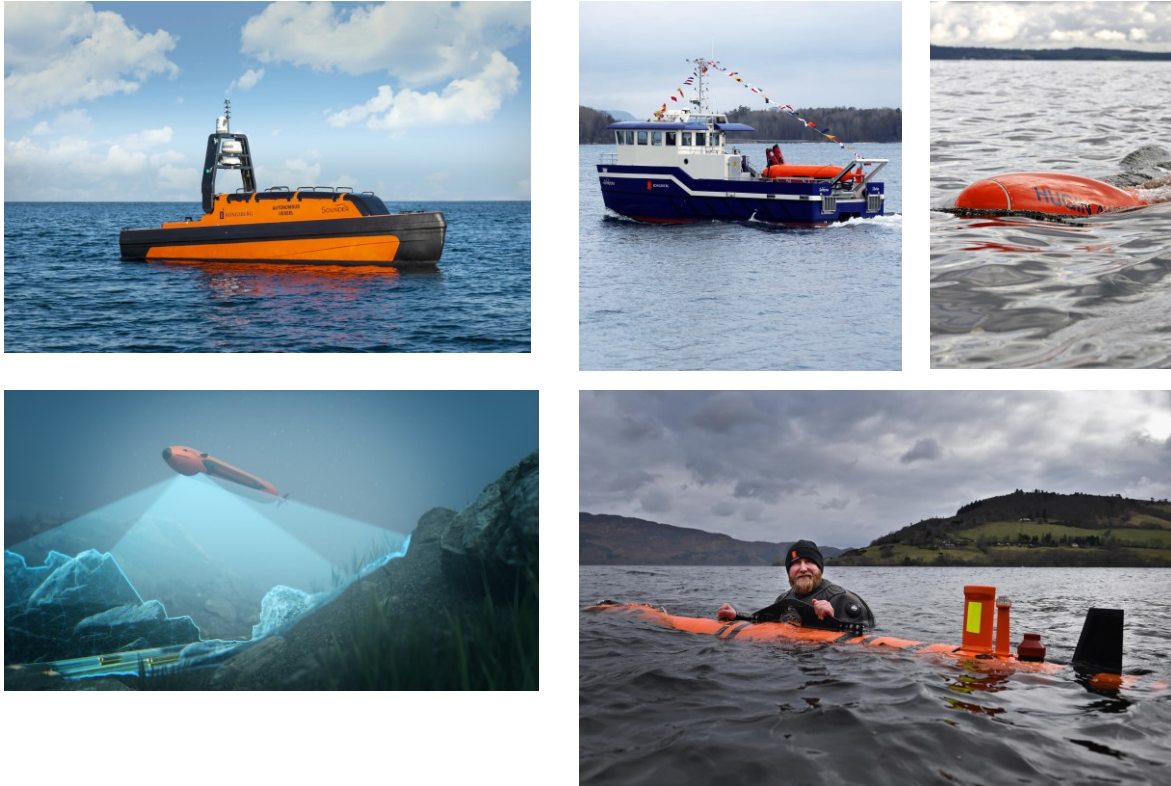


*Figure 1-3: The figure illustrates robots with limited space available for transducers and transducer electronics. Pictures from Kongsberg Maritime AS.*

## 1.4 Research questions and structure of thesis

With this inspiration and these new requirements in mind, we initiated a Ph.D.-project with the following research questions:

1. What is the state of the art for single crystal underwater transducers?
2. How is the usable frequency band of underwater transducers affected by use of single crystals with high electromechanical coupling?
3. How should a 1-3 piezocomposite transmitter and a tonpilz transmitter be designed to maximize the usable frequency band for underwater applications?
4. How is the compactness of a 1-3 piezocomposite transmitter and a tonpilz transmitter affected by use of single crystals?

The research questions, approaches used to answer them, and types of outcomes are summarized in **Table III**. Each question has its own chapter in this document, Chapters 2, 3, 4 and 5. Theory, methods, results, discussion, and conclusion are presented in the relevant

chapter. Another very important question is: *How realistic is it to implement high coupling materials in practical applications?* A full answer to this question is left for future work, but some information is provided in Chapters 6, 7 and 8. In Chapter 6, the performance of the piezocomposites fabricated during the Ph.D. project is presented. The performance was measured at room temperature, small electrical field, and small mechanical stress. Chapter 7 summarizes a literature study on material parameter variations due to temperature, stress, and electric field. Chapter 8 summarizes a literature study on the state of the art for textured ceramics. The thesis is concluded in Chapter 9.

The choice of document structure, with each chapter aiming at answering one research question, necessitated repetition of information found in the articles. Collocation of results was essential to point out how research presented in different articles contribute to answering a specific research question. To help a reader that is already familiar with the articles to skip repetitions, text and figures that are taken directly from the included articles are printed on a light grey/teal background, as shown below:

Text and figures that are taken directly from the included articles are printed on a light grey/teal background.

*Table III: Research questions, approaches, and types of outcomes*

Questions	Approaches	Types of outcomes
1. State of the art	Literature review	See Chapter 2
2. Usable frequency band, impact	Theory study and 1D modelling	Article1, part 1
3. Usable frequency band, design	Optimization of matching layers: 1D modelling 3D FEM modelling + fabrication	Article 1, part 2 Article 3
	Tonpilz design: 1D modelling	Article 2
4. Compactness	Theory study + 3D FEM modelling Fabrication of prototype	Article 4

## 1.5 Two types of transmitter design

The Ph.D. project was concentrated on two types of transducer designs for which a high  $k_{33}$  can be utilized, the tonpilz and the 1-3 piezocomposite plate. The investigations considered transducers used as transmitters, not as receivers. Sherman and Butler [16] gave the following categorization of transmitter designs: “While spherical and ring sources are omnidirectional in at least one plane, the piston type transducers generally projects sound into one direction with a directionality that depends on its size compared to wavelength. Large arrays of these transducers are used to project highly directional, high intensity beams of sound into a particular area (...) and are commonly used in underwater acoustics. (..) Tonpilz lumped mode transducers are typically operated in the range from 1 kHz to 50 kHz, (..) and piezoelectric plates, diced plates or piezoelectric composites are used from about 50 kHz to beyond 2 MHz.” The tonpilz transducer has a piezoelectric driving section between a head mass and a tail mass, shown schematically to the left in Figure 1-4. A large tail-to-head mass ratio is desirable as it yields a large head velocity, radiating the most power. Piezocomposites consists of piezoelectric material embedded in a polymer matrix. For a composite with 1-3 connectivity the piezoelectric material is connected only along a single (1) direction, while the polymer is connected along three (3) directions [16]. Arrays of piezoelectric pillars are arranged in a polymer matrix as shown to the right in Figure 1-4. In a piezocomposite transducer there is a backing behind the composite and often one or more matching layers between the composite and water. The included articles consider composites with air backings. Air or air-like materials with very low acoustic impedance reflect the sound from the back end of the composite, increasing efficiency at the front end.

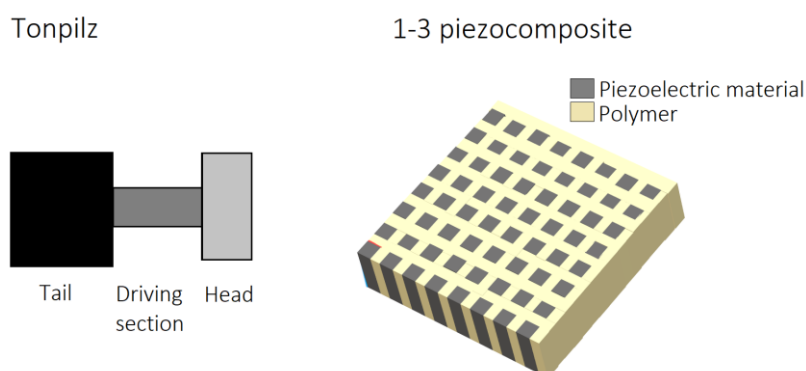


Figure 1-4: The two considered designs. Left: Tonpilz. Right: 1-3 piezocomposite plate

## 1.6 Complexity of research questions

The answers to many of the research questions might seem to be given by the quote on page 5 by Amin et al. [8] and by simple comparison of the parameters of Table II. Figure 1-5 illustrates why application specific investigation is needed. In this figure, the performance of the single crystal PIN24%-PMN-PT is compared to the performance of PZT5H1 for a simple 1-3 piezocomposite design. The composite has volume fraction active material 40 %, air backing, water load and no matching layers. The matrix material is an epoxy with Young's modulus 1 GPa. The performance was calculated using a FEM model with periodic boundary conditions. These calculations are not included in any of the articles and Figure 1-5 serves as an initial illustration only.

- Figure 1-5a and Figure 1-5b show transmitting voltage response, TVR [17]. The single crystal composite has a larger -3 dB bandwidth than the PZT composite, but far from a threefold increase.
- Figure 1-5c shows the electrical impedance magnitude, and we see that the single crystal material gives a larger distance between the resonance frequency and the anti-resonance frequency than what is the case for the PZT material.
- The large difference between the resonance frequency and the anti-resonance frequency for the single crystal is reflected in Figure 1-5d, which shows the sum of transmitted voltage response (TVR) and received voltage response (RVS) [17]. In this figure, the -12 dB bandwidth is much larger for the single crystal composite than for the PZT composite, but for the -6 dB bandwidth it is the other way around. Figure 1-5e shows the electroacoustic efficiency, transmitted acoustic power per applied real electrical power, but note that dielectric loss was not included in the model.
- The large difference between the resonance frequency and the anti-resonance frequency for the single crystal is also reflected in Figure 1-5f, which shows electrical impedance phase, untuned. The u-shape is wider for the single crystal composite than for the PZT composite, but the PZT composite has a smaller total phase variation.
- Note from Figure 1-5a that the increase of the TVR for the single crystal composite compared to the PZT composite is smaller at resonance than at high and low frequency.

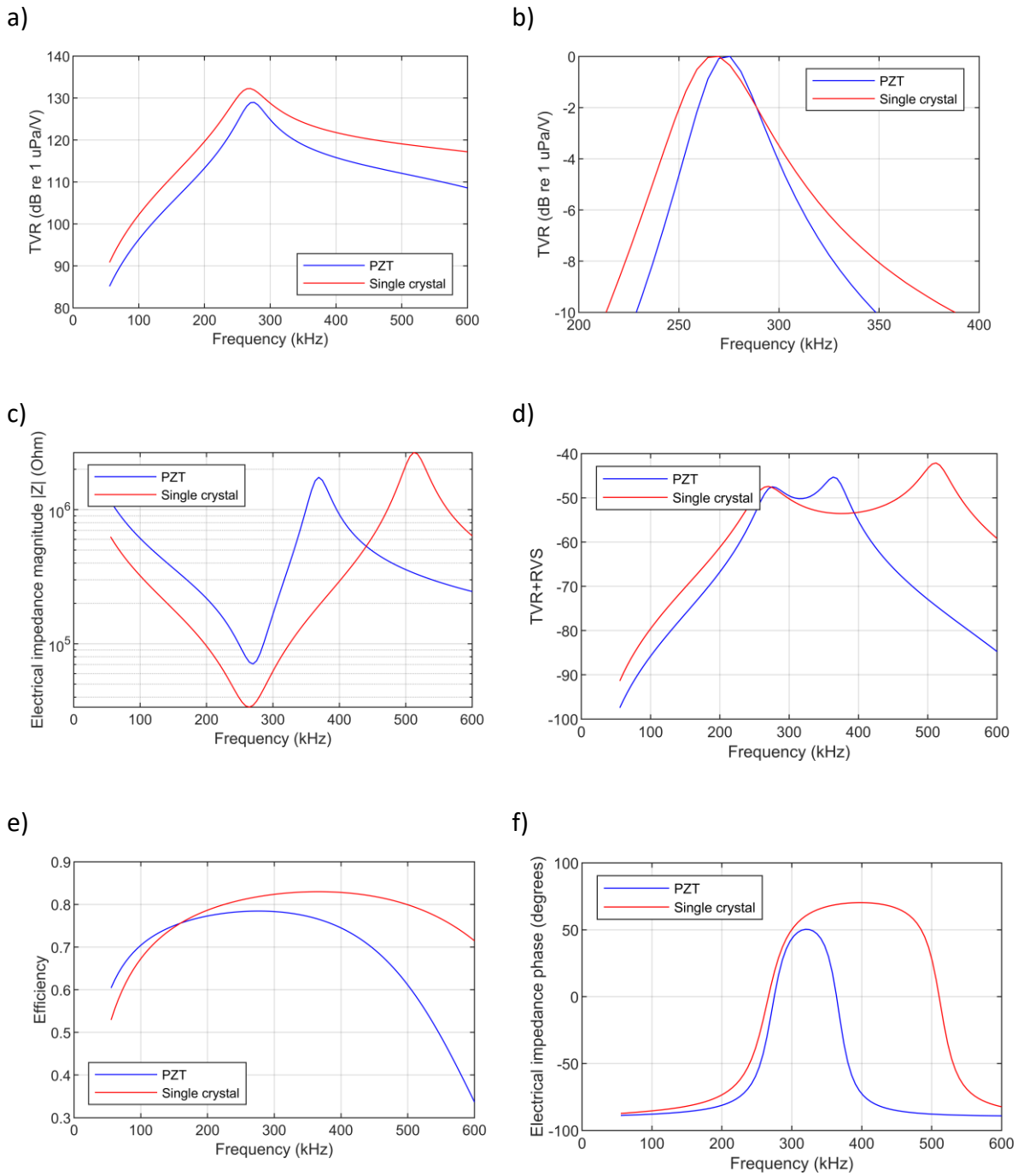


Figure 1-5: Performance for single crystal PIN24%-PMN-PT composite (red) compared to soft type VI PZT5H1 (blue). a) Transmitting voltage response, b) Transmitting voltage response, normalized and for a smaller frequency range, c) Electrical impedance magnitude, d) Transmitting voltage response + Receiving voltage sensitivity, e) Efficiency, f) Electrical impedance phase, untuned.





## 2 State of the art for single crystal underwater transducers

This chapter aims at answering research question 1 “What is the state of the art for single crystal underwater transducers”?

### 2.1 Method

The state of the art for single crystal underwater transducers was reviewed through a literature study. The main search was performed at the end of 2018, through Web of Science, IEEE Xplore and JASA. Following the search, alerts were placed at Web of Science, IEEE Xplore and Google Scholar.

### 2.2 Results

The by far largest group of researchers in this field is the one affiliated with the US Office of Naval Research (ONR), with two cooperating centres at Pennsylvania State University (Penn State) and Naval Undersea Warfare Centre (NUWC). The professors Cao (Penn State) and Zhang (former Penn State) are authors of extensive review articles on single crystals in general [18]-[21]. The focus of this Ph.D. project, on the other hand, was articles that specifically treat underwater transducer designs. Many of the articles regard stability of the crystals under applied mechanical, electrical, and thermal loads [6],[8],[22]-[27]. This will be discussed in Chapter 7.

The majority of the reported naval single crystal designs are of the tonpilz type [12], [22]-[25], [28]-[33]. In 2007, researchers from NUWC reported a 16-element array of tonpilz transducers [8]. Each tonpilz incorporates four stacks of PMN-PT single crystal. These stacks are made from plates rather than conventional rings. An earlier version of the element was reported by Powers et al. [28], and they explain that large crystal rings were not available at the time of the design. The head was designed to be “simultaneously lightweight, stiff and large relative to the stack area in order to provide an optimal mechanical quality factor to maximize the bandwidth”. The theory of optimum mechanical quality factor was described in the article by Moffett et al. that was mentioned in Chapter 1 [13], and this theory will be further treated in Chapter 3. In [28], the head material was given as an aluminium-beryllium alloy. This alloy has high stiffness to

help prevent head flexure, and the head flexure was further controlled by the evenly spread stacks. The material of the heavy tail mass was a machinable tungsten alloy [28]. Prestress was applied using a Belleville spring. The effective coupling coefficient was reported to be 0.75, compared to 0.55-0.6 for a typical PZT transducer. The source level from the 16-element single crystal tonpilz array was compared to the source level from a conventional ceramic tonpilz array. The source level was plotted versus normalized frequency, from 0.5 to 2.5. For a fixed number of Volt-Amperes, the single crystal array provided 15 dB additional source level at the high and low ends of the frequency band. It was shown in a presentation by Robinson [34] that the tuned electrical impedance phase was smaller than  $50^\circ$  in the frequency band 0.7-2.5 for the single crystal array compared to 0.8-1.55 for the conventional array. The earlier version of the tonpilz element was reported to have dimensions 35x35x40 mm and a nominal centre frequency of 20 kHz [28].

Also in 2007, PennState researchers Montgomery, Meyer and Bienert evaluated the system impact of using a single crystal tonpilz element compared to a doubly resonant hybrid magnetostrictive-piezoelectric tonpilz element (MPT) [31]. They stated that “recent work has shown that PMN-PT based tonpilz elements with a single resonance have a device electromechanical coupling coefficient greater than 0.86”. The impact analysis was summarized as follows: “The benefits of the PMN-PT based transmit system are obvious in all categories; weight, volume, power consumption. In addition, when all the transmit system components are included in the cost, the cost of the transmit sub-system for the two transduction types is nearly equivalent. As such, a PMN-PT projector will be instrumental in reducing payload size and power consumption in future small AUVs, while maintaining performance.”

A tonpilz element incorporating one stack of eight PMN-PT rings was reported by Thompson, Meyer and Markley in 2014 [33]. A tonpilz utilizing the 32 mode of PMN-PT was also reported [12][32]. The targeted application for the latter work was broadband (>100%), 45 kHz, synthetic aperture arrays for unmanned underwater vehicles [32]. For 33 mode tonpilzes, the high compliance leads to short resonators. A less than ideal aspect ratio reduces the effective coupling coefficient and thus the bandwidth, and the 32 mode design was proposed to address

this issue. Robinson et al. [29] reported use of the 32 mode in a Low Frequency Range Tracking Transducer to provide tracking pinger transmit capabilities to small-diameter vehicles. The volume and weight of the transducer element was reduced by 90% compared to a PZT-based pinger transducer.

The 32 mode tonpilz has been studied also by Zhang et al. from Science and Technology on Sonar Laboratory in Hangzhou, China [35]. Using a thin light beryllium alloy head mass, a thick heavy tungsten alloy tail mass and three blocks of 32 mode single crystal, a 32 mode tonpilz with resonance frequency 21 kHz was designed, fabricated, and measured. The transmitting voltage response (TVR) of the transducer had ripple within  $\pm 3.5$  dB from 16 to 91 kHz.

Another alternative mode provided by single crystals is the shear 36 mode. Single crystal material with  $d_{36} = 2200$  pC/N,  $k_{36} > 0.8$  and high elastic compliance,  $190 \cdot 10^{-12}$  m<sup>2</sup>/N, is available [36]. Van Tol et al. [37] [38] developed a 36 mode tonpilz transducer with resonance frequency 2 kHz and a size of only three inches in diameter and 2.5 inches in depth.

Researchers from the acoustics groups in Scotland have contributed significantly to the field of single crystal underwater transducers. Marin-Franch, Cochran and Kirk compared PMN-32%PT to PZT5H in 2004 [39], concluding that “the new single crystal material will be capable of outperforming the present widely used ceramic for almost all practical applications”. For underwater applications, they evaluated an array made from a 200 kHz single crystal 1-3 composite, using the hard-setting CY1301/HY1300 as the matrix material. They added a quarter-wavelength thick matching layer and used a material with low acoustic impedance as backing. The calculated transmit-receive quality factor was 0.99 for PMN-PT, compared to 1.75 for PZT-5H. Robertson et al. from Centre for Ultrasonic Engineering at The University of Strathclyde in Glasgow investigated cross talk in single crystal piezocomposite arrays [40][41]. One of these arrays had resonance frequency around 1 MHz, which is in the upper end of the relevant frequency range for underwater transducers.

Pham Thi et al., France, did also fabricate single crystal piezocomposites in the relevant frequency range [42], and so did Wang et al. [43]. Wang is affiliated with Shanghai Institute of Ceramics, China. One of the co-authors of [43] is Haosu Luo. He is the co-author of several

articles [43]-[48] concerning fabrication of piezocomposites with resonance frequencies around 1 MHz. Many of these composites were targeted for NDT applications, but the articles contain useful machining and fabrication instructions. Kim and Roh from School of Mechanical Engineering in Korea modelled single crystal 1-3 piezocomposites incorporated in tonpilzes [49]-[51].

Generation II and III, ternary (PIN-PMN-PT) and Mn-doped ternary single crystals were developed to provide extended operating temperatures and electric field driving ranges [52], see Chapter 7. These materials have been incorporated in tonpilzes by several of the mentioned research groups [22][53][54].

So far, this state-of-the-art-chapter has been concentrated on tonpilz or composite designs. A few other designs are also worth mentioning. Particularly interesting is the single crystal segmented cylinder transducer reported by NUWC researchers [8][13]. Theoretically, the effective coupling coefficient of a cylinder is equivalent to the material coupling [34], and the reported design had an effective coupling coefficient of 0.867. The design allows a low mechanical quality factor, 0.91 in [13], and this enables a bandwidth close to optimum. Cylinder projectors are frequently used for communication [34], [55]-[57].

Single crystal cymbal transducers were also reported [58]-[60], and in 2017 Guo et al. [61] made a comprehensive analysis of Mn:PIN-PMN-PT single crystals for Class IV flexensional transducers. In 2013, improved performance of a cantilever mode piston transducer by use of PIN-PMN-PT single crystals was demonstrated [62]. An advantage analysis of PMN-PT material for free-flooded ring transducers was performed in 2011 [63].

Wallace, together with Cochran and several others [64], investigated a parametric array design. Their aim was to use a small device of expensive single crystal to produce a low frequency beam. They concluded that “the ease with which this technique can be employed with modern instrumentation suggests that it is viable for commercial implementation with PMN-PT single crystal material even in the highly cost-competitive underwater sonar market”.

Together with Parker and Marin-Franch, Cochran also reported an “Ultrabroadband single crystal composite transducer for underwater ultrasound” [65]. In a previous work they

presented a multilayer ultrasonic transducer with layers of nonuniform design, yielding resonant harmonics not observed in the usual odd harmonic response of a conventional structure. They now replaced PZT by single crystal in their multilayer structure, and by extensive material characterization and design optimization they achieved a -6 dB transmit-receive bandwidth of 125 %.

The authors of [65] emphasized the general importance of optimizing the thickness of the matching layers for a broadband design, as “the geometric quarter-wavelength thickness usually assumed of a matching layer is fundamentally a narrowband property”. Optimization of matching layers for single crystal underwater transducers is not treated in any of the articles resulting from the literature search. In light of the importance of an optimum mechanical quality factor, explained by Moffett et al. [13], we considered this to be an interesting topic for further investigation and a natural starting point for the Ph.D. project. The frequency range of interest for commercial and scientific underwater transducers includes the low frequencies provided by tonpilz designs, but also the higher frequencies usually obtained by piezocomposite designs with matching layers.



### **3 Impact of the electromechanical coupling coefficient on the usable frequency band**

This chapter aims at answering research question 2 “How is the usable frequency band of underwater transducers affected by use of single crystals with high electromechanical coupling?”

Among the listed advantages of single crystals, the impact of the electromechanical coupling coefficient,  $k$ , on the bandwidth is the least intuitive. The coupling coefficient determines the distance between the resonance frequency and the anti-resonance frequency. It is evident from Figure 1-5 that this distance is of importance for the width of the band in which sound can effectively be transmitted or received. However, it is also evident that the benefit of a high coupling coefficient is heavily dependent on the definition of bandwidth. For example, if defining bandwidth by the transmit-receive-sensitivity of Figure 1-5d, the -12 dB bandwidth is much larger for the single crystal composite than for the PZT composite, but for the -6 dB bandwidth it is the other way around.

In Article 1, we investigated the impact of  $k$  on the frequency response of two different parameters, the electromechanical transfer function and the electrical power factor.

#### **3.1 The impact of $k$ on the transfer function bandwidth**

The term bandwidth is often associated with pulse length and is conventionally defined by the -3 dB points of the electromechanical transfer function, alternatively by the -3 dB points of the transmitting voltage response (TVR [17]). One of the objects of Article 1 was to isolate the impact of  $k$  on the electromechanical transfer function from the impact of other material parameters.

##### **3.1.1 Theory**

Four fundamental concepts for this study are given below: The electromechanical coupling coefficient, the electromechanical transfer function, the Butterworth-Van Dyke (BVD)



transducer model, and the mechanical quality factor. Another central model, the Mason model, was given in Figure 1-1.

Electromechanical coupling causes changes in mechanical stiffness,  $K_m$ , and electrical capacitance,  $C$ , when the electrical or mechanical boundary conditions are changed. The relative changes are equal and can be defined as [1]:

$$k^2 = \frac{K_m^D - K_m^E}{K_m^D} = \frac{C_f - C_0}{C_f} \quad (9)$$

The superscripts D and E denote electrical open and short circuit conditions, and the subscripts  $f$  and  $0$  denote mechanical free and clamped conditions. The parameter  $k$  is called the electromechanical coupling coefficient, and it can be shown [1] that  $k^2$  gives the ratio of converted mechanical energy to input electrical energy under static or quasi-static conditions. The coupling coefficients for different materials are given in Table II, for different modes. The coupling coefficient of a bar resonator will not necessarily be equal to the material  $k_{33}$ . If the aspect ratios are not consistent with a pure mode, see Figure 1-2, the effective  $k$  is reduced compared to  $k_{33}$ . The effective  $k$  can also be reduced by dynamic increase in stiffness. This reduction is dependent on the electrode arrangement [66]. For a complex transducer, e. g. a tonpilz,  $k$  can be additionally reduced by inactive elements, such as glue joints, cables, and stress bolts [66].

The electromechanical transfer function,  $H(f)$ , is defined by

$$H(f) = u(f)/V(f) \quad (10)$$

where  $u(f)$  is normal velocity at the face of the transducer, and  $V(f)$  is the voltage at the electrical terminal of the transducer. The conventional definition of the transfer function bandwidth is the range of frequencies where

$$20 \log_{10} \frac{|H(f)|}{|H(f_0)|} \geq -3 \text{ dB} , \quad (11)$$

with  $f_0$  being the frequency where the transfer function  $H(f)$  has its maximum value. For a constant real-valued load, the transfer function bandwidth is equal to the bandwidth of the acoustic power.

From Article 1

The Mason model was presented in Figure 1-1. It is a 1D model and does not account for lateral modes. The Mason model is a distributed model, meaning that the mass and stiffness of the resonator is distributed throughout the structure rather than lumped into discrete components. The model assumes boundary conditions that makes the resonator vibrate in a specific, clean, mode. The simple model of Figure 1-1 is for one layer of piezoelectric material. The model can be extended to include matching layers or the head and tail of a tonpizl.

The Butterworth Van-Dyke (BVD) transducer model [67] is a lumped-model simplification of the distributed Mason model around a selected resonance. Figure 3-1 shows the electrical equivalent BVD circuit for a single degree of freedom system.

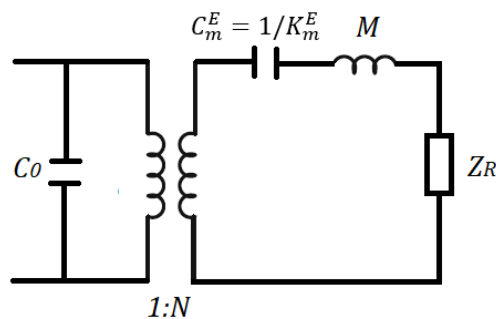


Figure 3-1: The BVD model. The circuit drawn here is for the case of no internal loss.  $M$  is the effective mass and  $Z_R$  is the radiation impedance.

For the BVD model, the electrical equivalent of the velocity  $u(f)$  is the current going into the mechanical, series, branch. The sharpness of a resonance is defined by the quality factor. The quality factor of the series branch of the BVD circuit is called the mechanical quality factor  $Q_m$ . Using the definition for an RLC series, we get

$$Q_m = 2\pi f_r (M/Z_R) \quad (12)$$

for a pure resistive load  $Z_R$ . For the BVD model, the transfer function bandwidth is given by  $1/Q_m$ .

### 3.1.2 Method

A piezoelectric plate in the thickness extensional mode was considered, for a simplified case where the back port was short circuited (air backing), and the front port was loaded by a real load of constant acoustic impedance  $Z_R$ . The frequency dependence that matching layers would introduce at the front port was not considered at this point. The simplified case was chosen to study the impact of  $k$ . The expression for  $H(f)$  derived from the two-port matrix representation of the 1D Mason model [68] was rewritten by using relations from Figure 1-1. The magnitude of the transfer function  $H(f)$  was plotted for different ratios of  $Z_c/Z_R$ , where  $Z_c$  is the open circuit acoustic impedance of the plate, given in Figure 1-1 as  $Z_c = A\rho\sqrt{c_{33}^D\rho}$  for the thickness mode. The results were presented in Article 1.

### 3.1.3 Results

Using the method described above, we found that the electro-mechanical transfer function  $H(f) = u(f)/V(f)$  for the plate can be written as

$$H(f) = \frac{N}{Z_R} \frac{1}{1 - \frac{1}{2 \sin^2 x} + \frac{k_t^2}{2x \tan x} + j \frac{Z_c}{Z_R} \left( -\cot x + \frac{k_t^2}{x} \right)} \quad (13)$$

The parameter  $x$  is a normalized frequency parameter,  $x = \pi ft/v = (\pi/2)(f/f_a)$ . For the simple case considered here, the factor  $N/Z_R$  is frequency independent and disappears when the transfer function is normalized. For frequency normalized to the anti-resonance frequency  $f_a$  and for a given ratio  $Z_c/Z_R$ , the normalized transfer function is dependent on  $k_t$  only. This is illustrated in Figure 3-2, for  $k_t = 0.9$  and  $k_t = 0.7$  and various values of  $Z_c/Z_R$ . The absolute widths of the transfer functions vary little between the two coupling factors, but the width relative to the resonance frequency is significantly larger for  $k_t = 0.9$ . This effect is illustrated in Figure 3-3, showing the same curves as in Figure 3-2, but now normalized to resonance and with a finer scale for the vertical axis. Note from Table II that the open circuit

characteristic acoustic impedances,  $z_c$ , of the single crystals are similar to those of the PZTs, due to similar  $\rho$  and  $c_{33}^D$  (or  $s_{33}^D$  for rods).

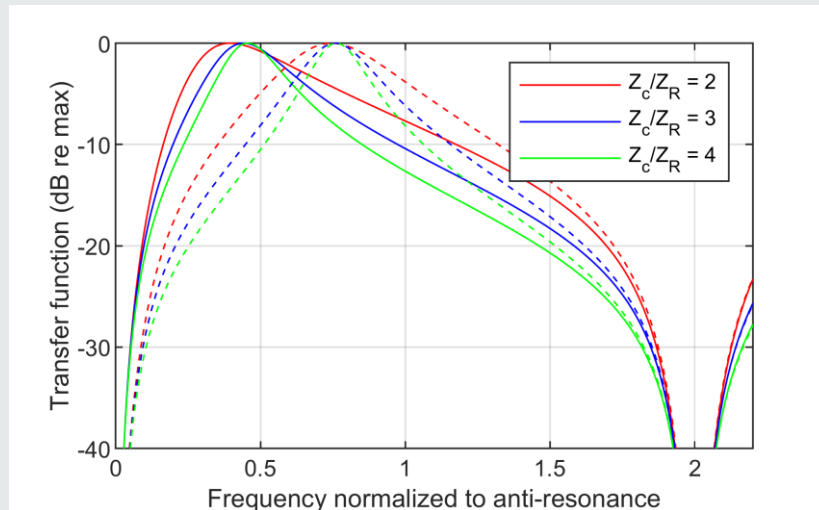


Figure 3-2: Normalized magnitude of the electromechanical transfer function for two transducers with  $k_t = 0.9$  (solid lines) and  $k_t = 0.7$  (dashed lines). Calculated with (13) for mismatch  $Z_c/Z_R = 2$  (red),  $Z_c/Z_R = 3$  (blue) and  $Z_c/Z_R = 4$  (green). The frequency axis is normalized to the anti-resonance frequency.

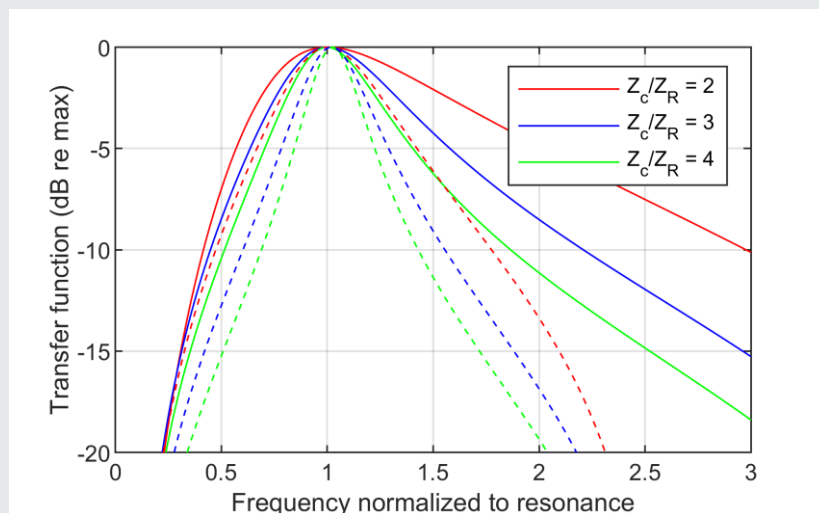


Figure 3-3: Normalized magnitude of the electromechanical transfer function for two transducers with  $k_t = 0.9$  (solid lines) and  $k_t = 0.7$  (dashed lines). Calculated with (13) for mismatch  $Z_c/Z_R = 2$  (red),  $Z_c/Z_R = 3$  (blue) and  $Z_c/Z_R = 4$  (green). Corresponding to Figure 3-2, but with frequency axis normalized to resonance, and with a finer scale for the vertical axis. In this figure, resonance is defined as the frequency where the transfer function has its maximum.  
From Article 1, slightly adapted

### 3.1.4 Discussion

The decrease in resonance frequency due to an increase in  $k_t$  can physically be explained as a softening of the piezoelectric material under short circuit conditions. Equations (13) was derived from the distributed Mason model for the air-backed plated. The effect of an increased  $k_t$  on the relative width can be seen also from the BVD model.

To find  $Q_m$  using the BVD model, the effective mass [66]  $M = (1/2)\rho At$  is inserted in (12), with  $A$ ,  $t$  and  $\rho$  being the area, thickness, and density of the plate. The expression for the effective mass,  $M$ , can be found by deriving the BVD model from the Mason model using series expansion. An expression for the resonance frequency  $f_r$  is also needed. Using the definition of the coupling coefficient (9),  $f_r$  is given by  $f_a$  as  $f_r = \sqrt{1 - k^2}f_a$  [69]. Note that for this expression for  $f_r$  to be valid,  $k$  must be the effective coupling coefficient for the structure, not the material alone, hence, dynamic conditions and any inactive components are also included. The resulting mechanical quality factor is given by

$$Q_m = \frac{\pi \rho v^D \sqrt{1 - k^2}}{2 Z_R} = \frac{\pi Z_c}{2 Z_R} \sqrt{1 - k^2} \quad (14)$$

*From Article 3, slightly adapted  
Included also in Article 1, but better explained in Article 3*

The method used to find expression (14) is not accurate for the plate, especially not for the case of high electromechanical coupling. It does however establish a first estimate for the decrease in  $Q_m$  provided by an increase of  $k$ .

If  $k$  is increased from 0.7 to 0.9,  $Q_m$  is decreased by a factor 0.61, according to (14), and the transfer function bandwidth,  $1/Q_m$ , is increased by 64 %. If  $k$  is increased from 0.6 to 0.9, the corresponding increase of transfer function bandwidth is 83 %. This is a significant increase, but nowhere near the tripled bandwidth we read about in [8]. The explanation lies in the definition of bandwidth. For many underwater transducer applications, transducer bandwidth is defined not only in terms of the transfer function bandwidth but also in terms of reactive electrical power.

## 3.2 Impact of $k$ on the electrical power factor

Object number 2 of Article 1 was to investigate the impact of  $k$  on a bandwidth that is restricted by the amount of reactive electrical power. In later sections, the term *usable frequency band* is preferred to describe a bandwidth that is not defined by the conventional -3 dB points of the electromechanical transfer function. The term *bandwidth* is however kept in the following section, as it is used in the central references.

### 3.2.1 Theory

#### Reactive electrical power and tuning:

The apparent electrical power,  $VI$ , into a transducer consists of a real part,  $|VI| \cos \theta$ , and a reactive part,  $|VI| \sin \theta$ , where  $V$  is the voltage,  $I$  is the electric current, and  $\theta$  is the phase of the transducer's electrical impedance. The reactive power flows back into the transmit electronics without contributing to the transmitted acoustic power. The reactive power should be limited to limit the amount of apparent power drained from the power source and limit the required size of the electronics. In a transducer, the impedance phase  $\theta$  is often tuned to zero at resonance. One way of doing this, is by adding an inductor in parallel with the capacitance  $C_0$  shown in Figure 3-1.

#### Stansfield's two bandwidth criteria:

In the book "Underwater Electroacoustic Transducers" by D. Stansfield [70], two bandwidth criteria were proposed: "The tuned transducer forms a bandpass filter between the amplifier and the load. By considering the impedance variation that a properly sized amplifier can tolerate, Stansfield has provided two criteria, for the magnitude and phase of the transducer admittance, to define the transducer bandwidth. The magnitude criterion requires that the variation in magnitude of the tuned admittance be within a factor of 2. The phase criterion restricts the phase variation to  $\pm 37^\circ$ , equivalent to power factor  $\geq 0.8$ . The useful bandwidth is then determined by whichever criterion is more stringent". This explanation of Stansfield's two bandwidth criteria is taken from the article by Moffett et al. [13][28].

Optimum mechanical quality factor:

Referring to Mason [71], Stansfield explained that there exists an optimum  $Q_m$  for the transducer design that maximizes the bandwidth according to the two criteria. The concept of an optimum  $Q_m$  was later presented also by Sherman and Butler, in their book “Transducers and Arrays for Underwater Sound” [69]. They used the BVD model, but unlike Stansfield they did not base their derivation on specific limits for admittance magnitude and phase. They started by showing how the electrical phase at the resonance frequency,  $\theta_r$ , is related to  $Q_m$ . The phase  $\theta_r$  can be found from [69]:

$$\tan \theta_r = \frac{B_r}{G_r} = 2\pi f_r \frac{C_0}{G_m}. \quad (15)$$

The electrical conductance and susceptance are denoted  $G$  and  $B$ , respectively. Electrical loss is ignored, and  $G_m$  is a symbol for mechanical conductance at resonance. Expression (15) is called the electrical quality factor,  $Q_e$ , and is “an important consideration when the transducer is connected to a power amplifier. Broadband power operation is difficult if  $Q_e$  is high, since then a large Volt-Ampere capacity from the power amplifier is needed for a given power requirement as a result of the shunted current through  $C_0$ ” [69].

Using  $G_m = N^2/R$ ,  $k^2 = N^2/(K_m^E C_f)$ , see equation (9) and Figure 3-1,  $Q_m = \frac{K_m^E}{2\pi f_r R}$ , and  $G_m = k^2 2\pi f_r C_f Q_m$ , the following relation was derived [69]:

$$Q_e = \tan \theta_r = \frac{C_0}{k^2 C_f Q_m}. \quad (16)$$

Here,  $R$  denote resistance in the mechanical branch of the BVD circuit and is equal to the real part of the radiation impedance  $Z_R$  if there is no internal loss. In section 3.1 the symbol  $Z_R$  was kept for the purely resistive radiation impedance, for consistency with the work by DeSilets et al. [72] referred to in Articles 1 and 3. From the definition of  $k$ , we have  $C_0 = C_f(1 - k^2)$ , yielding [69]

$$Q_m Q_e = (1 - k^2)/k^2. \quad (17)$$

Sherman and Butler's optimization criterium is minimization of the sum of  $Q_e$  and  $Q_m$ . This sum is minimum when  $Q_m = Q_e$ , and the optimum  $Q_m$  is therefore given by:

$$Q_{opt} = \frac{\sqrt{1-k^2}}{k}. \quad (18)$$

Moffett et al. [13] used a slightly larger value for the optimum mechanical quality factor,  $1.245Q_{opt}$ , based on Stansfield's bandwidth criteria. This alternative value was also mentioned in Sherman and Butler as providing "broader response, but with slight ripple". The maximum relative bandwidth resulting from  $1.245Q_{opt}$  is [13]:

$$BW_{max} = 0.98 \frac{k}{\sqrt{1-k^2}}. \quad (19)$$

which is approximately equal to the bandwidth resulting from the inverse of (18). Moffett et al. [13] has commented on this in their article, stating that "there is an optimization approach that requires equality of the mechanical and electrical quality factors. (..) The resulting bandwidth, however, turns out to be the same".

Equation (19) gives the nearly three-fold increase of bandwidth for single crystal compared to PZT8, as promised in [8]. The bandwidth  $BW_{max}$  is plotted in Figure 3-4, showing an increase by a factor 2.75 from  $k = 0.6$  to  $k = 0.9$ . From  $k = 0.7$  to  $k = 0.9$ , the bandwidth is approximately doubled. Note that the quality factors are defined at the mechanical resonance. The maximum bandwidth is therefore given relative to the resonance frequency  $f_r$ , not relative to the centre of the band.



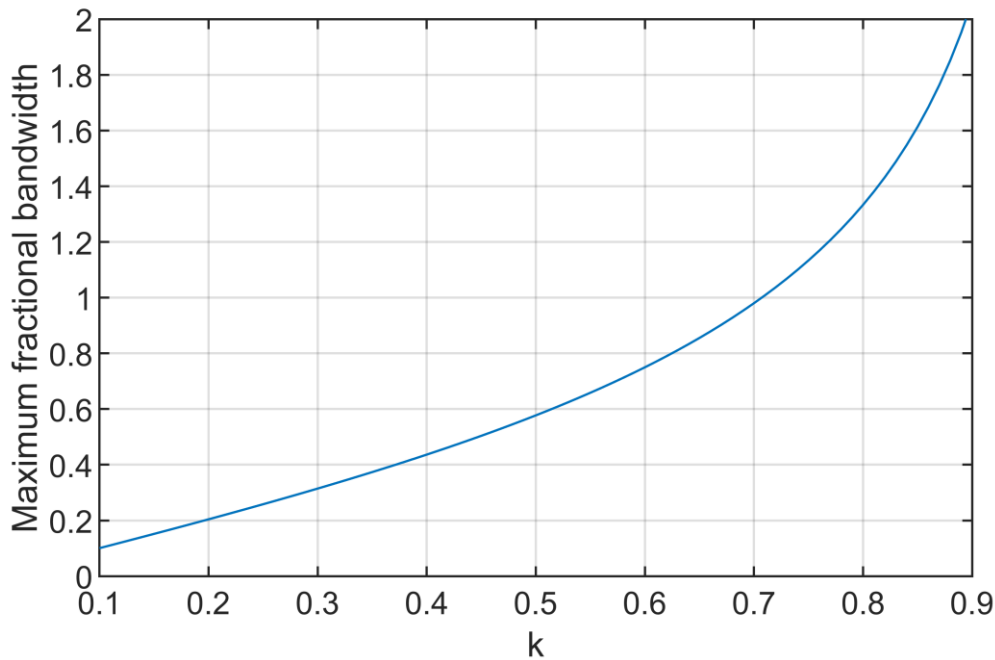


Figure 3-4: Maximum bandwidth  $BW_{max}$ , calculated using (19). This figure corresponds to fig. 4 in [13].

Tuned electrical power factor:

The electrical power factor is defined as  $PF = \cos \theta$ . Using the BVD model, Sherman and Butler derived an expression for the parallel tuned power factor as a function of frequency  $f$  [69]:

$$PF = \cos \theta = 1/\sqrt{1 + \tan^2 \theta} \quad (20)$$

$$\tan \theta = \left[ \frac{1 - k^2}{k^2} \frac{1}{Q_m} - Q_m + \frac{1 - k^2}{k^2} Q_m \left( \frac{f}{f_r} - \frac{f_r}{f} \right)^2 \right] \left( \frac{f}{f_r} - \frac{f_r}{f} \right). \quad (21)$$

In this expression,  $\theta$  is the electrical impedance phase after tuning.

Equation (21) was derived by expressing the electrical admittance of the untuned BVD circuit as  $Y = j2\pi f C_0 + G_m / \left[ 1 + jQ_m \left( \frac{f}{f_r} - \frac{f_r}{f} \right) \right]$ , tuning by adding an inductor with inductance  $L_p = 1/(2\pi f_r)^2 C_0$ , and by using (17). In Figure 3-5, the tuned power factor is plotted for

the cases of Figure 3-2 and Figure 3-3. The quality factor is extracted from Figure 3-3. Figure 3-5 corresponds to Fig. 2.12 in [69].

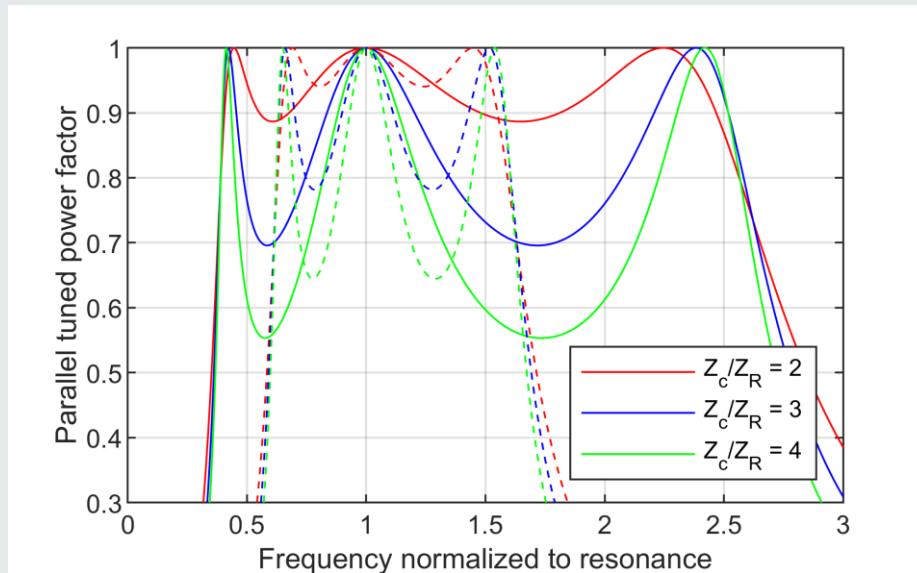


Figure 3-5: Parallel tuned electrical power factor for two transducers with  $k_t = 0.9$  (solid lines) and  $k_t = 0.7$  (dashed lines). Calculated with (20) and (21) for mismatch  $Z_c/Z_R = 2$  (red),  $Z_c/Z_R = 3$  (blue) and  $Z_c/Z_R = 4$  (green).  $Q_m$  is extracted from Figure 3-2. The frequency axis is normalized to resonance.

*From Article 1, slightly adapted*

### 3.2.2 Method

It can be seen from Figure 3-5 that a large  $k$  gives a wide distance between the flanks of the power factor. The hypothesis was that this distance could be related to the expression for maximum bandwidth. The aim was to make the concept of an optimum quality factor easier to understand, and to illustrate in what way  $k$  limits the obtainable bandwidth for an application that is restricted by reactive electrical power. A quadratic equation for the nodes of (21) was found in Sherman and Butler's book [69]. This equation was used to derive an expression for the maximum distance between the outer nodes. The result was published in Article 1.

### 3.2.3 Result

Assuming  $Q_m > 0.5$ , it was found that the largest obtainable fractional frequency band between the outer maxima of the tuned power factor is given by:

$$\frac{\Delta f}{f_r} = \frac{k}{\sqrt{1 - k^2}} \quad (22)$$

*From Article 1, slightly adapted*

### 3.2.4 Discussion

The derived expression (22) is approximately equal to the expression for  $BW_{max}$  (19). The two equations express different quantities and are arrived at using different approaches. Note that the upper flank of the curves in Figure 3-5 has a slope that can make the band where the power factor  $PF$  is acceptable somewhat wider than the band within the outer nodes of (21), depending on the limit set for  $PF$ . For smaller  $Z_c/Z_R$ , the upper node will be shifted down in frequency and the upper power factor flank will be less steep. The distance between the outer nodes of (21) is therefore not an accurate measure of maximum bandwidth, but the result is useful for understanding the importance of  $k$  for the power factor. It shows how  $k$  impact the frequency band in which an acceptable electrical phase can be achieved. This is the band for which there is a nearly triple increase in going from  $k = 0.6$  to  $k = 0.9$ , or a doubling in going from  $k = 0.7$  to  $k = 0.9$ . We know however from Figure 3-5 that the ripple within the flanks is dependent on  $Q_m$ .

The maximum distance between the outer maxima of the power factor is given by  $k$  only, while  $Q_m$  can in theory be infinitely regulated by changing the mechanical transducer design. We know from equation (14) that in addition to the reduction in  $Q_m$  obtained by an increase in  $k$ , we can obtain a further reduction of  $Q_m$  by decreasing  $Z_c/Z_R$ . The ratio  $Z_c/Z_R$  can be decreased by increasing the load area compared to the area of the active material, or by use of matching layers.

For optimum bandwidth defined by Stansfield's criteria,  $Q_m$  should be equal to  $1.245 \sqrt{1 - k^2}/k$ , which equals 0.6 for  $k = 0.9$ . For many designs,  $Q_m = 0.6$  is unrealistic to

achieve. It is however evident from Figure 3-5 that  $PF > 0.8$  between the flanks can be achieved for  $Z_C/Z_R < 2$ . This corresponds to  $Q_m < 1.4$ , see (14). The transfer function bandwidth at  $Q_m = 1.4$  is only 70%, while  $PF$  is larger than 0.8 in a band of width approximately equal to 200 %. For some applications a large increase in power factor bandwidth can be beneficial, even if the transfer function magnitude has a larger variation than 3 dB in the power factor bandwidth. The benefit will depend on whether the electronics can handle a variation in magnitude better than a variation in phase.

### 3.3 Conclusion

Research question 2 was “*How is the usable frequency band of underwater transducer designs affected by use of single crystals with high electromechanical coupling?*” The answer to this question depends on how the usable frequency band is defined for a given application.

The conventional definition of bandwidth is the – 3 dB points of the electromechanical transfer function magnitude. For this definition, an increase of  $k$  from 0.7 to 0.9 increases the bandwidth by a factor 1.64, according to the lumped BVD model for a plate in the thickness mode, see (14). A more accurate value can be found from the distributed Mason model calculations of Figure 3-3.

As explained by Moffett et al. [13] for the case of an underwater transmitter, “this definition of bandwidth applies to constant-voltage drive conditions, it is not realistic for practical conditions, such as when a high-power transducer is driven near resonance by an amplifier that is not greatly oversized for its job”. For such conditions, the usable frequency band is restricted also by the amount of reactive electrical power. The term *usable frequency band* is preferred since *bandwidth* is associated with the -3 dB points of the transfer function. When reactive electrical power is taken into account, increasing  $k$  from 0.7 to 0.9, increases the *maximum achievable* usable frequency band from 100 % to 200 %, relative to the resonance frequency  $f_r$ . This conclusion is based on the lumped BVD model. Note also that even if the maximum *achievable* bandwidth is increased, the *actual* bandwidth depends on the acoustic matching.



## 4 Maximizing the usable frequency band for selected underwater transducer designs

This chapter aims at answering research question 3 “How should a 1-3 piezocomposite transmitter and a tonpilz transmitter be designed to maximize the usable frequency band for underwater applications?”. An air-backed 1-3 piezocomposite plate with matching layers is treated in section 4.1, and a tonpilz transducer is treated in section 4.2. The usable frequency band for the relevant applications was defined by both the electromechanical transfer function and the electrical power factor. The allowed variation of these two parameters was specified in each case.

### 4.1 Piezocomposite with matching layers

Acoustic matching means to match the acoustic impedance of the piezoelectric part,  $Z_C$ , to the acoustic impedance of the load,  $Z_R$ . The  $Z_C/Z_R$  of a piezocomposite plate can be reduced by reducing the area of the active material, but a small fraction of active material leads to a reduction in the effective  $k$  of the composite. This is treated in Chapter 6. Usually, piezocomposite plates are instead matched to water by adding one or more matching layers of quarter wavelength thickness. Optimization of matching layers to maximize the usable frequency band was presented theoretically in Article 1 and experimentally in Article 3. This chapter gives a summary of the theoretical work, while the experimental work is presented in Chapter 6.

#### 4.1.1 Theory

The matching layers reduce the ratio  $Z_C/Z_R$ , by increasing the  $Z_R$  that is seen from the composite. When one matching layer is added to the composite and designed following the conventional guidelines given by DeSilets et al. [72],  $Z_C/Z_R$  is reduced to  $(Z_C/Z_R)^{1/3}$  at the design frequency. For two added matching layers,  $Z_C/Z_R$  is reduced to  $(Z_C/Z_R)^{1/7}$ . Unfortunately, the large reduction of  $Z_C/Z_R$  is present in a limited passband only. This can be seen in Figure 4-1, where  $Z_C/Z_R$  is calculated as a function of frequency for two conventional matching layers added to a plate with acoustic impedance 15 MRayl. Outside

the passband,  $Z_c/Z_R$  increases rapidly. The frequency-dependence introduced by the matching layers complicates the expression for the power factor. The simple BVD expression, (21), can no longer be used. The mechanical quality factor is defined at the resonance frequency, but outside the passband, the acoustic matching is significantly poorer than at resonance, see Figure 4-1.

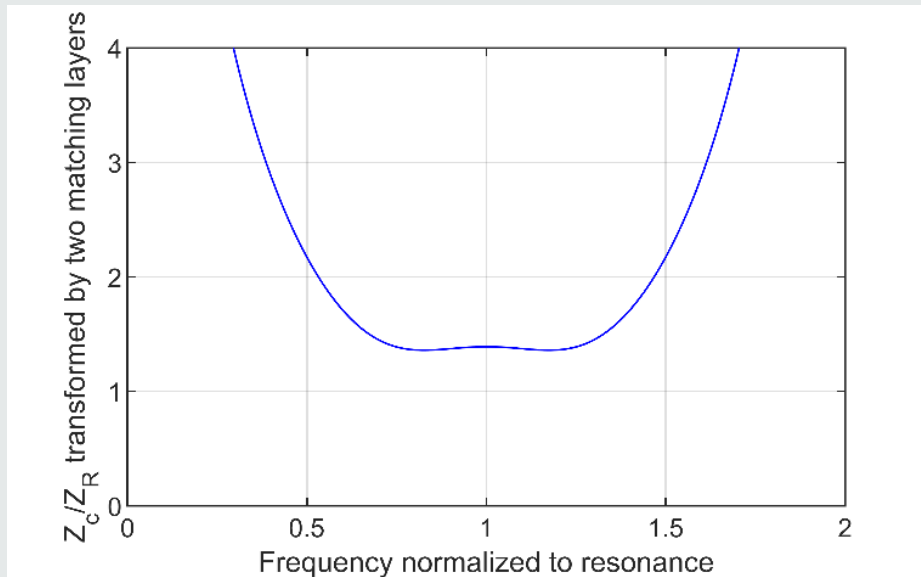


Figure 4-1: Transformed  $Z_c/Z_R$  for two conventional matching layers added to a plate with acoustic impedance 15 MRayl [72].

From Article 3

#### 4.1.2 Method

In Article 1, a hypothetical single crystal piezocomposite plate with  $k = 0.87$ ,  $Z_c = 14$  MRayls, air-backing and two matching layers was considered. Adding a larger number of matching layers would give a larger reduction of  $Z_c/Z_R$  and a wider passband, but it would also increase the fabrication complexity of the following experimental study, described in Article 3.

The following method was used for the optimization part of Article 1:

1. Using the 1D Mason model, the electromechanical transfer function and the tuned electrical power factor were calculated for the case of two conventional matching

layers designed following the guidelines given by DeSilets et al. [72]. Conventional matching layers are optimized for a maximally flat passband.

2. Large ripple was observed in the resulting tuned electrical power factor, and we proposed that this was attributed to the frequency dependence of the matching layers. The incentive for this proposal will become evident in section 4.2, where the performance of the piezocomposite is compared to the performance of a tonpiliz.
3. The matching layer passband can be extended by separating the resonances of the complex system more widely than what is done when optimizing for a maximally flat passband. This can be allowed for applications that do not require a flat band, but rather a selection of narrow-band pulses at a variety of frequencies.

Many underwater applications can utilize information from the transducer far beyond the -3 dB limit, restricted by the dynamic range of the electronics. The actual dynamic range varies between applications. We chose to define a usable frequency for the transducer by its -12 dB frequency band, i.e. where

$$20 \log_{10} \frac{|H(f)|}{|H(f_0)|} \geq -12 \text{ dB}. \quad (23)$$

This limit was chosen to represent the performance of a typical electronic transmit stage. Changing its value would alter some results, but the methods presented in the paper would still be valid. As for the amplitude limit, there also does not exist an exact limit for the electrical power factor. We used a more relaxed criterium than Stansfield, and defined the usable frequency band to the frequencies where

$$PF = \cos \theta > 0.5. \quad (24)$$

This corresponds to an electrical phase  $|\theta| < 60^\circ$ . This is a choice representing the limitations of a typical electronic transmit stage. The value may be changed without invalidating the methods presented in this study.

*From Article 1, slightly adapted*



4. To find the matching layer impedances and thicknesses that give the optimum separation of the resonances under these criteria, a gradient-based numerical algorithm implemented in MATLAB's Global Optimization Toolbox was used. Matching layer impedance and thickness within a set span were sent as input to a Mason model program. For each run, the width of the usable frequency band was calculated using (23) and (24), with  $\theta$  being the phase after tuning the impedance phase to zero at  $f_r$ . The inverse width was minimized by the global optimization algorithm.
5. The resulting usable frequency band for the single crystal piezocomposite transducer was compared to the results for a similar PZT piezocomposite transducer with  $k = 0.69$  and  $Z_c = 15$  MRayls.

### 4.1.3 Results

Calculated transfer function magnitude and tuned power factor are shown in Figure 4-2 for the case of two conventional matching layers, and in Figure 4-3 for the case of two matching layers optimized under the given criteria. The usable frequency bands of Figure 4-3 are  $1.88f_r$  for the single crystal transducer, compared to  $1.21f_r$  for the PZT transducer.

### 4.1.4 Discussion

#### Limited separation of resonances:

Equation (22) establishes a design target of a large usable band for transducers with high coupling coefficients. The equation was derived for the ideal case of frequency independent matching, and the system considered has only one resonance. The complex system of piezocomposite plus matching layers has more than one resonance. For the PZT transducer, large separation of the resonances provides an extension of the usable band compared to the width given by (22). This effect can also be seen for the single crystal transducer, but to a smaller extent. The -12 dB criterium limits the possible separation of the resonances. Hence, increasing  $k$  from 0.69 to 0.87 could not double the usable band. However, the achieved 55 % increase in usable bandwidth is still considerable.

*From Article 1, slightly adapted*

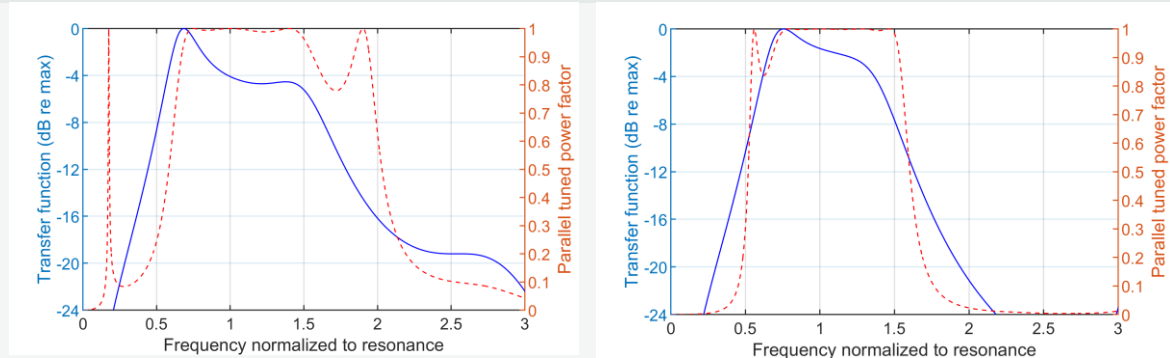


Figure 4-2: Composite with air-backing and two conventional matching layers. The layers have quarter wavelength thicknesses and impedances calculated according to [72]. Blue line: Electromechanical transfer function magnitude. Red line: Electrical power factor after tuning at the resonance frequency using a parallel inductor. Left: Single crystal,  $k = 0.87$ . Right: PZT,  $k = 0.69$ .

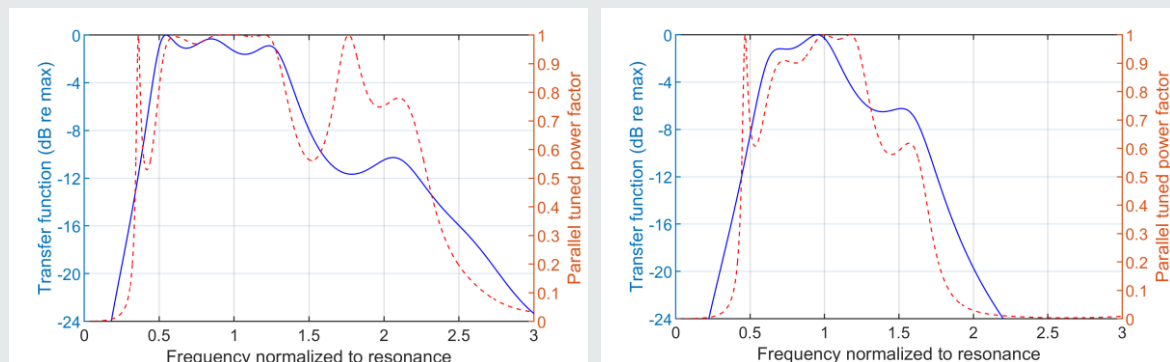


Figure 4-3: Composite with air-backing and two optimized matching layers. The layers have quarter wavelength thicknesses and impedances calculated according to [72]. Blue line: Electromechanical transfer function magnitude. Red line: Electrical power factor after tuning at the resonance frequency using a parallel inductor. Left: Single crystal,  $k = 0.87$ . Right: PZT,  $k = 0.69$ .

From Article 1, slightly adapted

If the transfer function was allowed to vary more than 12 dB, the resonances of the single crystal composite could have been separated further. Note that transducer directivity increases with frequency, causing the far field acoustic source level to decrease less at the high frequency end than what is the case for the transfer function magnitude. However, even if further separation was allowed, ripples in the acoustic matching passband must be balanced against ripples in the power factor passband.

#### Design of matching layers for optimum passband:

As pointed out by Cochran et al. [65], and generally recognized by transducer designers, the conventional quarter-wavelength matching layer thickness is a narrowband property. A quarter wavelength thickness at  $f_r$  will introduce a stopband at  $2f_r$ . Besides, the guidelines given by DeSilets et al. [72] are based on the acoustic impedance for open circuit conditions ( $Z_c$ ), and they are suited for matching at  $f_a$ , or for cases where  $k$  is low and  $f_r \approx f_a$ . For  $k = 0.87$  there is a large difference between  $f_r$  and  $f_a$ , and conventional matching gives a skew transfer function. As a result, the  $-3$  dB bandwidth found from the conventional design of Figure 4-2 is in fact larger for the PZT composite than for the single crystal composite. Use of the short circuit acoustic impedance  $Z_c\sqrt{1 - k^2}$  instead of  $Z_c$  when calculating the matching layer impedances will improve this, but also result in a flatter and narrower passband. The opposite effect is required to ensure decent matching in a wide band, to prevent power factor ripple.

As utilized in Article 1, extension of the passband is possible by separating the resonances of the complex system more widely. This will however reduce the flatness of the passband and increase the pulse length of a pulse spanning the entire band. Short pulse length is required for many medical applications. For many underwater designs, on the other hand, the aim is to ensure versatility by providing a selection of more narrowband pulses at a variety of frequencies. The transducer operator might want to use 300 kHz near the bottom and 200 kHz for deeper waters, while perhaps 700 kHz to achieve high resolution inspection of a particularly interesting object. During marine resource surveys, multifrequency narrowband data are collected and used to identify the genus of the scattered objects. Measurements of acoustic backscatter made over a wide frequency band have the potential for improved classification [73][74].

Restriction of the usable frequency band by relative or absolute amount of reactive power:

For several of the reported naval single crystal applications, the acoustic source level is calculated for a fixed amount of power source Volt-Amperes (apparent power), to illustrate potential savings in the size of the power source. For the case of a fixed amount of apparent power, it makes sense to restrict the *relative* amount of reactive power, thus require a minimum level for the power factor. For a constant voltage source, the *absolute* amount of reactive power is perhaps more relevant. Having restrictions on the power factor rather than electrical susceptance,  $B$ , might be conservative. Still, for some transmit stages it is important to restrict the electrical phase  $\theta$ . Being AC signals, the voltage and current drained from the source varies periodically between maximum and minimum, and the time of maximum instantaneous current relative to the time of maximum instantaneous voltage may impact the performance of amplifier components, dependent on component size and frequency.

One could argue that instead of reducing the power factor ripple at the cost of a larger variation for the transfer function, one could accept the power factor ripple and reduce the voltage whenever the reactive current or electrical phase exceeds critical levels. The exact implications of such a power source design is not considered here, but it will complicate the system and prevent use of wideband single crystal transducers with some existing transceivers.

## 4.2 Tonpilz transducer

Design of single crystal tonpilz transducers was covered in Article 2. The purpose of this article was to answer two sub questions:

1. What does it take to reduce  $Q_m$  to  $Q_{opt}$  in a tonpilz design?
2. The acoustic matching of the tonpilz design is frequency independent. How does this affect the transfer function and power factor, and how does a tonpilz with a standard  $Q_m$  (from approximately 2 and above) perform compared to a piezocomposite plate with matching layers?

### 4.2.1 Theory

To evaluate  $Q_m$  for various tonpilz designs, we used the BVD model for a fixed-end, mass-loaded piezoelectric bar, see Figure 4-4. The fixed-end can be provided by a large tail-to-head mass ratio. The piezoelectric bar has actual mass  $M_c$ . When the length  $l$  of the bar is much smaller than a quarter wavelength,  $l \ll \lambda/4$ , the dynamic mass,  $M_d$ , of the bar is  $M_d = \frac{1}{3}M_c$  (See e.g. Sherman and Butler's book [66], chapter 4.2.2 Effect of the Mass of the Bar). The resonance frequency  $f_r$  and the mechanical quality factor  $Q_m$  will then be:

$$2\pi f_r = \sqrt{\frac{K}{M+M_c/3}} \quad (25)$$

$$Q_m = 2\pi f_r \frac{M+M_c/3}{R} \quad (26)$$

where  $M$  is the mass of the tonpilz head and  $K$  is the stiffness of the bar. For a real load and no loss,  $R$  is equal to the acoustic load impedance  $Z_R$ .

Flexural modes in the head should be placed outside the operating frequency band of the transducer. Expressions for the flexural head modes of a tonpilz can also be found in Sherman and Butler's book (chapter 5.3.1. The Tonpilz Projector [16]). For a square head, the frequency of the lowest flexural head mode is given by:

$$f_f = 1.12 \frac{c_h M}{A^2 \rho_h \sqrt{1-\sigma^2}} \quad (27)$$

where  $c_h$ ,  $\rho_h$  and  $\sigma$  are the speed of sound, the density, and the Poisson ratio of the head material. Increasing head mass  $M$  will increase the frequency of the first flexural head mode.

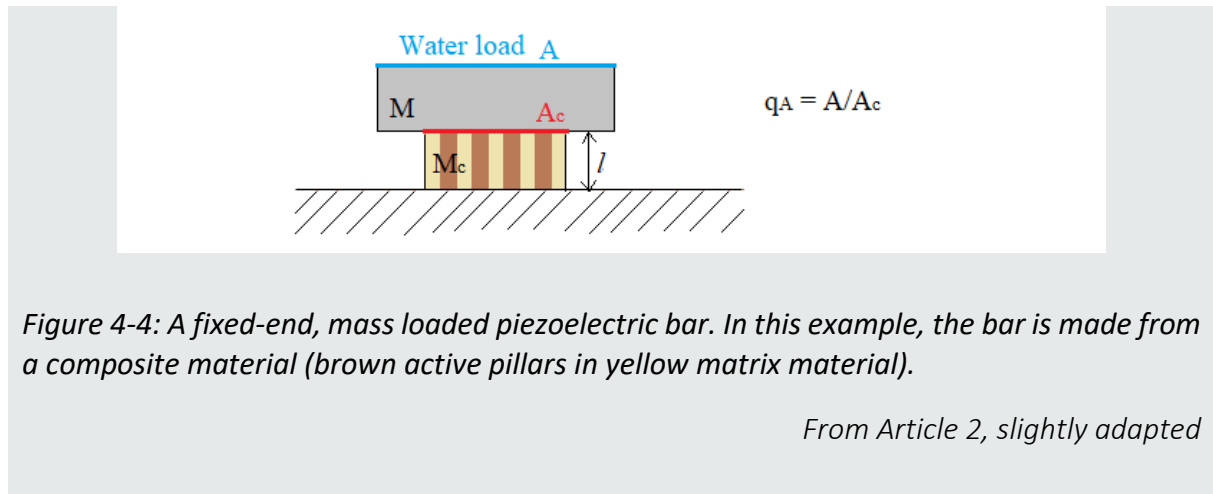


Figure 4-4: A fixed-end, mass loaded piezoelectric bar. In this example, the bar is made from a composite material (brown active pillars in yellow matrix material).

*From Article 2, slightly adapted*

#### 4.2.2 Method, sub question 1: What does it take to reduce $Q_m$ to $Q_{opt}$ ?

Below is a description of three things that was done to simplify the  $Q_m$ -evaluation. A shorter version of this description is included in Article 2.

Equal, effective material parameters in tonpilz and piezocomposite:

We wanted to compare the tonpilz to the piezocomposite of Article 3. The initial model of this piezocomposite gave an effective coupling coefficient of  $k = 0.82$ . The 33 mode requires pillars of a certain aspect ratio. In the piezocomposite of Article 3, these pillars are supported by a hard-set epoxy matrix. The epoxy clamps the pillars and causes a reduction of the coupling coefficient compared to  $k_{33} = 0.9$ . In a tonpilz, the pillars are supported by the head and tail mass, and the epoxy can be omitted. Nevertheless, the effective coupling coefficient of a tonpilz will be reduced by other mechanisms, such as glue and pre-stress bolt [66]. These effects were not included explicitly in our model, but the effective coupling coefficient resulting from them was estimated to approach 0.8, see table 4.2 in Sherman and Butler [66]. For easier comparison, the effective coupling of the piezocomposite and the tonpilz were both set to 0.82. This was obtained by using the effective composite material parameters also for the driving section of the 1D tonpilz model. Effective stiffness is needed to calculate the BVD model

resonance frequency, (25). The effective stiffness<sup>1</sup> was found using  $K = A_c c_{33}^E / l$ , where  $A_c$  is the area of the driving part and  $c_{33}^E$  is the effective stiffness coefficient of the composite material [75]. The composite that the effective material parameters are based on had 40 % volume fraction active material. It is therefore important to remember that the area of single crystal is 40% of  $A_c$ . To visualize this, imagine a tonpilz like the one in [28], where several single crystal pillars are distributed over a given area  $A_c$ . This is also illustrated in Figure 4-4. The yellow matrix of Figure 4-4 can be air, like in [28].

Expressing  $Q_m$  for the tonpilz by  $M$  and area ratio  $q_A = A/A_c$

We wanted to calculate  $Q_m$  for fixed resonance frequency  $f_r$  and head area  $A$ . For the case of no loss and real loading,  $R$  is given by  $\rho_w v_w A$  and thus also fixed. The symbols  $\rho_w$  and  $v_w$  denote the density and the speed of sound for water. By inserting  $K = A_c c_{33}^E / l$  and  $M_c = \rho A_c l$  into (25), we see that for a given  $M$ , there will be a fixed relationship between the length  $l$  and the area  $A_c$  of the driving section:

$$l = \frac{-(2\pi f_r)^2 M + \sqrt{(2\pi f_r)^4 M^2 + 4((2\pi f_r)^2 \rho A_c / 3) A_c c^E}}{2((2\pi f_r)^2 \rho A_c / 3)} \quad (28)$$

The length  $l$  can therefore be eliminated from the expression for the mass  $M_c$ . The bar area  $A_c$  can be given as a fraction of  $A$ ,  $A_c = A/q_A$  see Figure 4-4. The mechanical quality factor  $Q_m$ , (14), will be given by  $M$  and  $q_A$ :

$$Q_m = 2\pi f_r \frac{M + \frac{\rho(A/q_A)(-(2\pi f_r)^2 M + \sqrt{(2\pi f_r)^4 M^2 + 4((2\pi f_r)^2 \rho A_c / 3) A_c c^E})}{6((2\pi f_r)^2 \rho A_c / 3)}}{\rho_w v_w A} \quad (29)$$

Expressing  $M$  by a reference mass  $M_p$ :

A reference mass was introduced to make the calculations independent of resonance frequency. The reference mass  $M_p$  was chosen as the mass of a half-wavelength resonator with area  $A$ , made from the composite material.

---

<sup>1</sup> There is a typo i Article 2,  $c_{33}^D$  should have been  $c_{33}^E$

For  $l > \lambda/4$ , the lumped assumption breaks down. In the real world, head flexure will also impose limitations on the suitable combinations of  $M$  and  $q_A$ . Using (27), the  $c_h/\rho_h$  ratio required to avoid head flexure for different designs was calculated. It was assumed that the frequency  $f_f$  of the first flexural head mode should be larger than  $2f_r$  to avoid interference with the main mode. A Poisson ratio of  $\sigma = 0.3$  was also assumed, as this is an estimate close to the value of most head materials.

#### 4.2.3 Results, sub question 1: What does it take to reduce $Q_m$ to $Q_{opt}$ ?

Mechanical quality factor versus  $q_A$  for various  $M$  is plotted in Figure 4-5. The  $c_h/\rho_h$  ratio required to avoid head flexure is shown in Figure 4-6.

#### 4.2.4 Discussion, sub question 1: What does it take to reduce $Q_m$ to $Q_{opt}$ ?

The optimum  $Q_m$  for  $k = 0.82$  is approximately 0.9, see section 3.2. According to Figure 4-5, this can be achieved by  $M = 0.025M_p$  and  $q_A = 5$ . Among the common head materials, magnesium has the highest velocity to density ratio,  $c_h/\rho_h = 2.8 \text{ m}^4\text{kg/s}$ . According to Figure 4-6, the head width must be smaller than  $0.3\lambda$  to avoid head flexure below  $2f_r$  for a magnesium head with  $M = 0.025M_p$ . Increasing  $Q_m$  from 0.9 to approximately 2 allows the head mass to be increased by a factor 4 for  $q_A = 5$ . Alternatively,  $q_A$  for the case of  $M = 0.025M_p$  can be reduced by almost a factor 3. A  $Q_m \approx 2$  design is much easier to implement, but how does it perform?



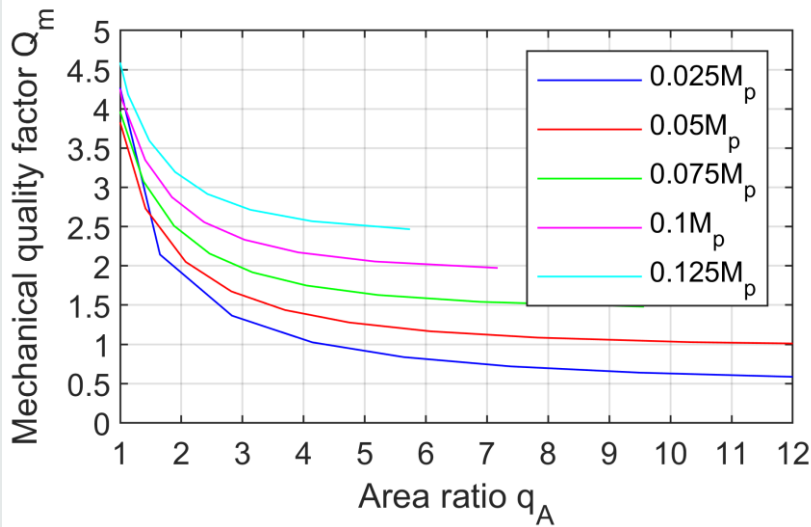


Figure 4-5: Mechanical quality factor versus area ratio  $q_A$  for different head masses. Calculated using (29), for a fixed-end tonpiliz with  $k = 0.82$ , modelled by the lumped BDV model. The masses are given in terms of the reference mass  $M_p$ .

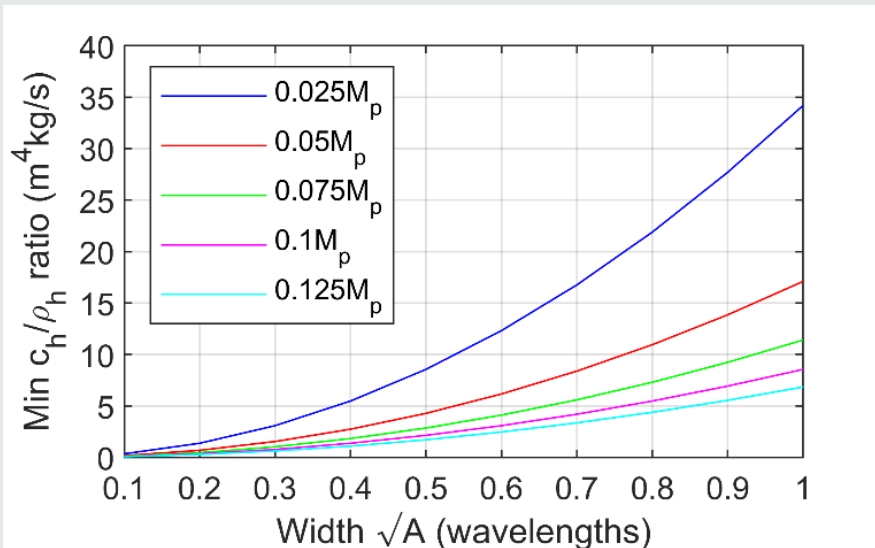


Figure 4-6: The  $c_h/\rho_h$  ratio needed for the first flexural mode of a square head to appear at twice the resonance frequency, plotted versus the width of the head. The width of the square head is equal to the square root of the head area  $A$  and is given in wavelengths of water. A Poisson ratio of  $\sigma = 0.3$  was assumed.

From Article 2, slightly adapted

#### 4.2.5 Method, sub question 2: Comparison of performance

Using a square magnesium head with  $M = 0.075M_p$  and an area ratio of  $q_A = 2.7$ , a tonpizl with  $Q_m \approx 2$  was obtained. Its performance was compared to that of an air-backed piezocomposite plate with two matching layers. The electromechanical transfer function and the parallel tuned electrical power factor for the two designs were calculated using the 1D Mason model. The matching layers added to the piezocomposite were designed following the guidelines given by DeSilets et al., however using the short circuit acoustic impedance instead of the open circuit impedance. The matching layers were not otherwise optimized.

#### 4.2.6 Results, sub question 2: Comparison of performance

Calculated transfer function magnitude and tuned power factor are shown in Figure 4-7.

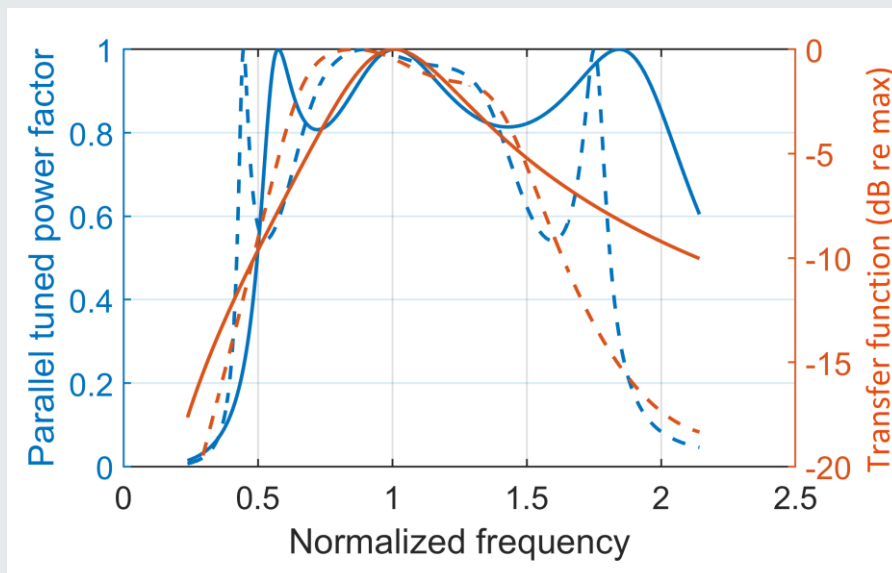


Figure 4-7: Parallel tuned electrical power factor (blue) and electromechanical transfer function (red). Comparison of a tonpizl design with  $k = 0.82$  and  $Q_m \approx 2$  (solid lines) and a design comprised of a composite plate (also  $k = 0.82$ ) and two added matching layers (dashed lines).

*From Article 2, slightly adapted*

#### 4.2.7 Discussion, sub question 2: Comparison of performance

The power factor for the tonpilz design has pronounced ripple, but it stays above 0.8 in a frequency band that is 150 %, relative to the resonance frequency. The piezocomposite has larger power factor ripple.

The distance between the  $-3$  dB points of the transfer function is larger for the piezocomposite than for the tonpilz, but the transfer function of the piezocomposite falls off more rapidly beyond the  $-3$  dB points. Figure 4-7 motivates the proposed extension of the acoustic matching passband for the piezocomposite in Article 1.

Note that even compared to the piezocomposite with optimized matching layers and  $k = 0.87$  of Article 1, the tonpilz with  $k = 0.82$  and  $Q_m \approx 2$  performs well. The tonpilz has a frequency range of approximately  $1.7f_r$  for  $PF > 0.5$  and smaller ripple within the flanks.

### 4.3 Discussion and conclusion

Research question 3 was: *How should a 1-3 piezocomposite transmitter and a tonpilz transmitter be designed to maximize the usable frequency band for underwater applications?*

In Article 1, we optimized two matching layers added to a 1-3 composite plate. The aim was to maximize the usable frequency band, defined by maximum ripple  $-12$  dB for the electromechanical transfer function and maximum ripple 0.5 for the electrical power factor. The resulting widths were  $1.88f_r$  for a single crystal composite with  $k = 0.87$ , compared to  $1.21f_r$  for a PZT composite with  $k = 0.69$ .

The matching layers are frequency dependent, and the degree of matching falls off rapidly outside the passband. To decrease the power factor ripple in the maximum achievable bandwidth, (22), we extended the acoustic matching passband compared to the case of conventional layers optimized for a maximally flat passband. The extension was achieved by separating the resonances of the complex system more widely. This can be allowed for applications where the aim is not to create one pulse spanning the entire band, but rather to ensure versatility by enabling a selection of narrow-band pulses at a variety of frequencies.

The tonpilz design can more accurately than a piezocomposite with matching layers be described by the BVD model that was used to derive the expression for optimum mechanical quality factor. In Article 2, the effective coupling coefficient was  $k = 0.82$ , for which optimum  $Q_m$  is approximately 0.9. Figure 4-5 and Figure 4-6 showed that optimum  $Q_m$  can be challenging to achieve in a practice. However, even for the case of  $Q_m \approx 2$ , the tonpilz design had a better power factor performance than the piezocomposite with two matching layers. The  $Q_m \approx 2$  tonpilz design gave power factor larger than 0.8 in a frequency band that was 150 %, relative to the resonance frequency, close to the value predicted by (22). The frequency independent acoustic matching inherent in the tonpilz design is beneficial for low power factor ripple in high  $k$  designs.

It is worth noting that the tonpilz had a large tail to mass ratio, while the piezocomposite had air backing. A clamped back end or high attenuation in an acoustically matched backing would reduce  $Q_m$  for the piezocomposite plate.

To decrease the  $Q_m$  of the tonpilz design below 2, the head flexing should be addressed. Disturbance from the first flexural resonance of the tonpilz head could be prevented by distributing the crystal bars evenly over the head area, see [28], or by tapering the head. This would allow a lighter head and thus a smaller  $Q_m$ . The curves of Figure 4-6 are calculated for square heads. For circular heads, the frequency of the first flexural mode is higher than for square heads [16], but square heads were chosen as they provide an array packing factor close to 1 and thus a large radiation resistance.

In this chapter, a tonpilz and a piezocomposite plate were considered. As reported in [13], the segmented cylinder is another interesting design for wideband single crystal transducers. Expressions for the effective coupling coefficient,  $k$ , and the mechanical quality factor,  $Q_m$ , of the segmented cylinder are found in Sherman and Butler [76]. For this design, an effective  $k$  close to the material  $k_{33}$  can be achieved, and a low  $Q_m$  is provided by a large difference between the water loaded area and the cross-sectional area between each segment.

The effective  $k$  of the PZT composites considered in Articles 1 and 3 are based on the soft PZT5H1. This PZT has  $k_{33} = 0.72$ . Single crystals, particularly the Mn-doped crystals of generation III, have lower internal mechanical loss than soft PZT. The single crystals therefore deserve to

be compared also to hard PZT, with  $k_{33}$  in the range 0.6 to 0.65.

## 5 Compactness of selected underwater designs

This chapter aims at answering the research question “How is the compactness of a 1-3 piezocomposite transmitter and a tonpilz transmitter affected by use of single crystals?”

Two factors that impact the compactness of the transmitter were considered:

1. Acoustic power provided at given input voltage (because transformer size is important for the total compactness).
2. The height of the transducer element (in the direction of sound).

### 5.1 Piezocomposite

This section deals with the compactness of piezocomposites, which was investigated in Article 4. Section 5.2 deals with the compactness of tonpilzes.

#### 5.1.1 Theory

For the length extensional 33 mode, the height required for a free piezoelectric bar to resonate at a given frequency is inversely proportional to the compliance. This can be seen from the Mason model in Figure 1-1, where the anti-resonance frequency,  $f_a$ , is inversely proportional to  $\sqrt{s_{33}^D}$ . For a material with high electromechanical coupling, there is a large difference between the compliance for open and short circuit conditions. The resonance frequency,  $f_r$ , is inversely proportional to  $\sqrt{s_{33}^E}$  for a lumped, quasi-static model. We see from Table II that some single crystals have  $s_{33}^E$  values that are approximately 2.5 times larger than those of the PZT materials, yielding an estimated 40 % reduction in height. Note that the single crystal materials and the PZT materials have approximately the same density.

Strain per electric field for a length extensional 33 mode bar is given by the piezoelectric constant  $d_{33}$ . Transmitted acoustic power per electric field is proportional to squared transducer face velocity.

The piezocomposites presented in Articles 1, 2 and 3 utilize the 33 mode of piezoelectric bars embedded in a polymer matrix. Single crystals do however provide high coupling not only in the longitudinally poled 33 mode, but also in the transversely poled length extensional mode.

High transverse coupling can be achieved when the crystals are poled along the [011] crystal direction, see Chapter 7. The resulting macroscopic symmetry gives  $k_{31} \neq k_{32}$ , and the highest transversely poled length extensional coupling occurs for the 32 mode [11][77]. For the 32 mode, the main extension is in the 2-direction, normal to the electric field which is in the 3-direction, see Figure 5-1. In this mode, the main resonance frequency is determined by the length in the 2-direction, rather than by the distance between the electrodes. For a given voltage, this enables an increase of the electric field by a decrease of the electrode spacing.

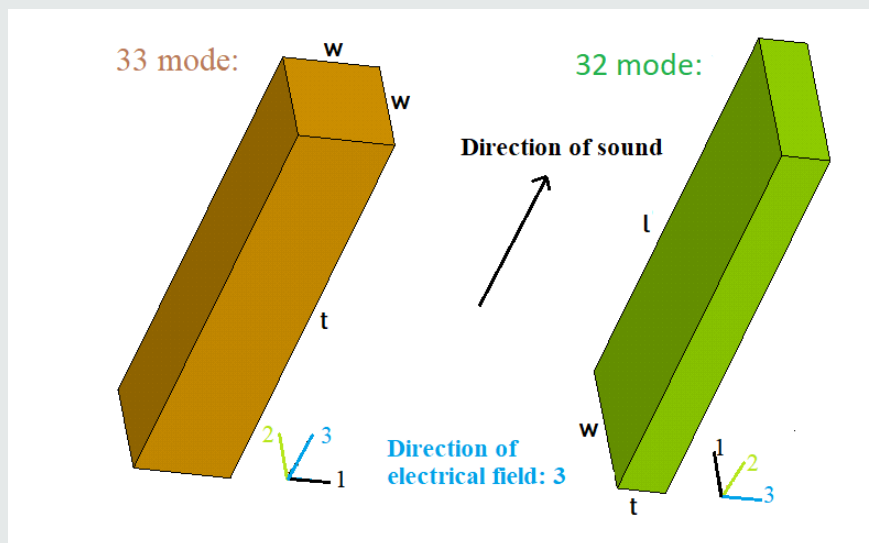


Figure 5-1: Geometry of 33 mode bar (left) and 32 mode block (right).

From Article 4, slightly adapted

For the 32 mode, the resonance frequency,  $f_r$ , is inversely proportional to  $\sqrt{s_{22}^E}$ , and the strain per electric field is given by  $d_{32}$ . Note from Table II that the [011] poled 24%PIN-PMN-PT has a  $s_{22}^E$  that is approximately four times higher than the  $s_{33}^E$  of PZT, and a  $d_{32}$  that is 2.6 times higher than the  $d_{33}$  of pz21.

### 5.1.2 Method

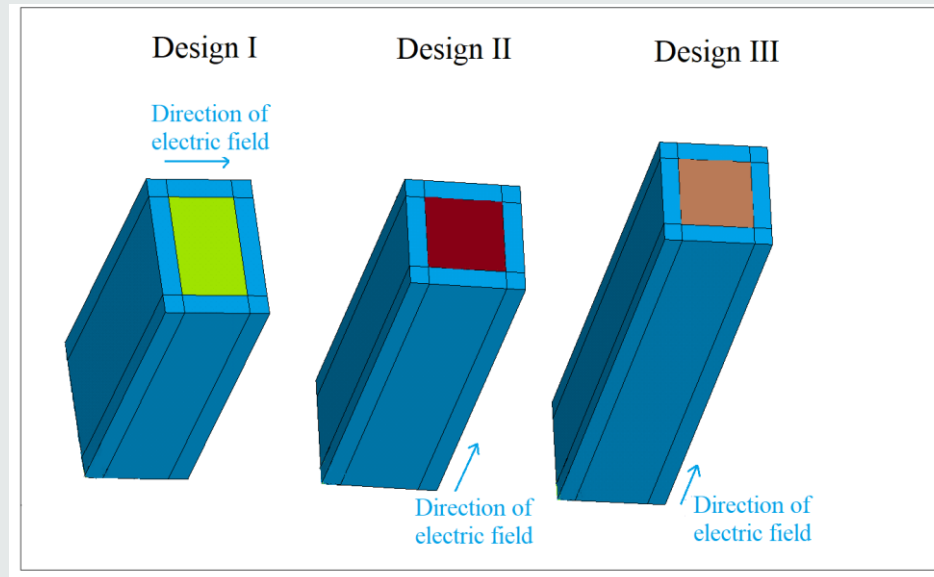
In Article 4, to account for dynamic effects and the influence of the polymer matrix, the compactness of piezocomposites was investigated using FEM models rather than the simple analytic relations presented in section 5.1.1. The composite height required for a given resonance frequency was calculated using FEM, and so was the acoustic power transmitted from water loaded composite at a given voltage. The main purpose of Article 4 was to investigate a piezocomposite that utilizes the 32 mode. However, through comparison to conventional piezocomposites, the article also provides information on the compactness of piezocomposites that utilize the 33 mode.

The designs compared in part A of Article 4 are presented in Figure 5-2. All the designs are piezocomposite plates with 1-3 connectivity, volume fraction active material 45 % and resonance frequency approximately 270 kHz. Design I is the 32 mode design, while Design II and Design III are conventional piezocomposites that utilizes the 33 mode of the embedded pillars. Design I and Design II both have single crystal 24%PIN-PMN-PT as the active material, poled along the [011] crystal axis for Design I and along the [001] crystal axis for Design II. Design III has PZT5H1 as the active material. Material parameters are found in Article 4. PZT5H1 is the same type of ceramics as pz21 from Table II, but from a different supplier. Transmitted acoustic power for the three designs was calculated, adding air backing and water load to unit cell FEM models with periodic boundary conditions. By using periodic boundary conditions, we exclude any vibration modes or reactive radiation impedance that are due to limited outer lateral dimensions.

The resonator length  $l$  for the 32 mode blocks was 2.5 mm, and the distance  $t$  between the electrodes was set to 0.5 mm for Design I. Although aiming for a small  $t$  for a large electric field, a moderate  $l/t$  aspect ratio was desirable for mechanical stability.

The width  $w$  of the 32 mode blocks determines the resonance frequency of the other transversely poled length extensional mode, the 31 mode. For the power comparisons in part A, the aspect ratio  $l/w$  of Design I was set to 3, to prevent the 31 mode from interfering with the 32 mode and thereby reduce the effective coupling coefficient of the main resonance.



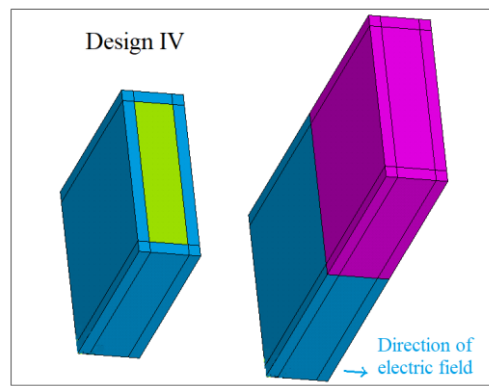


	Design I	Design II	Design III
Mode	32	33	33
Active material	[011]-poled PIN24%	[001]-poled PIN24%	PZT5H1
Active material type	Single crystal	Single crystal	PZT
Young's module $E$ , passive material (GPa)	1	1	1
$l$ (mm)	2.5		
$w$ (mm)	0.83	0.64	0.64
$t$ (mm)	0.5	3.4	4.9
Aspect ratio $l/w$	3		
Aspect ratio $l/t$	5		
Aspect ratio $w/t$	1.7	1/5.3	1/7.6
Kerf width (mm)	0.3	0.3	0.3

Figure 5-2: Unit cells of the piezocomposite designs of part A. Active materials in a matrix of polymer kerf filler (blue). The active parts are, from left to right: 32 mode single crystal (green), 33 mode single crystal (dark brown), and 33 mode PZT (light brown).

From Article 4, slightly adapted

The 31-type extension can however be used to add an extra, usable, frequency band to a 32 mode transducer. For a fourth design presented in part B of the article, the aspect ratio  $l/w$  was decreased compared to Design I, to obtain a transducer with two closely located usable frequency bands. The aspect ratio was set to  $l/w = 1.25$ , as a compromise to achieve a high effective coupling in the 32 mode and a low resonance frequency for the 31 mode. This design was called Design IV and is shown in Figure 5-3. In Article 4, the extra mode is denoted Mode 2 rather than the 31 mode, as the chosen aspect ratio is not compatible with pure 31 mode vibration. A full transducer based on Design IV was modelled, adding one acoustic matching layer to the composite. Design IV was adapted to fabrication, and fabrication of the composite is reported in Chapter 6.



Design IV	
Active material	[011]-poled PIN24%
Active material type	Single crystal
Young's module $E$ , passive material (GPa)	1
$l$ (mm)	2.44
$w$ (mm)	1.94
$t$ (mm)	0.5
Aspect ratio $l/w$	1.25
Aspect ratio $l/t$	5
Aspect ratio $w/t$	4
Kerf width in direction 1 (mm)	0.41
Kerf width in direction 3 (mm)	0.6
Volume fraction active material	39%
Matching layer impedance $Z_{ml}$ (MRayl)	3
Matching layer thickness (mm)	2.4

Figure 5-3: Design IV. Left: Piezocomposite unit cell with 32 mode single crystal (green) and polymer kerf filer (blue). Right: The unit cell with acoustic matching layer added (pink).

From Article 4, slightly adapted

### 5.1.3 Results

Comparison of the FEM modelled Design I, Design II, and Design III revealed the following:

1. Acoustic power at given voltage: Design I (32 mode single crystal,  $t = 0.5$  mm) provided more than twenty times more power than Design II (33 mode single crystal) and almost fifty times more power than Design III (33 mode PZT5H1), see Figure 5-4.
2. Height of transducer element: The composite of Design I (32 mode single crystal) was 26 % lower than the composite of Design II (33 mode single crystal) and 49 % lower than the composite of Design III (33 mode PZTH1), see Figure 5-2.

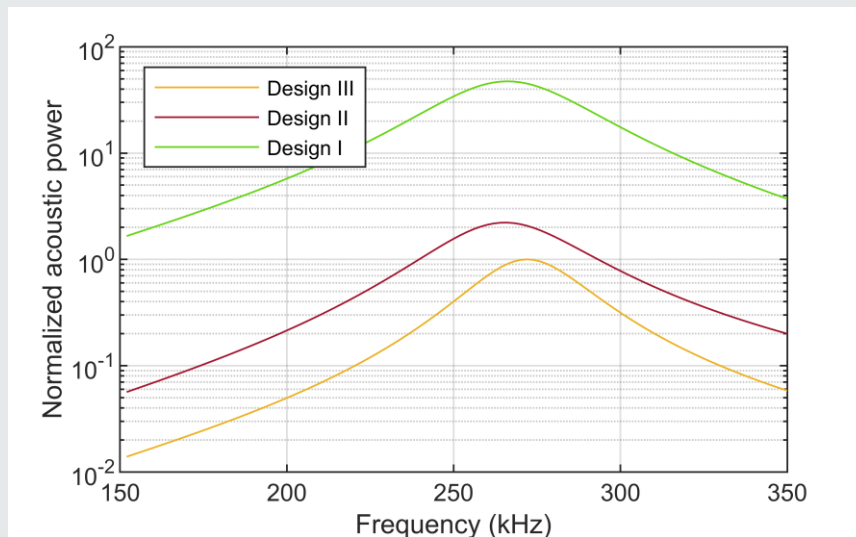


*Figure 5-4: Normalized acoustic power per area, calculated for water loaded composite, using FEM model with periodic boundary conditions.*

For Design I, the effective coupling coefficient of the composite was calculated to 0.85. For Design IV, the calculated effective coupling coefficient of the 32 mode was reduced to 0.78. The reason for choosing Design IV rather than the Design I for fabrication, was the potential for making a transducer that can be operated over a wide frequency range. The modelled wideband performance can be seen in Figure 5-5 and Figure 5-6. These figures show electrical impedance and acoustic power, calculated after adding one matching layer to the Design IV

composite. The frequency band centred around 260 kHz is due to the 32 mode resonance. The matching layer has  $\lambda/4$  thickness at 260 kHz. Mode 2, caused by extension in the 1-direction, is located close to 500 kHz.

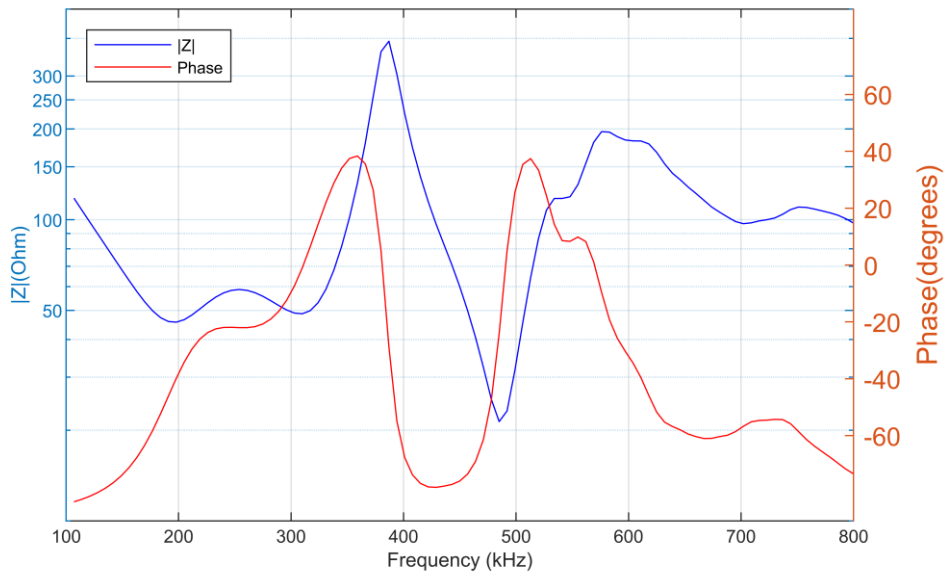


*Figure 5-5: Electrical impedance, magnitude and phase, calculated for Design IV transducer. The composite had air backing, one matching layer and water load. The impedance was calculated using FEM model with periodic boundary conditions. The magnitude per unit cell was divided by 36 to represent the fabricated composite. The fabricated composite is presented in Chapter 6. It consisted of  $4 \times 9 = 36$  parallel connected active blocks.*

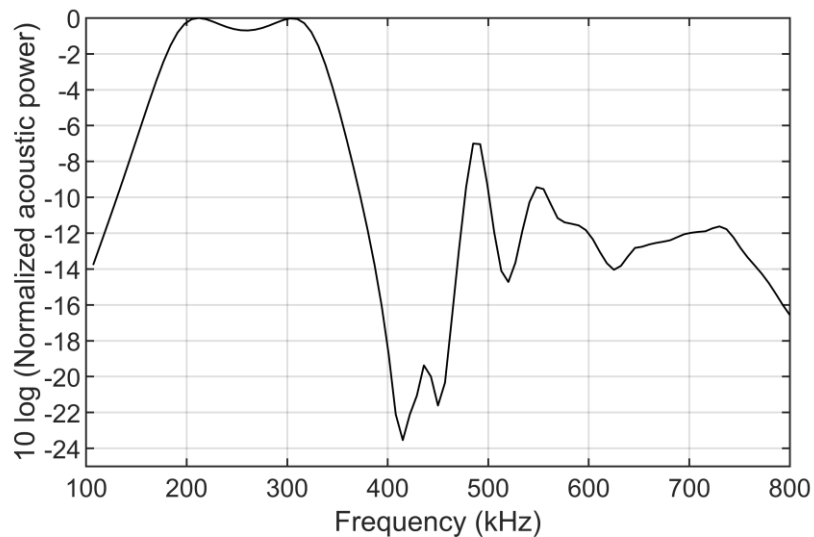


Figure 5-6: Normalized acoustic power, calculated for the Design IV transducer. The composite had air backing, one matching layer and water load. The acoustic power was calculated using FEM model with periodic boundary conditions.

From Article 4

#### 5.1.4 Discussion

A simple investigation of how use of single crystals impacts the compactness of the transducer was performed by comparing Design I, Design II and Design III. The reduction in composite height, see Figure 5-2, and the increase of acoustic power at given voltage, see Figure 5-4, were quantified. The reduction of height gives an obvious contribution to compactness. Increase of acoustic power at given voltage will also contribute to compactness. When a lower voltage is required to obtain a given acoustic power, insulation distances can be decreased, and voltage transformers can be reduced in size or even eliminated. A smaller composite height and a smaller transformer enable a smaller transducer housing and a decrease of total weight.

The investigation of Design IV adds a more complicated aspect to the question of compactness. The properties of single crystals enable alternative designs that can contribute significantly to total system compactness, exemplified in Design IV through the combination of alternative modes and wide bandwidths. Evaluation of the usable frequency bands of Design IV would

thematically belong to Chapter 4, but Design IV was included in the present chapter to show a complex, compact design.

In the 1D analysis of Chapter 4, a usable bandwidth was defined by both the -12 dB points of the electromechanical transfer function and by reactive electrical power below 50 %. Similar criteria were used in Article 4. However, the -12 dB points of the electromechanical transfer function was replaced by the -12 dB points of the acoustic power, calculated using the acoustic elements of the FEM program. In Chapter 4 and Article 1, the reactive electrical power for a single crystal transducer was compared to the reactive electrical power for a PZT transducer. This comparison was made easier by tuning the electrical impedance phase to zero at the resonance frequency, as is often done in practical applications. As there was no comparison of electrical power to other transducers in Article 4, and as the electrical phase was already zero at 300 kHz, close to the centre of the first frequency band, we omitted the complication of a tuning inductor for this compact design. The reactive power restriction of  $PF > 0.5$ , equivalent to phase between  $-60^\circ$  and  $+60^\circ$ , was set for untuned transducer. From Figure 5-6 and Figure 5-5, the resulting usable frequency bands are found to be 175-380 kHz, 475-500 kHz and 535-600 kHz. It is however noted in the article that the upper band partly originates from a third, spurious mode. This mode has far from piston-like displacement, see displacement plot in the article.

The impedance was calculated for a unit cell with periodic boundary conditions. The fabricated composite, see Chapter 6, was made from 4x9 active blocks. This gives an aperture of 9.9x9.4 mm<sup>2</sup>, which is approximately 2.3x2.2 wavelengths of water at the lowest usable frequency 175 kHz. For this aperture size, there is only a small deviation in radiation reactance introduced by the periodic boundary conditions [78].

The impedance magnitude for 4x9 parallel connected blocks varies between 20 and 300 Ohm within the bands that were defined as usable, see Figure 5-5. Only applications that can handle this range can make use of the full bands. This impedance range can normally be handled without need for an impedance transformer. Reducing  $t$  below 0.5 mm would decrease the impedance further, which would further reduce the voltage required for a given

power. Note however, that at some point, a further reduction of impedance will be undesired, due to electrical matching and increased current.

An ideal design might try to merge the bands of the 32 mode and of Mode 2 into one. This might be achieved by increasing the bandwidth of the first band beyond 380 kHz, by adding more than one acoustic matching layer to the front, or by optimizing the matching layer thickness differently, e. g. as done in Articles 1 and 3. However, the FEM modelling revealed that there is a frequency between the 32 mode and Mode 2 at which the blocks show flexural vibration with almost no sound transmission in the 2-direction. This flexural motion creates a stop band, making it very difficult to create one continuous band using this transducer design.

*From Article 4, slightly adapted*

It is not straight forward to quantify the benefit in terms of compactness that Design IV provide. In addition to the small composite height and the low voltage needed, the design provides the advantage of enabling transmission at 175 kHz and 500 kHz from the same transducer.

Several practical issues must also be taken into account when evaluating the benefit of using single crystals for a given application. In Article 4, the single crystal material 24%PIN-PMN-PT was compared to PZT5H1, which has a  $d_{33}$  that is doubled compared to hard PZT materials, see Table II. Hard materials are used for applications that require low loss or pressure resilience. Single crystals offer higher  $Q_m$  values than soft PZT. Mn-doped PIN-PMN-PT can provide  $Q_m$  above 500 [22], but at the expense of a decrease in  $d_{33}$ . The  $Q_m$  of [011]-poled 24%PIN-PMN-PT is 300-400 [79], which can justify a comparison to hard PZT for applications that require low loss. However, single crystals experience stress induced phase transitions. This was demonstrated for [011]-poled 24%PIN-PMN-PT by Carka et al. [80]. Phase transitions cause variation of material parameters, as explained in Chapter 7. An additional thing that must be considered for a given transducer design, is how much the single crystal can expand before it breaks or degrades.

## 5.2 Tonpiliz

The compactness of the tonpiliz design was treated only indirectly, in Article 2. The work presented in Article 2 was discussed in Chapter 4. We found that to approach the low optimum  $Q_m$  for the high coupling single crystal materials, a light tonpiliz head is required. One way of making the tonpiliz head lighter, is by reducing the height of the head.

The fixed back-end is obtained by a large tail to head mass ratio [16]. A lighter head enables a lighter tail, and thereby the possibility of a smaller tail height.

As seen in section 5.1, the compliance of the single crystals impacts the height of the active material for a given resonance frequency. High compliance in high coupling alternative modes, like the 32 mode, has been utilized for tonpiliz designs, see the state of the art report in Chapter 2. The largest compliance coefficient value is found for  $s_{66}^E$ . Values as large as  $190 \cdot 10^{-12} \text{ m}^2/\text{N}$  are available [36]. The face shear 36 mode transducer developed by Van Tol et al. [37][38] had resonance frequency 2 kHz and a total depth of only 2.5 inches (6.4 cm).

In Article 2, treating a 33 mode tonpiliz design, head masses and frequencies were normalized. Table IV was not part of the submitted work but is included here to make the benefits in terms of compactness easier to visualize. The table shows heights and weights for various 33 mode tonpiliz designs with  $f_r = 50 \text{ kHz}$ , fixed back-end and square magnesium head.

*Table IV: Heights and weights for tonpiliz designs with various  $Q_m$ , see theory section 4.2.1.*

Active material	pz26	pz26	pz26	PIN24	PIN24	PIN24
$Q_m$	4.6	3.5	2.3	2.2	1.4	1
Area ratio $q_A$	2.3	3.1	4.7	3.3	5.1	7.3
Height, active material	10 mm	10 mm	10 mm	6 mm	6 mm	6 mm
Height, head	6.2 mm	4.7 mm	3 mm	3.2 mm	2 mm	1.4 mm
Weight, head	2.7 g	1.9 g	1.2 g	1.3 g	0.8 g	0.6 g
Area $(\lambda/2)^2$						



### 5.3 Conclusion

The research question of chapter 4 was “How is the compactness of a 1-3 piezocomposite transmitter and a tonpilz transmitter affected by use of single crystals?” Quantitative investigations of compactness were performed for the piezocomposite design, through FEM modelling. The active materials single crystal 24%PIN-PMN-PT and polycrystalline PZT5H1 were compared. For a conventional 1-3 piezocomposite, utilizing the 33 mode, the acoustic power at a given voltage was approximately doubled for the single crystal material versus the PZT material. The composite height was reduced by 30 %. Required voltage is important for compactness because of transformer size.

When poled along the [011] crystal direction, the single crystal material provides high electromechanical coupling also in the 32 mode. By utilizing this mode in a 1-3 piezocomposite, the acoustic power at a given voltage was increased by almost a factor fifty compared to the conventional 33 mode PZT design. The composite height was reduced by 49 %. These calculations were based on a 32 mode design with aspects ratios  $l/w = 3$  and  $l/t = 5$ , where  $l$  is the resonator length,  $w$  the width and  $t$  the distance between the electrodes.

An additional benefit of the 32 mode design is the opportunity to obtain an extra, usable frequency band by utilizing a mode akin to the 31 mode. A transducer platform can be more compact if relevant information, at various frequencies, can be collected by a smaller number of different transducers.

In addition to reduction of resonator length, reduction of required voltage, and possible increase of the usable frequency range, the desire for a low  $Q_m$ , and thus a light head, will impact the compactness of tonpilz transmitters.

A smaller element height and a smaller transformer enable a smaller transducer housing and a decrease of total weight.

## 6 Performance of fabricated piezocomposites

As stated by the thesis title, the purpose of the Ph.D. project was to investigate the impact of single crystal properties on underwater transducer designs. The properties considered in chapters 3, 4 and 5 were the electromechanical, piezoelectrical and elastic properties from the datasheets, measured at low field and room temperature. The impact of these properties on the usable frequency band and on the compactness of underwater transmitters was modelled in the submitted articles and discussed in the previous chapters. Chapters 6, 7 and 8 however, are dedicated to practical considerations, divided into the following topics:

- Chapter 6: Performance of fabricated single crystal piezocomposites. Is the modelled performance possible to obtain in practice? The method presented in Article 1 was investigated experimentally in Article 3, and Article 4 includes impedance measurements for a fabricated 32 mode piezocomposite. The piezocomposites were fabricated by Kongsberg personnel using Kongsberg facilities, and the practical achievements should not be attributed to the Ph.D. project. The measurements and the evaluation of the results do however belong to the project and are presented here in Chapter 6.
- Chapter 7: Changes in properties due to temperature, stress, or electrical field. Experimental investigation of such changes was not performed during the Ph.D. project, but the topic was investigated through a literature study, presented in Chapter 7.
- Chapter 8: State of the art for textured ceramics. Disadvantages of the single crystals include the temperature, stress, and field stability discussed in Chapter 7, low fracture toughness, and the fact that the crystals are expensive and time-consuming to grow. Textured polycrystalline ceramics can potentially provide almost as high coupling as the single crystals, possibly with fewer practical limitations. The state of the art for textured ceramics was investigated through a literature study which is summarized in Chapter 8.

Two different types of single crystal 1-3 piezocomposites were fabricated and evaluated during the Ph.D. project. The conventional type, utilizing pillars vibrating in the 33 mode, is presented in section 6.1. The other type, utilizing blocks vibrating in the 32 mode, is presented in section 6.2.

## 6.1 The 33 mode piezocomposite

An experimental follow-up of Article 1 was reported in Article 3. The aim was to demonstrate experimentally that a wide frequency band with power factor larger than 0.5 could be obtained by separating the system resonances more widely than for the case of a maximally flat acoustic matching layer passband. Two 1-3 piezocomposite transducers were fabricated, measured, and compared. The transducers had  $f_r \approx 500$  kHz. One of the composites had active material single crystal PMN-28%PT, while the reference composite had active material polycrystalline ceramic PZT5H1. Two matching layers were added to each composite. The matching layers were optimized using the approach described in Article 1. The composites were air-backed. Electrical impedance measurements and a pulse-echo measurement were reported in Article 3. Transducer schematics are shown in Figure 6-1.

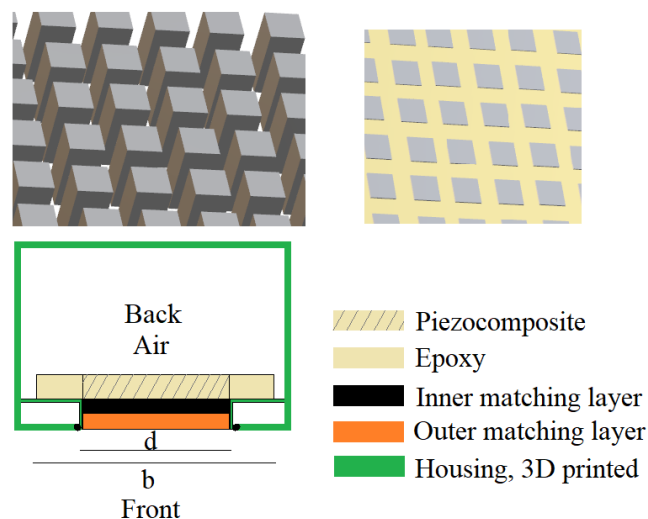


Figure 6-1: Schematical transducer design, Article 3.

There are two important outcomes of the investigations of Article 3:

1. The electromechanical coupling coefficient of the fabricated single crystal composite was in good agreement with modelling.
2. The electrical power factor of the fabricated single crystal transducer was in good agreement with modelling.

The results that these conclusions are based on are presented below, together with a summary of the design choices made for the single crystal composite.

### 6.1.1 Design choice: Composite materials

PMN-28%PT (CTS Corporation, Lisle, IL, USA ) was used as the active material for the single crystal composite. Material data reported by Kim et al. [81] was used for the modelling, because these data provided a better fit for the measured resonance frequency than the data provided by the supplier. PMN-28%PT is a generation I single crystal, and not suited for use under high field, temperature, or mechanical stress. It is however cheaper than generation II and III materials, and therefore better suited for trial-and-error prototyping. PZT5H1 is among the polycrystalline materials with highest  $k_{33}$  and was therefore chosen as the active material of the reference composite.

Epotek 301-2 (Epoxy Technology, Inc., Billerica, MA, USA) was chosen as the passive composite material because it is a well-established filler with minimal shrinkage and excellent structural stability.

Material data are given in Article 3.

### 6.1.2 Design choice: Pillar aspect ratio

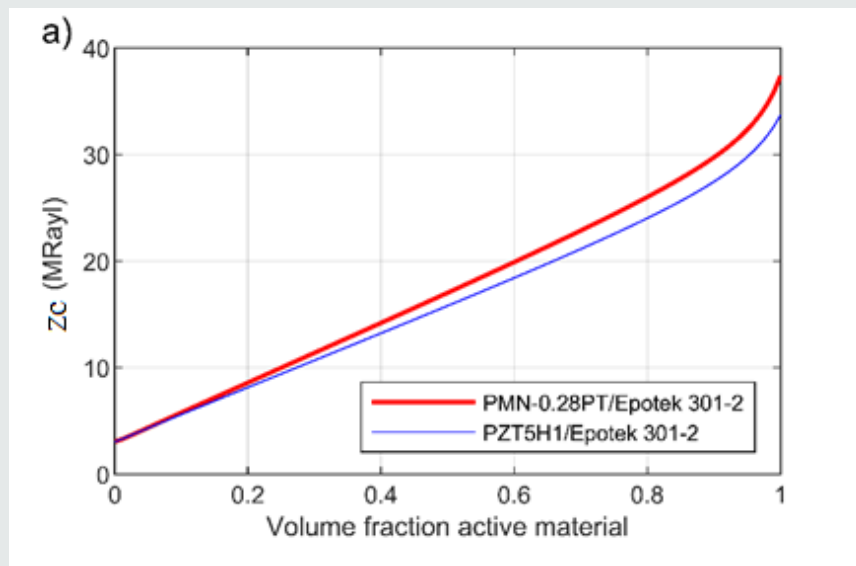
Fabrication methods for PZT composites in the underwater frequency range are well established. The single crystals have however lower fracture toughness and are more easily depoled than PZT. Would the existing fabrication methods degrade the performance of the single crystals? The single crystal material supplier (CTS Corporation, Lisle, IL, USA) does not recommend pillar aspect ratio above 3, as they consider the benefits of a larger aspect ratio to

be small compared to the increasing fabrication challenges. Hence, the thickness-to-width aspect ratio was set to 3 for the single crystal pillars, and this constituted the starting point for the composite design. The PZT pillars had aspect ratio 3.8, see Article 3.

### 6.1.3 Design choice: Volume fraction active material

Volume fraction active material was set to 0.4, based on the following calculations:

Effective composite parameters were calculated using the 1D model reported by Smith and Auld [75]. The effective parameters vary with volume fraction active material. Effective characteristic acoustic impedance and effective electromechanical coupling coefficient are shown in Figure 6-2. Due to clamping from the hard-set Epotek 301-2, the effective coupling coefficient is reduced compared to the  $k_{33}$  of the active materials.



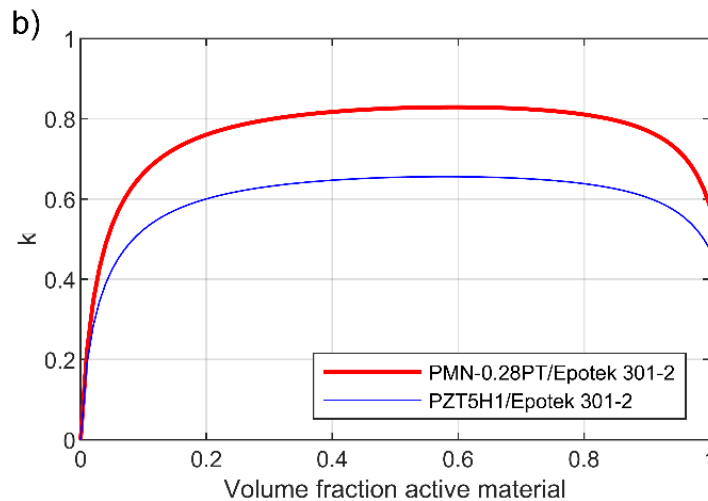


Figure 6-2: Effective composite parameters versus volume fraction active material, for PMN-0.28PT/Epotek 301-2 (red line) and PZT5H1/Epotek 301-2 (blue line). a) Characteristic acoustic impedance. b) Electromechanical coupling coefficient. Calculated using the model reported by Smith and Auld [75].

As explained in Chapter 3, a small mechanical quality factor  $Q_m$  is needed to minimize the power factor ripple. To minimize  $Q_m$ , (14), the composites should have minimum  $Z_c$  and maximum  $k$ . Matching layers can reduce the ratio  $Z_c/Z_R$  in (14), by increasing the  $Z_R$  that is seen from the composite. Two added conventional matching layers reduce the ratio to  $(Z_c/Z_R)^{(1/7)}$  at the design frequency. The  $Q_m$  resulting from inserting  $(Z_c/Z_R)^{1/7}$  and using the results from Figure 6-2 in (14) is shown in Figure 6-3.

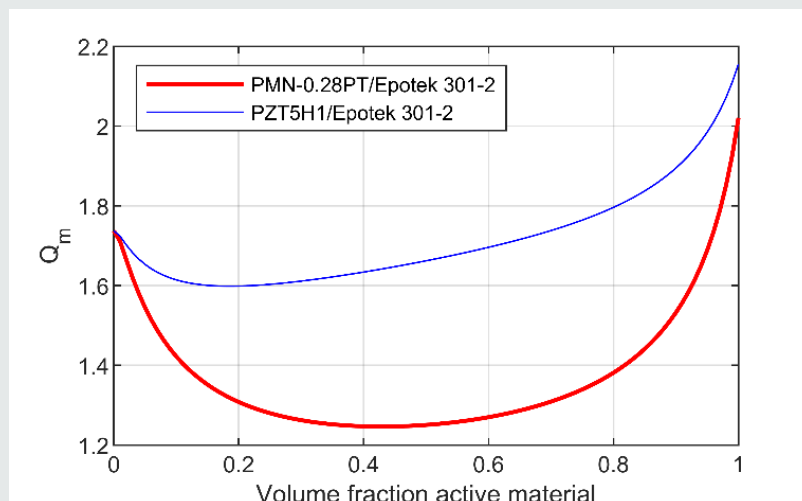


Figure 6-3:  $Q_m$  versus volume fraction, for acoustic load impedance 1.5 MRayl.

From Article 3, slightly adapted

Figure 6-4 shows electrical impedance for composites with volume fraction active material equal to 0.3 and 0.4. The impedance was calculated using a 3D FEM model with periodic boundary conditions and no loading. For volume fraction 0.3, a spurious mode interferes with the anti-resonance frequency of the single crystal composite. For volume fraction 0.4, on the other hand, the first spurious mode is moved to  $2.3f_r$ , which is outside of the maximum bandwidth that can be calculated from (21). The distance between the resonance frequency and the anti-resonance frequency is also increased compared to the case of volume fraction 0.3. The effective coupling coefficient can be calculated from this distance, and at volume fraction 0.4 it was calculated to  $k = 0.83$  for the single crystal composite and  $k = 0.64$  for the PZT composite. These numbers are in reasonable agreement with the 1D model of Figure 6-2, for which the coupling coefficients are 0.817 and 0.646. From this we can assume that at volume fraction 0.4, the coupling is neither reduced by low pillar aspect ratio, nor by interference from spurious modes. A lower volume fraction could have been used for the PZT composite. However, at volume fraction 0.4,  $Q_m$  for the PZT composite is 2 % higher than the minimum value at volume fraction 0.2. This increase in  $Q_m$  was considered negligible, and volume fraction 0.4 was used for both composites.

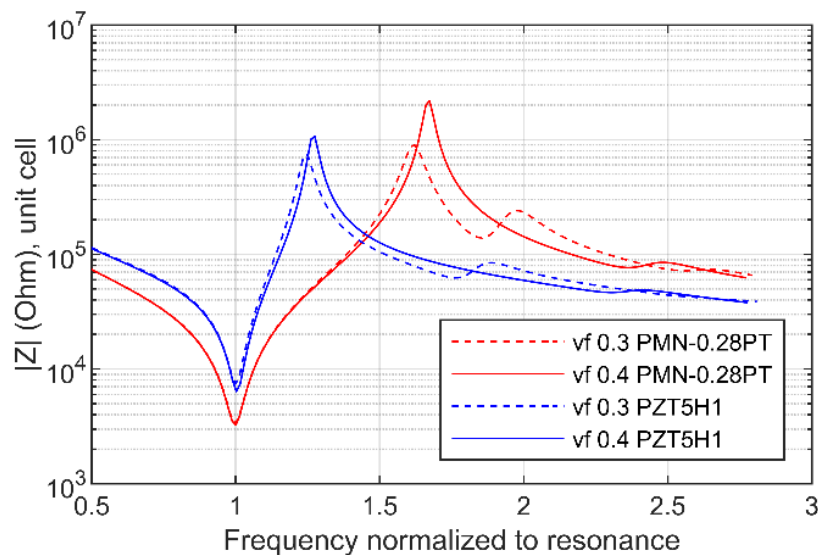
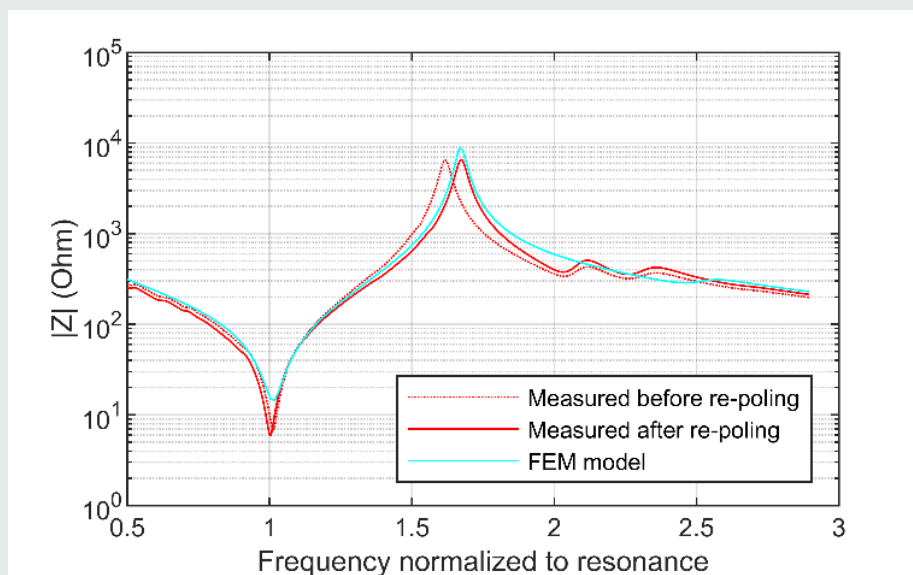


Figure 6-4: Electrical impedance magnitude  $|Z|$  for different volume fractions (vf) active material. The frequency is normalized to  $f_r$ . The impedance is calculated using a 3D FEM model with periodic boundary conditions and no loading.

#### 6.1.4 Result: Measured electrical impedance for the single crystal composite

Measured electrical impedance for the fabricated single crystal composite is shown in Figure 6-5. The impedance was measured in air, before and after re-poling. The frequency axis was normalized to the resonance frequency, 518 kHz. The effective coupling coefficient calculated from the final measurements was 0.83, in agreement with the modelling.



*Figure 6-5: Electrical impedance for the single crystal composite. The frequency is normalized to the resonance frequency 518 kHz. Dotted red line: Measured before re-poling. Solid red line: Measured after re-poling. Cyan line: 3D FEM model, fitted material parameters, see Article 3.*

*From Article 3, slightly adapted*

Figure 6-5 includes a FEM modelled curve for which the material parameters of PMN-28%PT were fitted to match the impedance measurements. The fitted parameters deviated less than 10% from material data reported by Kim et al. [81]. Note that this was a simplified fitting, focused on the main resonance, using one adjustment factor per parameter matrix. The fitted data are listed in Article 3. Complete parameter matrixes could not be measured for the single crystal plates before dicing of the pillars, but the permittivity  $\epsilon_{33}^T$  measured for the plates was



10% higher than the permittivity used for the fitted curve of Figure 6-5. This may indicate that the single crystals were to some extent affected by the fabrication, even if a degradation was not reflected in the measured coupling coefficient.

The effective coupling coefficient of the PZT composite was measured to 0.64, also in agreement with modelling. The PZT composite had resonance frequency 550 kHz. For measurements of the PZT composite, see Article 3.

### 6.1.5 Design choice: Use of FEM model for optimization of matching layers

During optimization of the matching layers for the single crystal composite, deviations between 1D Mason modelling and FEM modelling were discovered. As described in Article 3, Epotek 301-2 was chosen for the outer matching layer and a mix of tungsten and epoxy was chosen for the inner matching layer. 1D modelled and FEM modelled electrical conductance for the single crystal composite with inner matching layer is plotted in Figure 6-6. The figure shows a single resonance around  $1.6f_r$  for the 1D model, but two interfering resonances around  $1.5f_r$  for the FEM model. The effective composite material parameters used for the 1D model was calculated using the model suggested by Smith and Auld [75]. Smith and Auld stated that “A composite can be treated as a homogenous medium with effective material parameters so long as the rod size and spacing are sufficiently fine compared with all relevant wavelengths”. The transverse wavelength of the inner matching layer was approximately 850 m/s. Dictated by the low aspect ratio of 3, the composite periodicity was 1.1 mm. This periodicity corresponds to one transverse wavelength at 775 kHz, or  $1.5f_r$ . The dashed curve of Figure 6-6 shows FEM calculated conductance for a much finer periodicity, 0.275 mm, confirming that the Smith and Auld model is a good approximation for fine-pitched composites.

The lesson learned from the observed deviations in Figure 6-6 is that even if a maximum pillar aspect ratio of 3 does not affect the achievable coupling coefficient, it does put some limitations on possible transducer designs.

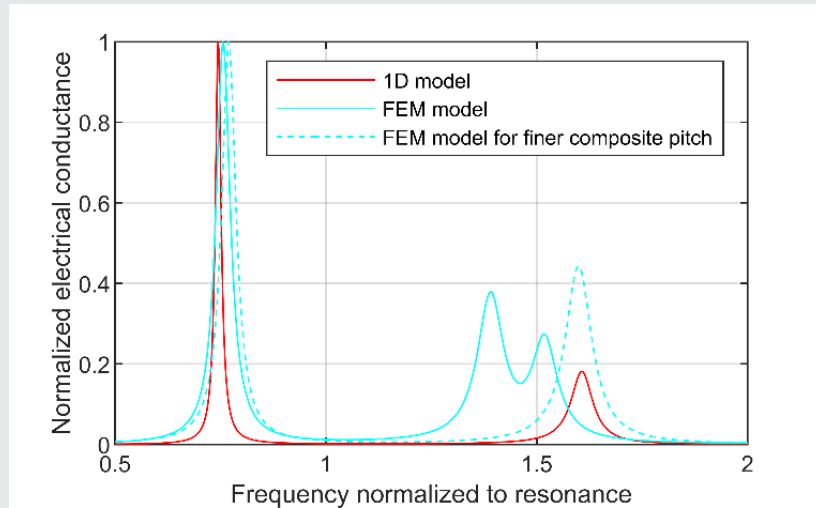


Figure 6-6: Single crystal composite with inner matching layer, air loaded.

From Article 3

The aim for the transducer design presented in Article 3 was to maximize the width of the frequency band with  $PF > 0.5$ . Due to the observed deviation from homogenous medium behavior, the optimum thicknesses of the two matching layers were found using the FEM model rather than the 1D model. In contrast to Article 1, a requirement for the electromechanical transfer function was not included in the optimization.

### 6.1.6 Results: Measurements of final transducers

Matching layers with the optimum design resulting from the FEM modelling were added to the fabricated composites. The electrical impedance was measured with water load at the front, using an Agilent 42941A impedance analyzer (Keysight Technologies, Santa Rosa, CA, USA). The tuned power factor was calculated from the electrical impedance phase, by theoretically adding a parallel inductor that tuned the phase to zero at the resonance frequency. For both composites, the measurements agreed very well with the FEM modelled results. This can be seen in Figure 6-7 and Figure 6-8. The width of the band with  $PF > 0.5$  was  $1.15f_s$  for the PZT transducer, compared to  $1.75f_s$  for the single crystal transducer. Referred to the centre

frequency instead of the resonance frequency, the widths are 114 % for PZT and 132% for single crystal.

Unnormalized, the usable frequency bands constitute 244 kHz – 1148 kHz for the single crystal transducer and 257 kHz – 865 kHz for the PZT transducer.

Following the approach of Article 1, the separation of the resonances was increased to widen the matching layer passband. This was allowed because we were not looking for one pulse spanning the entire band, and we could therefore accept more than the conventional -3dB ripple for the acoustic power. The resulting electrical conductance varies approximately 12 dB within the power factor bandwidths. For a constant voltage source, real electrical power is proportional to the electrical conductance. Acoustic power, however, is dependent also on the electroacoustic efficiency. Transmitting voltage response, TVR, [17] calculated from a pulse-echo measurement is shown in Figure 6-9. To perform the pulse-echo measurement, the transducer was mounted in a waterproof housing and submerged, and this was done only for the single crystal transducer. The efficiency was calculated from the pulse-echo measurement, using an estimate for the directivity index, see Article 4. The efficiency is shown in Figure 6-10.

The general offset in efficiency compared to the FEM model might be due to an inaccurate estimate of directivity. More concerning is the low measured efficiency for frequencies near  $2f_s$ . The resonance here is apparently less effective than modelled, causing a decrease in transmitting voltage response of 16 dB at  $2.2f_s$  compared to the value near resonance. The efficiency also decreases more rapidly below  $0.7f_s$  than expected. Even when there is no need for less than 3 dB TVR variation in the usable band, 20 dB variation will probably exceed the dynamic range of many applications.

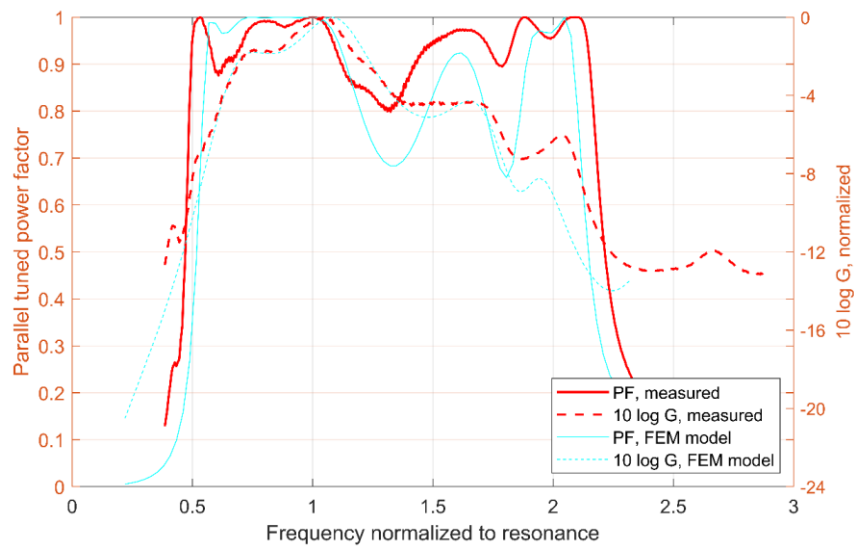


Figure 6-7: Single crystal composite with two matching layers. Red: Measured: Cyan: 3D FEM model. Solid: Parallel tuned power factor, calculated from electrical impedance phase. Dashed: Electrical conductance.

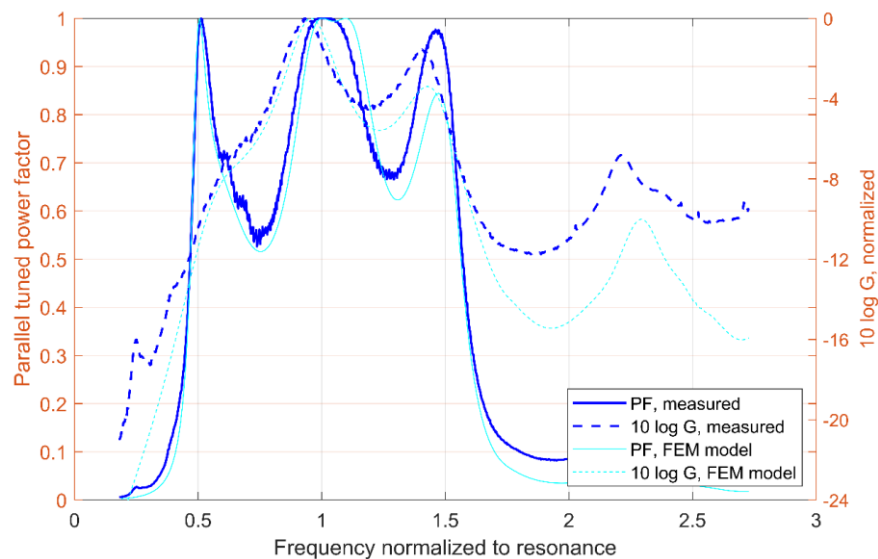


Figure 6-8: PZT composite with two matching layers. Blue: Measured. Cyan: 3D FEM model. Solid: Parallel tuned power factor, calculated from electrical impedance phase. Dashed: Electrical conductance.

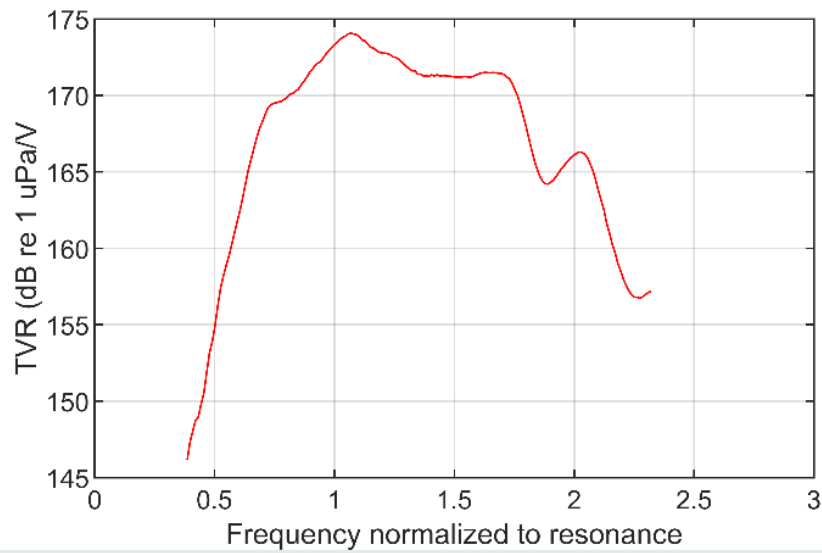


Figure 6-9: Transmitting voltage response, TVR, for the single crystal transducer. Calculated from the pulse-echo measurements.

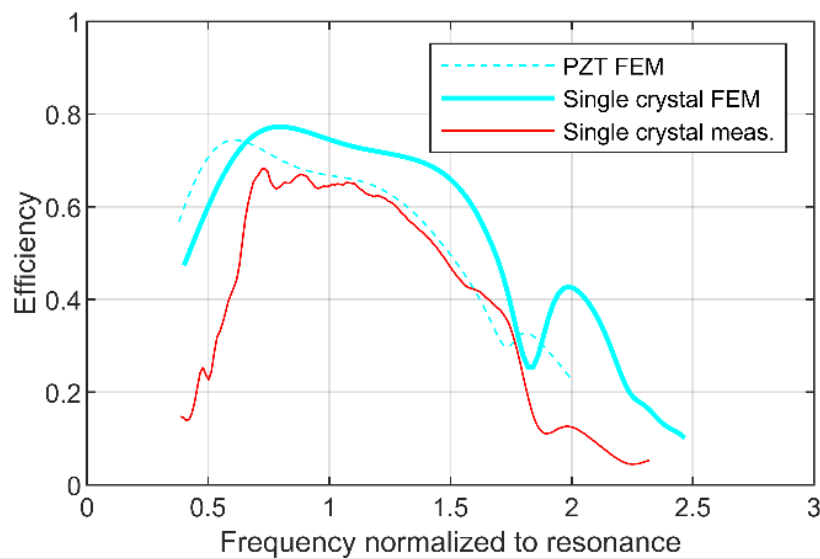


Figure 6-10: Electroacoustic efficiency. Cyan lines: calculated using the FEM model. Thick cyan line: Single crystal composite. Thin, dashed cyan line: PZT composite. Red line: efficiency for the single crystal composite, estimated from the pulse-echo measurements using reciprocity and estimated directivity index.

From Article 3, slightly adapted

### 6.1.7 Conclusion:

The fabricated single crystal composite with  $f_r = 518$  kHz had effective  $k$  close to the modelled value, which was  $k = 0.83$  for a volume fraction of 40% PMN-28%PT in a matrix of Epotek 301-2. The method of Article 1 was used in practice, to obtain tuned power factor larger than 0.5 in a band of width  $1.75f_r$ .

## 6.2 The 32 mode 1-3 piezocomposite

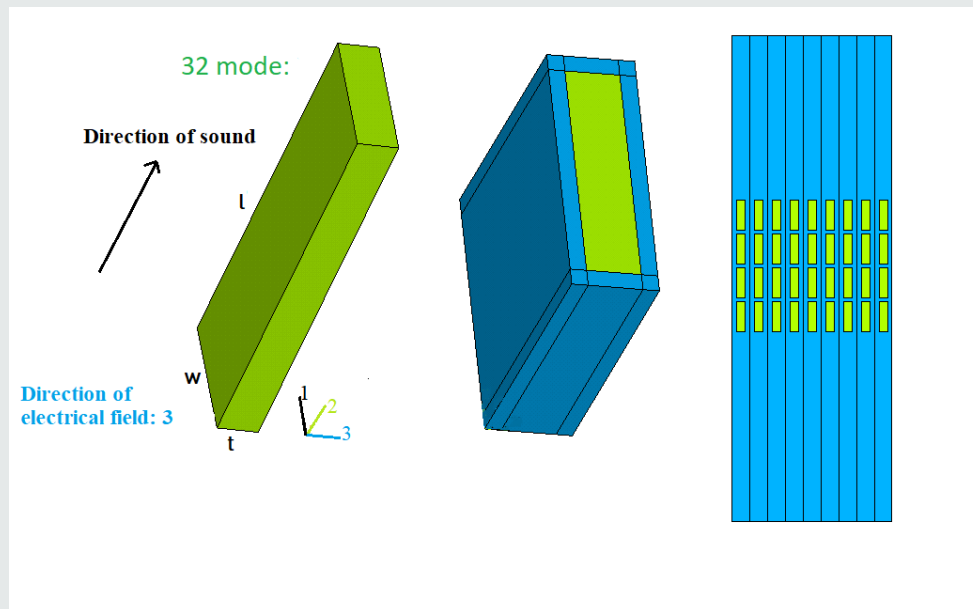
As described in Chapter 5, Article 4 treats the design of 32 mode 1-3 piezocomposites.

In the 32 mode, the main resonance frequency is determined by the length in the 2-direction, rather than by the distance between the electrodes. For a given voltage, this enables an increase of the electric field by a decrease of the electrode spacing. The aim of the design presented in Article 4 was to make use of this advantage in combination with the high  $k_{32}$  and  $d_{32}$  of [011] poled single crystal, to make an underwater transducer that provides large strain per voltage over a wide frequency band.

*From Article 4, slightly adapted*

To investigate the practical challenges of the 32 mode 1-3 piezocomposite design, a prototype composite was fabricated. Design IV from Article 4 was chosen for the fabrication. Design IV utilizes a mode akin to the 31 mode to add an extra, usable frequency band to the 32 mode composite. The electrical impedance of a fabricated composite was measured in air and compared to the FEM modelled impedance.

The fabricated composite consisted of 4 x 10 single crystal blocks. The electrical connection to one column of 4 blocks was lost during fabrication. This left 4x9 active blocks, as illustrated in Figure 6-11. The active aperture was 9.4x9.9 mm<sup>2</sup>, but excess polymer was left outside the active area on two sides, making the total width 40 mm in the 1-direction. Measured and modelled electrical impedance for the composite are shown in Figure 6-12. The measurements were performed using the Agilent 42941A impedance analyzer.



	Design IV
Active material	[011]-poled 24%PIN-PMN-PT
Active material type	Single crystal
Young's modulus $E$ , passive material (GPa)	1
$l$ (mm)	2.44
$w$ (mm)	1.94
$t$ (mm)	0.5
Aspect ratio $l/w$	1.25
Aspect ratio $l/t$	5
Aspect ratio $w/t$	4
Kerf width in direction 1 (mm)	0.41
Kerf width in direction 3 (mm)	0.6
Volume fraction active material	39%

Figure 6-11: Design, fabricated composite. Left: Single crystal block. Centre: Composite unit cell. Green: [011]-poled 24%PIN-PMN-PT single crystal. Blue: Polymer. Right: Assembly of 4x9 active blocks.

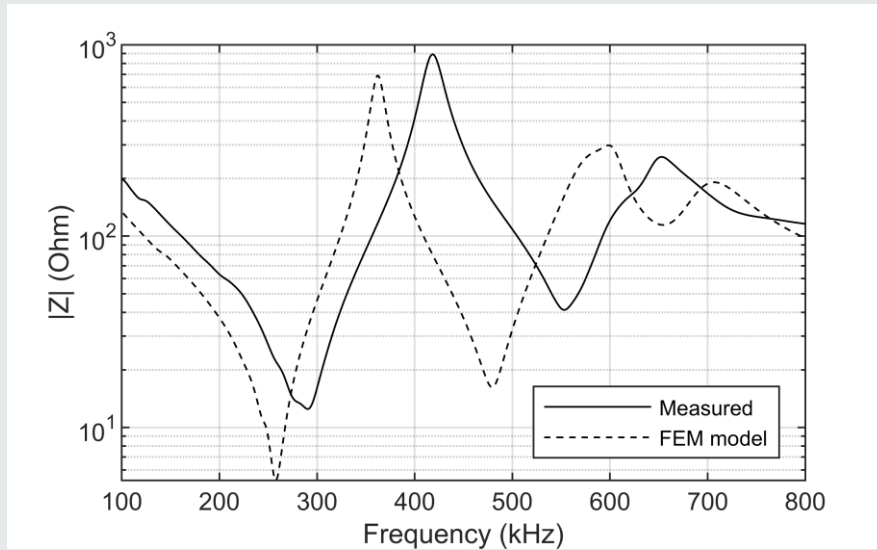


*Figure 6-12: Electrical impedance for the composite of Design IV, all  $4 \times 9 = 36$  blocks parallel connected, no matching layer and no acoustic loading. Solid line: Measured for fabricated composite. Dashed line: Calculated using FEM.*

*From Article 4, slightly adapted*

For the FEM model, the 32 mode resonance is located at 258 kHz. The second resonance is located at 482 kHz. In Article 4, this mode was called Mode 2, as the aspect ratio is not compatible with a pure 31 mode.

The structure of the measured impedance spectrum was well captured by the FEM model. However, there are some important quantitative differences. The fabricated composite showed 15 % increased resonance frequency, a higher impedance magnitude, and slightly wider peaks than the predictions from the FEM model. The widened peaks may be caused by underestimation of losses or by variation between the 36 piezoelectric blocks connected in parallel inside the composite. The increased impedance, most notable at low frequencies, can be explained by a reduced permittivity compared to the values provided in the data sheet. This agrees with the measured free capacitance of the blocks being approximately 15 % lower than estimated from the data sheet permittivity value, and the measured free



capacitance for the final composite being reduced by another 15 %. Likewise, the shift in resonance frequencies may be explained by deviations of actual material parameters from the nominal data sheet values. Slight tweaking of the material values used as input to the FEM model could have been done to match the calculated spectrum to the measured spectrum. However, it was decided not to do this, and rather present results calculated directly from data sheet values.

*From Article 4*

Calculated effective coupling coefficient for the 32 mode was 0.78 for the FEM model and 0.8 for the fabricated composite. However, as noted in section 6.1, depoling may have occurred even if it is not reflected in the effective coupling coefficient.

The increased resonance frequency of Mode2 causes interference with the third mode near 600 kHz. Adjusting the length  $l$  of the blocks for the next prototype could possibly prevent this interference.

### 6.2.1 Conclusion

A 1-3 composite with a high coupling 32 mode and a closely located additional mode akin to the 31 mode was successfully fabricated. Measured free capacitance is lower than modelled, and the measured impedance shows that the resonance is wider than expected from FEM calculations. One explanation for the widening is variation between the 36 piezoelectric blocks connected in parallel inside the composite, and this will cause a reduction of peak acoustic power compared to modelling.

## **7 Literature study: Changes in properties due to temperature, stress, or electric field**

The conclusions of Chapters 3, 4 and 5 were that single crystals provide significant increase of the usable frequency band and significant increase of acoustic power at a given voltage. The theory section of Chapter 3 showed that an increase in the electromechanical coupling coefficient,  $k$ , from 0.7 to 0.9 can double the maximum bandwidth. The modelled Design IV presented in Chapter 5 showed that a nearly tripled piezoelectric constant,  $d$ , and use of the high coupling 32 mode can multiply the acoustic power at given voltage by almost fifty. The fabricated composites in Chapter 6 were shown to have electromechanical coupling coefficients close to the modelled values. The fabricated composites were however measured at low signal, room temperature and no external stress. The next logical step is to investigate how the performance is affected by temperature, stress, and electric field. A literature study on this topic is presented below. Experimental investigations are left for future work.

Single crystals have been extensively tested for use in naval applications. In the abstract of one of the articles from the Naval Undersea Warfare Center, Ewart et al. [6] states that “Compared to lead zirconate titanate (PZT) ceramics, the large electromechanical coupling factor provides significant increases in transducer bandwidth. The superior strain energy density generates higher source level across the band, and the lower Young’s modulus allows considerably smaller transducers. These payoffs occur even when PMNT crystals are subject to navy operating conditions such as uniaxial mechanical compressive stresses up to 42 MPa, electric fields up to 1.2 MV/m, and a temperature range from 5 to 50 °C.” The compressive stress can be due to prestress, which is common for the tonpilz design, or due to water depth. Pressure at 1000 m water depth is equivalent to 10 MPa.

For quantitative ocean science, it is crucial that the material parameters not only provide payoffs, but also provide stability over the relevant range of operational conditions. Phase transitions can cause significant changes in the material parameters of single crystals, and to understand the behavior versus temperature, stress, and electric field, it is important to have knowledge of these transitions.

## 7.1 Theory, phase transitions

An introduction to phase transitions can be found in the book *Lead-free piezoelectrics*, edited by S. Priya and S. Nahm [5],[82]-[85], and this book constitutes the basis for the theory in this section. Useful definitions for the summary are given in Table V.

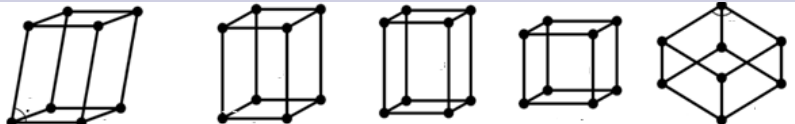
An approximate sketch of the phase diagram for PZT is shown at the left-hand side of Figure 7-1. PZT is produced by high temperature sintering. Each grain of the ceramic is a crystal, and as the temperature cools through the Curie temperature,  $T_C \approx 325^\circ\text{C}$ , there is a structural transition from the non-ferroelectric cubic state, C, to a ferroelectric state. The ferroelectric state is tetragonal, T, or rhombohedral, R, depending on composition. The boundary that marks transition in phase due to change in composition is called a morphotropic phase boundary (MPB). Sandwiched between the R and T phases is a monoclinic, M, phase, acting as a structural bridge between R and T. This bridging phase is the key to high piezoelectric properties. The increased number of thermodynamically equivalent states near MPB can substantially enhance the alignment of randomly oriented ferroelectric domains, allowing optimum polarization under an applied electrical field [83]. The direction of the polarization vector is [001] in T and [111] in R, while the monoclinic symmetry allows the polarization vector to continuously rotate in a plane and contributes to enhanced polarization and strain [5].

The polycrystalline ceramic lead magnesium niobate-lead titanate PMN-PT ( $\text{Pb}(\text{Mg}_{1/3}\text{Nb}_{2/3})\text{O}_3\text{-PbTiO}_3$ ) is also ferroelectric, of the relaxor type. MPB compositions of PMN-PT have properties comparable to soft PZT5H at room temperature [86]. An approximate sketch of the phase diagram for PMN-PT is shown to the right in Figure 7-1. The T-C transition happens at approximately  $325^\circ\text{C}$  for PZT, while at approximately  $125^\circ\text{C}$  for PMN-PT. Note also that for a PZT with 46% Ti-content, a R-T (via M) transition happens at a temperature of approximately  $225^\circ\text{C}$ , while for PMN-0.3PT this transition happens at a temperature of only approximately  $80^\circ\text{C}$ . The R-T transition is ferroelectric-ferroelectric. It does not depolarize the material, but a change in lattice parameters brings about possible changes in material properties.

Polycrystalline PZT has been the dominating piezoelectric material for several decades. However, at the end of the last century, ultrahigh piezoelectricity was discovered for single

crystal PMN-PT near the MPB. The ultrahigh properties appeared when rhombohedral single crystal was poled along a nonspontaneous  $\langle 001 \rangle$  direction. Similar behavior was found also for single crystal lead zinc niobate-lead titanate PZN-PT ( $\text{Pb}(\text{Zn}_{1/3}\text{Nb}_{2/3})\text{O}_3\text{-PbTiO}_3$ ). Single crystal PMN-PT and PZN-PT provide  $k_{33}$  up to 0.94 and  $d_{33}$  up to 2500 pC/N [5]. Single crystal PZT is more difficult to grow, and provide smaller improvements,  $d_{33} \approx 1200$  and  $k_{33} \approx 0.8$  [92].

Table V: Definitions, material theory

Term	Definition
Ferroelectric	Spontaneous polarization that can be reversed by an electrical field [87]. PZT and PMN-PT are ferroelectric materials.
Relaxor	Ferroelectric materials having a high permittivity value over a broad temperature range, and strong frequency dispersion in the dielectric response [88]. PMN-PT is a relaxor.
Coercive field, $E_c$	The negative external electrical field (opposite the direction of polarization) at which the direction of polarization switches [89]
Curie temperature, $T_c$	The material loses its piezoelectric properties above this temperature.
Crystalline solids	The atoms or groups of atoms of the solid are arranged in a regular order (crystal lattice), as opposed to amorphous solids. The crystalline solids can be further divided into single crystalline and polycrystalline solids [90]
Single crystalline solid	The regular order extends over the entire crystal. [90]
Polycrystalline solid	Contains many small single crystalline regions surrounded by grain boundaries. Includes most metals, rocks, ceramics [90].
Lattice systems [91]	 <p>Monoclinic Orthorhombic Tetragonal Cubic Rhombohedral</p>
Crystallographic notation	Coordinates in square brackets, [100], denote a direction vector. Coordinates in angle brackets, $\langle 100 \rangle$ , denote a family of directions. In the cubic crystal system, $\langle 100 \rangle$ would mean [100],[010] and [001]. Coordinates in parenthesis, (100), denote a plane.

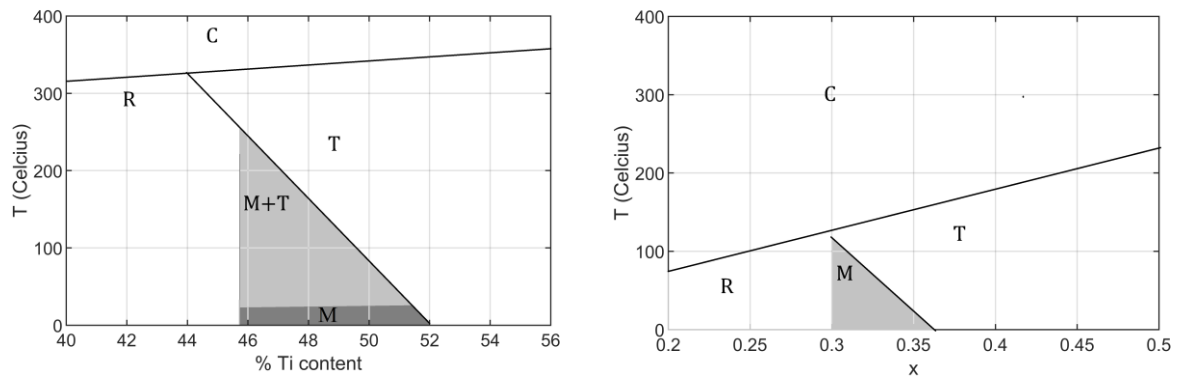


*Figure 7-1; Approximate sketch of phase diagrams. Left: PZT. Right: PMN-PT. For accurate diagrams, see [5].*

The origin of the ultrahigh properties of the relaxor-PT single crystals is a complex topic. There exists both a polarization rotation theory and an adaptive phase model. The polarization rotation theory is an extension of the one mentioned for PZT, saying that the enhanced piezoelectric properties near MPB are a result of enhanced polarizability, arising from the coupling between equivalent energy states, allowing optimum domain reorientation during poling. The spontaneous polarization of the R phase lies in one of the eight possible  $\langle 111 \rangle$  directions. When an electric field in excess of the coercive field  $E_c$  is applied in the [001] direction ([001]-poling), the spontaneous polarization will reorient such that four of the eight possible  $\langle 111 \rangle$  crystal variants are present [93]. Under operation, an electric field applied to the poled crystal in the [001]-direction makes the polar direction incline closer to [001] in each domain, causing a monoclinic distortion. This is illustrated in Figure 7-2. The four equivalent domains have the same energy state and hence low driving force for domain wall movement, resulting in a stable domain state. The exploitation of single crystal orientation to produce a stable domain configuration is termed “domain engineering” [86].

To summarize the adaptive phase model, McLaughlin et al. [26] chose the following wording: “MPB compositions of PMN-PT systems are in a multiphase state. Co-existence of R, M, T and also O (orthorhombic) phases affects electromechanical properties and result in complex phase behavior”. Studies have revealed significant changes in single crystal material parameters due to ferroelectric-ferroelectric phase transitions [93]. As explained above, phase transitions can

be induced by changes in temperature and/or electric field, but they can also be induced by stress, mechanically forcing the lattice structure to change.

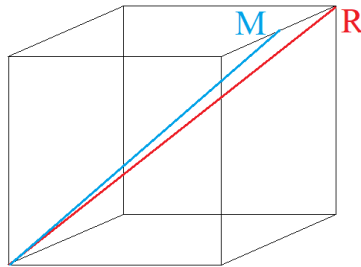


*Figure 7-2: A large electric field applied in the [001]-direction makes the polar direction incline closer to [001] in each domain, causing a distortion from rhombohedral R phase to monoclinic M phase.*

## 7.2 Parameter variation reported in literature

For PMN-28%PT from CTS, the datasheet value for the R-T phase transition temperature is  $T_{RT} = 90\text{ °C}$  [10]. The R-T phase transition causes the material's piezoelectric activity to change at  $T_{RT}$ , and also on approach to  $T_{RT}$ , with a significant impact on the piezoelectric performance of the material [94]. The transition temperature  $T_{RT}$  decreases towards the MPB, and McLaughlin et al. [26] reported strong temperature dependence for the properties of [001] poled PMN-32%PT. In their study,  $d_{33}$  increased from 2000 pC/N at 5°C to 3000 pC/N at 50°C, while the dielectric coefficient  $\epsilon_{33}^T$  increased from 7700 at 5°C to 13200 at 50°C. The temperature of the final transition to T depends on the size of the simultaneously applied electric field. At high electric field (approximately 1000 V/mm), the transition to T happened as early as 60°C. This transition marked a dramatic drop of  $d_{33}$ ,  $\epsilon_{33}^T$  and  $s_{33}^E$ . The relative permittivity  $\epsilon_{33}^T$  was decreased to 1900 and  $d_{33}$  was decreased to 700 pC/N.

Qiu et al. [94] studied PMN-29%PT which is further from the MPB than PMN-32%PT. They found that the main phase transition zone for this material occurred in the range 80 - 120°C. At 100 V/mm, the stiffness coefficient  $c_{33}^D$  decreased from  $16 \cdot 10^{10}$  N/m<sup>2</sup> at 40°C to  $14 \cdot 10^{10}$  N/m<sup>2</sup> at 80°C, the thickness mode coupling coefficient  $k_t$  decreased from 0.5 at 40°C to 0.35 at 80°C and the permittivity  $\epsilon_{33}^S$  increased from approximately 900 at 40°C to approximately 1400 at 80°C.

A phase transition from the rhombohedral, R, phase to what is most likely an orthorhombic, O, phase is induced by mechanical stress. McLaughlin et al. measured strain and electric displacement under combined electric field and mechanical stress at six temperatures, 5, 20, 40, 50, 60 and 80°C. The electrical field varied from 0 to 1500 V/mm, while the uniaxial mechanical prestress varied between 0 and 30 MPa. Illustrative 3D phase transition maps can be found in their article [26]. The maps show that:

- as the temperature increases, the R-O phase transition occurs at lower stresses.
- at a given temperature the stress required to drive the phase transition increases with increasing electrical field. An electrical field in the poling direction can effectively prevent the phase transition caused by the stress.
- Without electrical bias, the R-O transition happens just above 10 MPa at room temperature.

Qiu et al. [94] created maps for PMN-29%PT, estimating the transition zone at room temperature and zero electrical bias to 10-12 MPa.

Upon removal of the stress, the R phase returns, and the polarization returns [8] [26]. By using a very small electrical bias, a preferred orientation is induced in the dipoles, and the electrical displacement can be recovered [93]. The stress induced phase transition is reversible, but the stress dependence of the material properties must be taken into account when designing for performance at elevated pressures. Also, application of stress decreases the coercive field  $E_c$ . This effect was shown by Webber et al. [93] to be much more pronounced for single crystal than for its random ceramic counterpart. Many tonpilz transducers are subjected to uniaxial stress through a prestress bolt.

PMN-28%PT, PMN-29%PT and PMN-32%PT are examples of Generation I single crystals. They are also called binary PMN-PT. Generation II and III single crystals were developed to increase  $T_{RT}$ ,  $T_C$ ,  $Q_M$  and  $E_c$ . The development of these new crystals was reviewed by Lun et al. in 2009 [52]. They reported that through the inclusion of lead indium niobate  $Pb(In_{1/2}Nb_{1/2})O_3$  to form ternary  $Pb(In_{1/2}Nb_{1/2})O_3$ - $Pb(Mg_{1/3}Nb_{2/3})O_3$ - $PbTiO_3$  (PIN-PMN-PT),  $T_{RT}$  is increased to >120°C and  $E_c$  is increased to 4.5 kV/cm (For PIN33%-PMN-PT,  $E_c$  is 5.5-7 kV/cm [10]). By doping with

manganese, Mn, to form Mn:PIN-PMN-PT,  $Q_M$  can be increased above 700. Lun et al. explained that Mn affects PIN-PMN-PT properties similar to PZT ceramics, making both of them “harder”. The decrease of  $d_{33}$  in Mn:PIN-PMN-PT is however small compared to that in acceptor-doped PZT ceramics. Mn:PIN-PMN-PT has  $d_{33}$  between 1080 and 1700 pC/N, which is still 2-4 times higher than that of soft PZT ceramics. Continuing the work of Qiu et al. [94], Liao et al. [27] tested three generations of piezocrystals, I: binary PMN-PT, II: ternary PIN-PMN-PT and III: doped ternary Mn:PIN-PMN-PT under mechanical uniaxial stress 0-60 MPa and temperature 20-200°C. The PIN-PMN-PT and Mn:PIN-PMN-PT samples had 33% PT-contents, while the PMN-PT results were taken from Qiu’s work (29% PT-contents). The temperature experiments showed that the R-T transition for PIN-PMN-PT occurred in the range 120°C to 160°C, about 30°C higher than for PMN-PT. The properties of PIN-PMN-PT, doped and undoped, were quite stable below 100°C. The following variation was reported for the temperature range 20°C to 80°C:

- $\epsilon_{33}^S$  varied 29 % for PIN-PMN-PT compared to 53.7 % for PMN-PT
- $k_t$  varied 1.4 % for PIN-PMN-PT compared to 19.2 % for PMN-PT
- $c_{33}^D$  varied 2.7 % for PIN-PMN-PT compared approximately 9% for PMN-PT

The phase transition zone induced by uniaxial compressive stress was shifted to around 20 MPa for PIN-PMN-PT, compared to 10-14 MPa for PMN-PT. For the Mn:PIN-PMN-PT, there was no obvious evidence of a phase transition zone. Liao et al. concluded that “this suggests that the Mn acceptor dopant has significantly hardened the material to allow it work under more demanding conditions than can be sustained with generation I and II”.

Note that the material parameters had a significant pressure dependence all the way from 0 MPa and up to the transition zone. For  $k_t$  and  $c_{33}^D$ , the dependence was almost linear. For PIN-PMN-PT,  $k_t$  decreased from 0.52 at 0 MPa to 0.38 at 20 MPa, and  $c_{33}^D$  decreased from 16  $10^{10}$  N/m<sup>2</sup> at 0 MPa to 13.5  $10^{10}$  N/m<sup>2</sup> at 20 MPa. The permittivity  $\epsilon_{33}^S$  increased from 800 at 0 MPa to 1200 at 10 MPa, and then with a smaller slope to 1300 at 20 MPa [27]. Yang et al. [95] investigated stress dependence of material parameters for hard and soft PZT, observing only small changes up to 40 MPa for the hard PZT, but 20% increase of  $d_{33}$ , 35% increase of  $k_{33}$  and 60 % decrease of  $s_{33}^E$  for the soft PZT.



In some underwater transducer designs, the active material experiences an effectively uniaxial pressure. In other designs, the active material operates under hydrostatic conditions. Gao et al. [96] investigated the effects of hydrostatic pressure on PIN-PMN-PT, by measuring the electrical impedance. They reported insignificant changes for  $k_{33}$ ,  $d_{33}$  and  $s_{33}^E$  at 65 MPa, but they observed a decrease in the mechanical quality factor  $Q_M$  from 100 at 0 MPa to 33 at 65 MPa. The PT-contents were not given, but the high coupling coefficient indicates a composition close to the MPB.

## 8 Literature study: State of the art for textured ceramics

Phase transitions are among the factors that may limit the use of single crystals in practical underwater applications. Other potential showstoppers are low fracture toughness and high material cost. The ongoing development of textured ceramics with single crystal-like properties can potentially provide a solution to at least some of these issues. In the review paper *Texture engineered ceramics – property enhancement through crystallographic tailoring* [7] Messing et al. state that “textured polycrystalline ceramics possess directional, single crystal-like properties as well as mechanical reliability and compositional versatility”. This chapter summarizes a literature study on the state of the art for textured ceramics, as a means for evaluating the realism of implementing high coupling materials in commercial underwater transducers.

### 8.1 Theory, texturing

“Texture” describes the preferred crystallographic orientation of grains in a polycrystalline material, and crystallographic texturing is widely used to enhance the performance of anisotropic polycrystalline materials [7]. The technique is highly investigated in the field of lead-free ceramics, motivated by present and upcoming environmental legislation concerning the use of lead-based materials in electronics.

In most cases, the property of interest (e. g. the piezoelectric constant) is maximized along a single crystallographic direction, and thus one-directional texturing (fibre texture) is sufficient to obtain property enhancement [7]. By texturing a material, one gets more efficient alignment of polar vectors, and/or one gets to utilize inherent piezoelectric anisotropy [97]. As explained by Zhang et. al [98], textured ceramics have the same  $\infty m$  symmetry as that of random ceramics after polarization, but as the grains are oriented and poled along a given direction, the overall piezoelectric properties are not statistically averaged by randomly oriented grains as observed in random ceramics. “However, analogous to ceramics with random grain orientation, the existence of grain boundaries generates a depolarization field and impedes the domain movement around the boundaries. Hence, the piezoelectric properties are slightly

lower than that of the single crystal counterparts”. Textured piezoelectrics can be domain-engineered like single crystals, but at the grain-by-grain level [7].

Different techniques have been developed in the last few decades to achieve ceramics with texture fraction > 90%. In 1997, a technique called Templated Grain Growth (TGG) was reported. In TGG, highly dense and oriented ceramics can be produced by using a small number of anisometric seeds dispersed in a fine matrix powder. The template particles grow at the expense of the fine randomly oriented powder, ensuring a large volume fraction of highly oriented grains. Being based on standard powder processing and sintering, TGG achieves texture at a significantly lower cost as compared to other techniques used for texturing [82]. Schematics of the TGG process is shown in Figure 8-1. The selection and preparation of the templates is a subject of special interest for TGG experiments, since the texture development and the template growth during annealing strongly depends on their number, size, distribution, and initial orientation [82]. In *Lead-free piezoelectrics*, Safari and Hejazi writes [84]: “It is obvious that higher electrical properties can be achieved if a template with the same composition as a matrix is used. However, it is difficult to make perovskite ceramics in high aspect ratio morphologies due to the isotropic properties of perovskite structure. Reactive-templated grain growth (RTGG) is a type of TGG in which templates are aligned in the matrix and the final composition forms as a result of some consecutive in situ reactions”. Details on template selection and texture evolution through calcination, pressing and sintering can be found in *Lead-free piezoelectrics* [5][82]-[85].

## 8.2 State of the art

The superior piezoelectric properties of single crystal PMN-PT make random PMN-PT an obvious candidate for texturing. PZT-based single crystals are more difficult to grow and have lower piezoelectric response [92]. It is important to remember that the ultrahigh piezoelectric response in relaxor single crystals near the MPB has its origin in polarization rotation and multiphase state. When aiming for this behaviour, accompanying disadvantages must be expected, see chapter 7 on phase transitions.

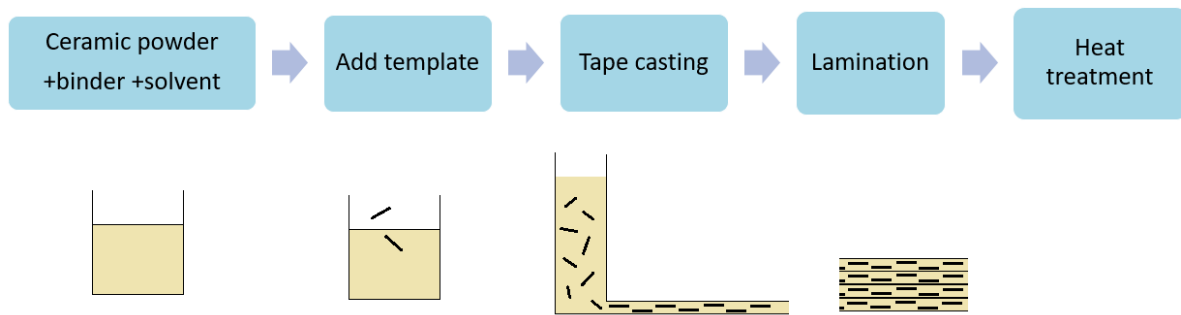


*Figure 8-1: Schematics of the TGG process. A slurry, consisting of the anisometric template particles mixed in the powder matrix together with solvents and binders, is poured into a reservoir behind a doctor blade. The carrier to be cast upon is set in motion. If gated with sufficiently fine gaps, the doctor blade will align the templates. The template particles are aligned parallel to the casting direction. The wet film goes into a drying box where solvents are evaporated. The resulting dry film is laminated, and after being cut into the desired shape and size, the stack of laminated films is called a green compact [97].*

Messing et al. [7] reviewed how different templates have been used to texture [001] oriented rhombohedral PMN-PT ceramics with composition near the MPB by TGG, achieving piezoelectric properties much larger than those of PZT-based ceramics. Barium titanate (BT) templates can yield  $d_{33} = 1150$  pC/N and  $T_c = 164$  °C, but with a large grain size that reduces the mechanical properties. The mechanical properties can be improved by using smaller BT templates with higher aspect ratio to produce smaller grain sizes and higher texture quality, at the cost of a smaller  $d_{33}$  ( $\approx 1000$  pC/N). The BT templates do not react with PMN-PT. They remain inclusions and reduce the strain response via mechanical clamping and the dielectric properties via a composite effect. This problem can be eliminated using strontium titanate ( $\text{SrTiO}_3$ ) templates, but the  $T_c$  is lowered to approximately 100 °C. Platelets of sodium bismuth titanate - lead titanate (NBT-PT) provide high density, fine grain size and excellent texture quality, resulting in  $d_{33} \approx 1000$  pC/N and  $T_c = 129$  °C. Messing et al. explained that in an untextured ceramic, crack propagation usually follows a path perpendicular to the applied stress. In contrast, texturing can affect the direction of crack propagation due to relatively low fracture energy of the interfaces between templated grains, thus promoting delamination.

Texturing with  $\text{SrTiO}_3$  templates was reported in a Ph.D. thesis from 2007 by Brosnan [86]. She investigated the effect of uniaxial pressure on textured ceramics, by fabricating tonpiz

elements from textured rings, applying stress via the prestress bolt, and measuring electrical impedance at different stress levels. For an 81 vol% textured PMN-28%PT tonpilz element, the effective coupling coefficient was 0.65 from 0 to 10 MPa, fell just below 0.6 at 17 MPa, and then fell to 0.45 at 20 MPa.

Not only the stress induced R-O transition, but also the temperature induced R-T transition is a concern for textured PMN-PT, as it is for single crystal PMN-PT. Messing et al. [7] reported that low  $T_{RT}$  and low  $T_c$  (90 – 170°C) limit the working temperature for textured PMN-PT near the morphotropic phase boundary, MPB. There is now extensive effort put into texturing of new systems with higher  $T_{R-T}$  and  $T_c$ . Systems in focus are ternary PIN-PMN-PT, but also PYN-PMN-PT and PMN-PZT, where PYN is an abbreviation for lead ytterbium niobate  $Pb(Yb_{0.5}Nb_{0.5})$ . According to Brova et al. [99] single crystals with 15-14 mol% PYN have comparable piezoelectric coefficients to PIN-PMN-PT crystals, but improved  $T_{R-T}$  (120-130°C). Motivated by this, they developed textured PYN-PMN-PT and obtained  $d_{33} = 754$  pC/N. High piezoelectric properties ( $d_{33} \approx 800$  pC/N) and phase transition temperatures 20-70 °C greater than PMN-PT has been demonstrated for textured PIN-PMN-PT. Mn-doping of these textured ceramics have been used to create hardened properties [ref. 100][ref. 101].

According to Messing et al. [7] texture fraction is no longer considered to be a property-limiting obstacle, as texture resulting from most fabrication techniques are now >95%. On the other hand, alignment of grains is a challenge. A misalignment of 10° reduces  $d_{33}$  by >25% compared to single crystal.

### 8.3 Commercially available textured ceramics

There is a lot of interesting research going on in the field of texture ceramics, but the range of commercially available materials is still limited. Two examples of commercially available textured ceramics are shown in Table VI. These materials can offer improved performance compared to PZT but are not yet at the level of single crystals. The permittivity  $\epsilon_{33}^T$  and the piezoelectric constant  $d_{33}$  are higher than for hard PZT, while the mechanical quality factor  $Q_m$  is higher than for soft PZT. The  $d_{33}$  is comparable to soft pZ1/PZT5H1, and approximately double the value for hard PZT. The values of the electromechanical coupling coefficient  $k_{33}$  and

the compliance coefficient  $s_{33}^E$  provide an advantage even compared to soft PZT. For  $k_{33} = 0.85$ , the maximum bandwidth (22) is increased by 60% compared to PZT5H1, while  $k_{33} = 0.79$  gives an increase of only 30 %.

*Table VI: Material data, textured ceramic from [ref. 102] and [ref. 103].*

	CTS Textured 2 <sup>nd</sup> Generation	Qortek TX101
$\rho$ (kg/m <sup>3</sup> )		7600
$k_{33}$	0.79-0.85	0.79
$d_{33}$ (10 <sup>-12</sup> C/N)	600 (1 <sup>st</sup> generation)	710
$g_{33}$ (10 <sup>-3</sup> Vm/N)		44.1
$s_{33}^E$ (10 <sup>-12</sup> m <sup>2</sup> /N)		38
$\epsilon_{33}^T$ ( $\epsilon_0$ )	1870	1795
$Q_m$		350
$T_c$ (°C)	203	
$E_c$ (kV/cm)	$\approx 7$	



## 9 Thesis conclusion

Research questions 1 and 2 read:

1. What is the state of the art for single crystal underwater transducers?
2. How is the usable frequency band of underwater transducers affected by use of single crystals with high electromechanical coupling?

The literature study, summarized in Chapter 2, showed that naval single crystal tonpilz and cylinder transducers have been built, demonstrating high electrical power factor in wide bandwidths. The theory behind this is well established [13][69] but was presented in an alternative way in Article 1, see Chapter 3. While the width of the electromechanical transfer function can be regulated by the transducer design, the width between the outer maxima of the tuned electrical power factor,  $\Delta f$ , is limited upwards by the electromechanical coupling factor  $k$  (see assumptions in Article 1). In Article 1, using the lumped BVD-model,  $\Delta f$  was shown to be equal to  $(k/\sqrt{1-k^2})f_r$ . An increase of  $k$  from 0.6 (some hard PZT ceramics) to 0.9 (typical single crystal) yields a three-fold increase of  $\Delta f$ , while an increase of  $k$  from 0.7 (soft PZT) to 0.9 yields a doubling of  $\Delta f$ . The ripple within the outer maxima of the power factor is dependent on the mechanical quality factor,  $Q_m$ , of the design, see (21) [69]. Low ripple has been demonstrated for single crystal designs with optimized  $Q_m$  [13]. Thus, for applications where the usable frequency band is restricted by the reactive electrical power, the high  $k$  of the single crystals provides a unique opportunity for extension of the usable band compared to PZT transducers.

In one of the reported naval tonpilz designs [8], 15 dB additional source level was provided in the high and low frequency ends, compared to a PZT transducer. The single crystals have higher piezoelectric  $d$ -constants than PZT ceramics, and thus provide larger strain per electric field. Other advantages are high elastic compliance and high electromechanical coupling in alternative modes. A 36 mode tonpilz with resonance frequency 2 kHz was designed by van Tol et al. [37][38], and high compliance  $s_{66}$  contributed to a small total depth of only 2.5 inches.



Tonpilzes are typically operated below 50 kHz [16]. Many commercial and scientific underwater applications require plane transducers in the frequency range 50 kHz to 1 MHz, often provided by piezocomposite designs. Research question 3 reads:

3. How should a 1-3 piezocomposite transmitter and a tonpilz transmitter be designed to maximize the usable frequency band for underwater applications?

The literature study did not reveal any underwater piezocomposite designs for which bandwidth restricted by power factor was investigated. The electrical power factor and the electromechanical transfer function for an air-backed piezocomposite plate were calculated in Article 2 and compared to the tonpilz design. For the tonpilz,  $Q_m$  can be regulated by the frequency independent acoustic matching inherent in the design. Piezocomposite plates, on the other hand, are usually matched to water by acoustic matching layers. This type of matching is frequency dependent, and the matching decreases rapidly outside the passband. A main contribution of this Ph.D. project was a demonstration of how single crystal piezocomposite transducers can be designed to maximize the frequency band with acceptable power factor, despite of the frequency dependence of the matching layers. It was shown theoretically in Article 1 and experimentally in Article 3 that widening of the matching layer passband by separation of the resonances can reduce the power factor ripple. A wider passband comes at the cost of a less flat passband, but the method can be used for applications where the aim is a selection of narrowband pulses at a variety of frequencies rather than one short pulse spanning the entire band. For the fabricated single crystal piezocomposite transducer of Article 3, the tuned power factor was larger than 0.5 in a band that was 175 % wide relative to the resonance frequency. The fabricated composite had an effective coupling coefficient of  $k = 0.83$ , in good agreement with modelling.

Underwater transducers can be used for exploring, mapping, visualizing, and analyzing the ocean and sea bottom. The frequency providing the best result will be dependent on the type of investigation. The transducer operator might want to use 300 kHz near the bottom and 200 kHz for deeper waters, while perhaps 700 kHz to achieve high resolution inspection of a particularly interesting object. Collection of all relevant information by *one* transducer instead

of two or more transducers can be a gamechanger for small robots and other small platforms, possibly justifying use of expensive single crystals even for commercial applications.

For the air-backed piezocomposite transducers in Articles 1 and 3, the two matching layers were optimized under a relaxed definition for the usable frequency band. The criterium was tuned power factor ripple less than 0.5. In Article 1 an additional criterium was set for the electromechanical transfer function, requiring less than 12 dB ripple. Articles 1 and 3 demonstrated that for applications where ripple of this magnitude can be accepted, single crystals enable wide usable bands also for underwater piezocomposite transducers in the frequency range above 50 kHz. The tonpilz design is however preferable for the lower frequencies, as the frequency independent matching enable smaller power factor ripple, see Article 2. According to (9) [69], very small ripple can be obtained for a lumped design with  $Q_m$  close to the optimum value. The optimum  $Q_m$  for single crystal designs is however very low, 0.6 for  $k = 0.9$ , or 0.9 for effective  $k = 0.82$  [69]. The latter case was investigated in Article 2, quantifying the design parameters necessary to obtain optimum  $Q_m$  for a tonpilz. For the example case discussed in the article, reducing  $Q_m$  from 2 to 0.9 require reduction of the head mass by a factor 4, or reduction of active area by a factor 3. These reductions make it more challenging to avoid head flexure, and an important take-home-message from Article 2 is that even for  $Q_m = 2$  the tonpilz had smaller power factor ripple than a piezocomposite with two conventional matching layers. The tonpilz with  $Q_m = 2$  also performed well compared with the piezocomposite with optimized matching layers reported in Article 3. The tonpilz had power factor larger than 0.5 in a band of width  $1.7f_r$ , and the ripple within the flanks was smaller than for the piezocomposite.

A wide usable frequency band contribute to a compact transducer system by reducing the number of transducers required to collect a given set of multi-frequency data. Other contributions to a compact transducer system were considered in Article 4, completing research question 4:

4. How is the compactness of a 1-3 piezocomposite transmitter and a tonpilz transmitter affected by use of single crystals?

In Article 4, piezocomposites with the active materials single crystal 24%PIN-PMN-PT and polycrystalline PZT5H1 were compared, using FEM modelling. For a conventional 33 mode 1-3 piezocomposite, the acoustic power at a given voltage was approximately doubled for the single crystal material versus the PZT material. The composite height was reduced by 30 %. Required voltage is important for compactness because of transformer size.

When poled along the [011] crystal direction, the single crystal material provides high electromechanical coupling also in the 32 mode. By utilizing this mode in a 1-3 piezocomposite, the acoustic power at a given voltage was increased by almost a factor fifty compared to the conventional 33 mode PZT design. The calculation was performed for a design where the distance between the electrodes was one fifth of the resonator length. The composite height was reduced by 49 % compared to the PZT design.

A special design was proposed in the second part of Article 4, utilizing both the 32 mode and a mode akin to the 31 mode. The aim was to provide a very compact transducer system by combining the advantages of a wide range of usable frequencies, a low voltage, and a small height. One conventional matching layer was added. The piezocomposite had a height of 2.5 mm, and FEM modelling predicted a usable frequency band from 175 kHz to 380 kHz for the 32 mode and from 475 kHz to 500 kHz for the mode akin to the 31 mode.

To investigate the practical challenges of this design, the piezocomposite was fabricated. The structure of the measured impedance spectra was well captured by the FEM model, but some quantitative differences were evident. The fabricated composite showed 15 % increased resonance frequency, a higher impedance magnitude, and slightly wider peaks than predicted by the model.

The 32 mode design opens for transducers that can be operated over a wide frequency range and driven by low voltages, making it well suited for mounting on compact platforms.

### **9.1 Future work**

Phase transitions are one of many issues that impact the performance of single crystals in practical applications. The literature study on phase transitions in Chapter 7 revealed large

material parameter variations with temperature, mechanical stress, and electric field for the generation I PMN-PT single crystals. For the generation II single crystals, PIN-PMN-PT, the ferroelectric-ferroelectric phase transition temperature is increased to  $>120^{\circ}\text{C}$  [52]. Liao et al. [27] reported 29 % variation of  $\epsilon_{33}^S$ , 1.5 % variation of  $k_t$ , and 2.7 % variation of  $c_{33}^D$  for 33%PIN-PMN-PT in the temperature range  $20^{\circ}\text{C}$  to  $80^{\circ}\text{C}$ . The phase transition zone induced by uniaxial compressive stress is extended to around 20 MPa for PIN-PMN-PT, compared to 10-14 MPa for PMN-PT. Note that the material parameters have a significant pressure dependence all the way from 0 MPa and up to the transition zone. Experimental investigations of the performance of a PIN-PMN-PT transducer at various water depths and temperatures are priority number one for future work. Any variation in performance will probably be largely dependent on the design of the transducer and its housing, so this work requires mechanical design expertise and several different prototypes, including both piezocomposites and tonpilzes.

Priority number two for future work is fabrication of a transducer with textured ceramics as the active material. According to Messing et al. [7] “textured polycrystalline ceramics possess directional, single crystal-like properties as well as mechanical reliability and compositional versatility”. The range of commercially available materials are however still limited. A future textured ceramic transducer should undergo the same evaluation of performance at various water depths and temperatures as a similar single crystal transducer. Moreover, the fabrication challenges for a textured ceramic piezocomposite should be compared to those of the 518 kHz single crystal piezocomposite fabricated for Article 3. It was shown in Article 3 and Chapter 6 that the measured impedance of the fabricated single crystal composite was in reasonable agreement with a FEM model based on material data from Kim et al. [81], and that the coupling coefficient calculated from the measurements was close to the modelled value. The composite was however fabricated with a pillar aspect ratio of only 3. The mechanical robustness for higher aspect ratios should be investigated, both for textured ceramics and for single crystals. The robustness for thick composites in the underwater frequency range might be different from the robustness experienced during fabrication of medical transducers.

A third future aspect to investigate is element to element variation in arrays, especially for tonpilzes for which the supplied rings might come from different locations of a grown block of

single crystal. For this aspect also, the conclusion might be different from the experience drawn from fabrication of the smaller medical transducers.

## References

- [1] C. H. Sherman and J. L. Butler, "Introduction", in *Transducers and arrays for underwater sound*, 2<sup>nd</sup> ed., Cham, Switzerland: Springer International Publishing, 2016, ch. 1, sec. 1.3-1.4, pp. 18-28.
- [2] W. P. Mason, *Electro-Mechanical Transducers and Wave Filters*, New York, NY: D. Van Nostrand Company, Inc., 1942, p. 205
- [3] C. H. Sherman and J. L. Butler, "Transducer models", in *Transducers and arrays for underwater sound*, 2<sup>nd</sup> ed., Cham, Switzerland: Springer International Publishing, 2016, ch. 3, sec. 3.2, pp. 110-127.
- [4] S. Sherrit and B. K. Mukherjee, "Characterization of piezoelectric materials for transducers", *Dielect. Ferroelect. Reviews*, CL#7-1466, pp. 175-244, 2007, [online] Available: <http://arxiv.org/abs/0711.2657>
- [5] W. Ge, J. Li, and D. Viehland, "Domain engineering and phase transformations" in *Lead-free piezoelectrics*, S. Priya and S. Nahm, Ed., New York, NY: Springer, 2012, ch. 1, pp. 3-20.
- [6] L. M. Ewart, E. A. McLaughlin, H. C. Robinson and J. J. A. Stace, "Mechanical and Electromechanical Properties of PMNT Single Crystals for Naval Sonar Transducers," *IEEE Trans. Ultrason. Ferroelect. Freq. Contr.*, vol. 54, no. 12, p. 2469, Dec. 2007.
- [7] G. L. Messing, S. Poterala, Y. Chang, T. Frueh, E. Kupp, B. Watson, R. Walton, M. Brova, A. Hofer, R. Bermejo, and R. Meyer, "Texture-engineered ceramics - Property enhancements through crystallographic tailoring", *J. Mater. Res.*, vol. 32, no. 17, pp. 3219-3241, Sep. 2017
- [8] A. Amin, E. McLaughlin, H. Robinson and L. Ewart, "Mechanical and Thermal Transitions in Morphotropic PZN-PT and PMN-PT Single Crystals and Their Implication for Sound Projectors," *IEEE Trans. Ultrason. Ferroelect. Freq. Contr.*, vol. 54, no. 6, p. 1090, Jun. 2007.
- [9] *Ferroperm matrix data*, Meggitt A/S, Apr. 2022, [Online]. Available: <https://www.meggittferroperm.com/materials/>
- [10] *Piezoelectric PMN-PT single crystal products*, CTS Corporation, Apr. 2022, [Online]. Available: <https://www.ctscorp.com/wp-content/uploads/2016.12.15-Single-Crystal-Brochure.pdf>
- [11] *Full set of elasto-piezo-dielectric properties of 24%PIN-PMN-PT poled along [011]*, CTS Corporation, Received by contacting CTS Corporation.

- [12] K. A. Snook, P. Rehrig, X. Jiang, W. Hackenberger, M. J.R and D. Markley, "Advanced Piezoelectric Single Crystal Based Transducers for Naval Sonar Applications," *IEEE Int. Ultrason. Symp*, Rotterdam, Netherlands, 2005.
- [13] M. B. Moffett, H. C. Robinson, J. M. Powers, and P. D. Baird, "Single-crystal lead magnesium niobate-lead titanate (PMN/PT) as a broadband high power transduction material," *J. Acoust. Soc. Am.*, vol. 121, no. 5, pp. 2591 – 2599, May. 2007.
- [14] Monterey Bay Aquarium Research Institute, Moss Landing, CA, *MBARI is advancing marine science and engineering to understand our changing ocean* (March 19, 2020), Accessed: Apr. 2022 [Online video]. Available: <https://vimeo.com/398905381?fbclid=IwAR3gVJQ7ixCimPKgBYzoUtnt0vJHizRuqsUANMvb2ts8OmFTBYKiyXtVwc>
- [15] Sebastien de Halleux, Saildrone, Alameda, CA, How a fleet of wind-powered drones is changing our understanding of the ocean (December 11, 2018), Accessed: Apr. 2022 [Online video]. Available: <https://www.youtube.com/watch?v=mqX2BmiEDnQ>
- [16] C. H. Sherman and J. L. Butler, "Transducers as projectors", in *Transducers and arrays for underwater sound*, 2nd ed., Cham, Switzerland: Springer International Publishing, 2016, ch. 5, sec. 5.3.1, pp. 207- 215
- [17] C. H. Sherman, and J. L. Butler, "Transducer evaluation and measurement", in *Transducers and arrays for underwater sound*, 2nd ed., Cham, Switzerland: Springer International Publishing, ch. 9, 2016, pp. 475 - 502.
- [18] E. Sun and W. Cao, "Relaxor-based ferroelectric single crystals: Growth, domain engineering, characterization and applications," *Progress in Material Science*, vol. 65, 2014.
- [19] J. Luo and S. Zhang, "Advances in the growth and characterization of relaxor-PT-based ferroelectric single crystals," *Crystals*, vol. 4, 2014.
- [20] S. Zhang, F. Li, X. Jiang, J. Luo and X. Geng, "Advantages and challenges of relaxor PbTiO<sub>3</sub> ferroelectric crystals for electroacoustic transducers - a review," *Progress in material science*, vol. 68, 2015.

- [21] S. Zhang and F. Li, "High performance ferroelectric PbTiO<sub>3</sub> single crystals: *Status and perspective*," *J. Appl. Phys.*, no. 111, 2012
- [22] N. Sherlock and R. J. Meyer Jr, "Modified Single Crystals for High-Power Underwater Projectors," *IEEE Trans. Ultrason. Ferroelect. Freq. Contr.*, vol. 59, no. 6, p. 1285, Jun. 2012.
- [23] N. Sherlock, "Relaxor-PT single crystals for broad bandwidth, high power sonar projectors," Ph.D. dissertation, Material Science and Engineering, The Graduate School, The Pennsylvania State University, State College, PA, 2010.
- [24] N. Sherlock and R. J. Meyer Jr., "Large signal response and harmonic distortion in piezoelectrics for SONAR transducers," *J. Electroceram*, 2012.
- [25] N. Sherlock and R. J. Meyer Jr, "Electromechanical Nonlinearities and Losses in Piezoelectric Sonar Transducer Materials," *IEEE Trans. Ultrason. Ferroelect. Freq. Contr.*, vol. 59, no. 8, p. 1618, Aug. 2012.
- [26] E. A. McLaughlin, T. Liu and C. S. Lynch, "Relaxor ferroelectric PMN-32%PT crystals under stress, electric field and temperature loading: II-33-mode measurements", *Acta Materialia*, vol. 53, no. 14, pp. 4001-4008, Aug. 2005
- [27] X. Liao, Z. Qiu, T. Jiang, M. R. Sadiq, Z. Huang, C. E. M. Démoré, and S. Cochran, "Functional piezocrystal characterisation under varying conditions", *Materials*, vol. 8, no. 12, pp. 8304-8326, Dec. 2015
- [28] J. M. Powers, M. B. Moffett and F. Nussbaum, "Single Crystal Naval Transducer Development," *IEEE ISAF*, Honolulu, HI, USA, 2000
- [29] H. Robinson, R. Janus, J. O'Neal, C. Mathews, J. Chase, and J. Moore, "Low frequency range tracking transducer" in *OCEANS*, Monterey, CA, USA, 2016, pp. 1-5.
- [30] R. J. Meyer Jr, T. C. Montgomery and W. J. Hughes, "Tonpilz Transducers Designed Using Single Crystal Piezoelectrics," *OCEANS*, Biloxi, MI, USA, 2002.



- [31] T. C. Montgomery, R. J. Meyer Jr and E. M. Bienert, "Broadband Transduction Implementation and System Impact," *OCEANS*, Vancouver, BC, Canada, 2007.
- [32] P. W. Rehrig, W. S. Hackenberger, X. Jiang, R. J. Meyer Jr and X. Geng, "Naval Device Applications of Relaxor Piezoelectric Single Crystals," *IEEE Ultrason. Symp.*, Munich, Germany, 2002
- [33] S. C. Thompson, R. J. Meyer and D. C. Markley, "Performance of tonpilz transducers with segmented piezoelectric stacks using materials with high electromechanical coupling coefficient," *J. Acoust. Soc. Am.*, vol. 135, no. 155, 2014.
- [34] H. Robinson, "US Navy PiezoCrystal Device Demonstrations", unpublished presentation, January 9, 2019
- [35] K. Zhang, Y. Chen and K. Peng, "The Study of 32-Mode Single Crystal Longitudinal Transducer," *IEEE/OES China Ocean Acoustics Symposium*, 2016
- [36] C. H. Sherman and J. L. Butler, "Transducers as projectors", in *Transducers and arrays for underwater sound*, 2nd ed., Cham, Switzerland: Springer International Publishing, 2016, ch. 5, sec. 5.8.2, p. 270.
- [37] D. J. Van Tol, R. J. Meyer, *Acoustic Transducer*, US Patent 7,615,912 B2 (November 10, 2009)
- [38] R. J. Meyer, T. M. Tremper, D. C. Markley, D. J. Van Tol, P. Han, J. Tian, Low profile, broad bandwidth projector design using  $d_{36}$  shear mode, *Navy Workshop on Transduction Materials and Devices*, Penn State, May 2010
- [39] P. Marin-Franch, S. Cochran and K. Kirk, "Progress towards ultrasound applications of new single crystal materials," *Journal of Materials Science: Materials in Electronics*, vol. 15, no.11, p. 715, Nov. 2004.
- [40] D. Robertson, G. Hayward, A. Gachagan and J. Hyslop, "Comparison of mechanical cross talk in single crystal and ceramic periodic piezoelectric composite arrays," *IEEE Ultrason. Symp.*, Honolulu, HI, USA, 2003.

- [41] D. Robertson, G. Hayward, A. Gachagan and V. Murray, "Comparison of the Frequency and Physical Nature of the Lowest Order Parasitic Mode in Single Crystal and Ceramic 2-2 and 1-3 Piezoelectric Composite Transducers," *IEEE Transactions on UFFC*, vol. 53, no. 8, 2006.
- [42] M. Pham Thi, H. Le Khanh and A.-C. Hladky-Hennion, "Fabrication and Characterization of Large Area 1-3 Piezo-composites based on PMN-PT Single Crystals for Transducer Applications," *IEEE Ultrason. Symp.*, Rome, Italy, 2009
- [43] H. Wang, H. Xu, X. He, H. Luo and Z. Yin, "Electric properties of single-crystal PMN-31% PT/epoxy 1-3 piezoelectric composites," *Phys. Stat. Sol.*, vol. 14, 2005.
- [44] Y. Zhang, S. Wang, D. Liu, Q. Zhang, W. Wang, B. Ren, and X. Zhao and H. Luo, "Fabrication of angle beam two-element ultrasonic transducers with PMN-PT single crystal and PMN-PT/epoxy 1-3 composite for NDE applications," *Sensors and Actuators A. Physical*, vol. 168, 2011
- [45] Y. Zhang, X. Zhao, W. Wang, B. Ren and H. Luo, "Fabrication of PIMNT/Epoxy 1-3 Composites and Ultrasonic Transducer for Nondestructive Evaluation," *IEEE Transactions on UFFC*, vol. 58, no. 9, 2011.
- [46] K. Chen, H. Chan, C. Choy, Q. Yin, H. Luo and Z. Yin, "Single crystal PMN-0.33PT/Epoxy 1-3 composites for ultrasonic transducer applications," *Transactions of IEEE UFFC*, vol. 50, no. 9, 2003.
- [47] W. Wang, S. Or, Q. Y, Z. Y, J. Jiao, C. Leung, X. Zhao and H. Luo, "Ternary piezoelectric single crystal PIMNT based 2-2 composite for ultrasonic transducer applications," *Sensors and actuators: A Physical*, vol. 196, 2013.
- [48] Q. Yue, D. Liu, J. Deng, D. Lin, W. Di, X. Li, W. Wang, X. Wang and H. Luo, "Design and fabrication of relaxor ferroelectric single crystal PIN-PMN-PT/epoxy 2-2 composite based transducer," *Sensors and Actuators: A Physical*, vol. 234, 2015.
- [49] J. Kim and Y. Roh, "Equivalent properties of 1-3 piezocomposites made of PMN-PT single crystals for underwater SONAR transducers," *Proc. of SPIE*, vol. 7978, 2011.

- [50] J. Kim and Y. Roh, "Homogenization of PMN-PT/epoxy 1-3 piezocomposites by resonator measurements and finite element analysis," *Sensors and Actuators A: Physical*, vol. 206, 2013.
- [51] Y. Roh and X. Lu, "Design of underwater tonpiliz transducer with 2-2 composite," *J. Acoust. Soc. Am.*, vol. 119, no. 3734, 2006.
- [52] J. Lun, W. Hackenberger, S. Zhang, and T. Shrout, "The progress update of relaxor piezoelectric single crystals", *IEEE Ultrason. Symp.*, Rome, Italy, 2009
- [53] J. Xia, J. Li, G. Xu and J. Xing, "High curie temperature relaxor piezoelectric single crystal broadband transducers," *Acoustics*, Hong Kong, 2012.
- [54] A. Mathieson, M. C. S. Sadiq and M. Lucas, "Characterization of a Langevin transducer incorporating Mn-doped piezocrystal material," *IEEE Ultrason. Symp.*, 2014.
- [55] D. Brown, "Broadband transducers for underwater communication," *J. Acoust. Soc. Am.*, vol. 123, no. 3006, 2008.
- [56] D. Brown, "Advances in Acoustic Communication and Navigation Transducers for Small Underwater Vehicles," *J. Acoust. Soc. Am.*, vol. 129, no. 2515, 2011.
- [57] C. Bachand, D. Brown and B. Aronov, "Evaluation transducer bandwidth and effectiveness on overall acoustic system performance," *J. Acoust. Soc. Am.*, vol. 132, no. 1920, 2012.
- [58] J. F. Tressler, T. R. Howarth and D. Huang, "A comparison of the underwater acoustic performance of single crystal versus piezoelectric ceramic-based "cymbal" projectors," *J. Acoust. Soc. Am.*, vol. 119, no. 2, 2006.
- [59] B. H. Houston, J. A. Bucaro, T. Yoder, L. Kraus, J. Tressler, J. Fernandez, t. Montgomery and T. Howarth, "Broadband Low Frequency Sonar for Non-Imaging Based Identification," *OCEANS*, Biloxi, MI, USA, 2002

- [60] R. J. Meyer Jr, A. Dogan, C. Yoon, S. M. Pilgrim and R. E. Newnham, "Displacement amplification of electroactive materials using cymbal flextensional transducer," *Sensors and Actuators A*, vol. 87, 2001.
- [61] R. Guo, S. Li, D. An, T. Han, J. Chen and W. Cao, "Comprehensive analysis of Mn:PIN-PMN-PT single crystal transducer for Class IV flextensional transducers," *Ceramics International*, vol. 44, 2018
- [62] J. Butler and A. L. Butler, "Cantilever mode piston transducer array," *Proceedings of Meetings on Acoustics*, vol. 19, 2013
- [63] H. Zheng-Yao and M. Yuan-Liang, "Advantage analysis of PMN-PT material for free-flooded ring transducers," *Chin. Phys. B*, vol. 20, no. 8, 2011
- [64] M. F. Wallace, H. Mulvana, P. Marin, K. Mayne, R. Wright, R. March, B. S. S. Spence and S. Cochran, "Parametric Array Design and Characterisation for Underwater Sonar and Medical Strain Imaging Applications," *IEEE Ultrason. Symp.*, New York, NY, USA, 2007
- [65] S. Cochran, M. Parker and P. Marin-Franch, "Ultrabroadband single crystal composite transducers for underwater ultrasound," *IEEE Ultrason. Symp.*, Rotterdam, Netherlands, 2005
- [66] C. H. Sherman and J. L. Butler, "Transducer characteristics", in *Transducers and arrays for underwater sound*, 2nd ed., Cham, Switzerland: Springer International Publishing, 2016, ch. 4, pp. 153-182
- [67] K. S. Van Dyke, "The piezo-electric resonator and its equivalent network", *Proc. IRE*, vol. 16, no. 6, pp. 742-764, Jun. 1928
- [68] T. Inoue, M. Otha and S. Takahashi, "Design of ultrasonic transducers with multiple acoustic matching layers for medical application", *IEEE Trans. Ultrason. Ferroelect. Freq. Contr.*, Vol. 34, no. 1, pp. 8-16, Jan. 1987

- [69] C. H. Sherman and J. L. Butler, "Electroacoustic transduction", in *Transducers and arrays for underwater sound*, 2nd ed., Cham, Switzerland: Springer International Publishing, 2016, ch. 2, pp. 31-73
- [70] D. Stansfield, "Bandwidth" in *Underwater Electroacoustic Transducers*, 1st ed., Bath, UK: Bath University Press, 1991, ch. 5, sec. 3, pp. 112–119
- [71] W. Mason, *Piezoelectric crystals and their application to ultrasonics*, New York, NY: Van Nostrand, 1950
- [72] C. S. DeSilets, J. D. Fraser and G. S. Kino, "The design of efficient broad-band piezoelectric transducers," *IEEE Trans. Son. Ultrason.*, Vol. 25, no. 3, pp. 115-125, May. 1978.
- [73] C. Bassett, A. De Robertis, C. D. Wilson, "Broadband echosounder measurements of the frequency response of fishes and euphausiids in the Gulf of Alaska", *ICES J. Marine Science*, vol. 75, no. 3, pp. 1131-1142, May. 2018
- [74] J. M. Jech, G. L. Lawson, and A. C. Lavery, "Wideband (15-260 kHz) acoustic volume backscattering spectra of Northern krill (*Meganyctiphanes norvegica*) and butterfish (*Peprilus triacanthus*)", *ICES J. Marine Science*, vol. 74, no. 8, pp. 2249-2261, Oct. 2017
- [75] W. A. Smith and B. A. Auld, "Modeling 1-3 composite piezoelectrics: Thickness-mode oscillations," *IEEE Trans. Ultrason. Ferroelect. Contr.*, vol. 38, no. 1, pp. 40-47, Jan. 1991
- [76] C. H. Sherman and J. L. Butler, "Transducers as projectors", in *Transducers and arrays for underwater sound*, 2nd ed., Cham, Switzerland: Springer International Publishing, 2016, ch. 5, sec. 5.3.1, pp. 196-197
- [77] *IEEE Standard for relaxor-based single crystals for transducer and actuator applications*, IEEE Standard 1859, 2017
- [78] C. H. Sherman and J. L. Butler, "Acoustic radiation from transducers", in *Transducers and arrays for underwater sound*, 2nd ed., Cham, Switzerland: Springer International Publishing, 2016, ch. 10, sec. 10.4.1, p. 461

- [79] CTS Corporation,  $Q_m$  value received by contacting CTS Corporation.
- [80] D. Carka, J. A. Gallagher, and C. S. Lynch, "Phase energy determined from stress and electric-field-induced phase transformations in  $[011]_c$  cut 0.24PIN-PMN-PT single crystals", *Crystals*, vol. 4, no. 3, pp. 377-389, Aug. 2014
- [81] Kim, J., Joh, C. and Roh, Y, 2013, "Evaluation of all the material constants of PMN-28%PT piezoelectric single crystals for acoustic transducers", *Sensors and Materials*, vol. 25, no. 8, pp. 539 - 552
- [82] H. Amornin, I. Coondoo, M. E. V. Costa, and A. L. Kholkin, "Ferroelectric Domains and Grain Engineering in  $\text{SrBi}_2\text{Ta}_2\text{O}_9$ " in Lead-free piezoelectrics, S. Priya and S. Nahm, Ed., New York, NY: Springer, 2012, ch. 2, sec. 2.1, pp. 53-55
- [83] H. J. Lee and S. Zhang, "Perovskite lead-free piezoelectric ceramics" in Lead-free piezoelectrics, S. Priya and S. Nahm, Ed., New York, NY: Springer, 2012, ch. 9, pp. 291-306
- [84] A. Safari and M. Hejazi, "Lead-free KNN-based piezoelectric materials" in *Lead-free piezoelectrics*, S. Priya and S. Nahm, Ed., New York, NY: Springer, 2012, ch. 5, pp. 139-152
- [85] T. Tani and T. Kimura, "Processing and properties of textured BNT-based piezoelectrics" in *Lead-free piezoelectrics*, S. Priya and S. Nahm, Ed., New York, NY: Springer, 2012, ch. 10, pp. 311-333
- [86] K. H. Brosnan, "Processing, properties, and applications of textured  $0.72\text{Pb}(\text{Mg}_{1/3}\text{Nb}_{2/3})\text{O}_3$ - $0.28\text{PbTiO}_3$  Ceramics", Ph.D. dissertation, Material Science and Engineering, The Graduate School, The Pennsylvania State University, State College, PA, USA, 2007
- [87] J. Fan, "A Meso-electro-mechanical model for PMN-PT-BT ceramics behavior", *Journal of Intelligent Material Systems and Structures*, vol. 15, no.3, p. 203, Mar. 2004
- [88] Relaxor ferroelectrics, The Rappe Group, Pennsylvania State University, Accessed Jun. 2022, [Online]. Available: <https://web.sas.upenn.edu/rappegroup/relaxor-ferroelectrics/>
- [89] S. C. Hwang, C. S. Lynch, and R. M. McMeeking, "Ferroelectric/ferroelastic interactions and a polarization switching model", *Acta Metal. Mater.*, vol. 43, no. 5, pp. 2073-2084, May. 1995

- [90] S. S. Li, "Classification of Solids and Crystal Structure", in *Semiconductor Physical Electronics Microdevices*, Boston, MA, US: Springer, pp. 1-19, 1993
- [91] A. Shirokanev, D. Kirsh, and A. Kupriyanov, "Development of a vector algorithm of three-dimensional crystal lattice parametric identification based on estimation of the spacing between adjacent lattice planes", *Procedia Engineering*, no. 201, 2017
- [92] Development of PZT-based single crystals as high-T<sub>c</sub> and high-performance piezoelectric materials, IEEE-UFFC (September 08, 2017), Accessed Apr. 2022, [Online video] Available: <https://www.youtube.com/watch?v=2K19hmw8zrk>
- [93] K. G. Webber, R. Zuo, and C. S. Lynch, "Ceramic and single crystal (1-x)PMN-xPT constitutive behavior under combined stress and electric field loading", *Acta Materialia*, vol. 56, no. 6, pp. 1219-1227, Apr. 2008
- [94] Z. Qiu, M. Sadiq, C. Démoré, M. Parker, P. Marin, K. Mayne, and S. Cochran, "Characterization of piezocrystals for practical configurations with temperature- and pressure-dependent electrical impedance spectroscopy", *IEEE Trans. Ultrason. Ferroelect. Freq. Contr.*, no. 9, 2011
- [95] G. Yang, S. Liu, W. Ren, B. K. Mukherjee, «Effects of uniaxial stress on the piezoelectric, dielectric, and mechanical properties of lead zirconate titanate piezoceramics", *Ferroelectrics*, no. 262, pp. 1181-1186, 2001
- [96] J. Gao, Z. Xu, F. Li, C. Zhang, Y. Liu, G. Liu, and H. He, "The effect of the hydrostatic pressure on the electromechanical properties of ferroelectric rhombohedral single crystals", *Applied physics letters*, no. 99, 2011
- [97] L. Liu, "Progress on the fabrication of lead-free textured piezoelectric ceramics: perspectives over 25 years", *J. Mater. Sci: Mater Electron*, no. 26, 2015
- [98] S. Zhang, B. Malic, J. Li, and J. Rödel, "Lead-free ferroelectric materials: Prospective applications", *J. Materials Research*, no. 5, 2021

- [99] M. J. Brova, B. H. Watson, R. L. Walton, E. R. Kupp, M. A. Fanton, R. J. Meyer, and G. L. Messing, "Templated grain growth of high coercive field CuO-doped textured PYN-PMN-PT ceramics", *J. Am. Ceram. Soc.*, vol. 103, no. 11, pp. 6149-6156, Nov. 2020
- [100] B. H. Watson, M. J. Brova, M. Fanton, R. J. Meyer, and G. L. Messing, "Textured Mn-doped PIN-PMN-PT ceramics: harnessing intrinsic piezoelectricity for high-power transducer applications", *Journal of the European Ceramic Society*, vol. 41, no.2, pp. 1270-1279, Feb. 2021
- [101] H. Leng, Y. Yan, H. Liu, M. Fanton, R. J. Meyer, and S. Priya, "Design and development of high-power piezoelectric ceramics through integration of crystallographic texturing and acceptor-doping", *Acta Materialia*, no. 206, 2021
- [102] H. Yegingil, *Textured tape cast piezoelectric materials utilizing templated grain growth (TGG)*, CTS Corporation, [Online], Accessed Apr. 2022, Available: <https://www.ctscorp.com/wp-content/uploads/Final-Textured-Tape-Cast-Piezoelectric-Materials.pdf>
- [103] Textured piezoceramics – TX101, Qortek, [Online], Accessed Apr. 2022, Available: [https://qortek.com/wp-content/uploads/2022/02/TX\\_101\\_Data\\_Sheets\\_rev\\_2\\_4\\_22\\_final.pdf](https://qortek.com/wp-content/uploads/2022/02/TX_101_Data_Sheets_rev_2_4_22_final.pdf)





## Article 1

E. S. Røed, M. Bring, F. Tichy, A. Henriksen, E.-M. Åsjord and L. Hoff, "Optimization of matching layers to extend the usable frequency band for underwater single-crystal piezocomposite transducers", *IEEE Trans. Ultrason., Ferroelect., Freq. Contr.*, vol. 69, no. 2, pp. 803-811, Feb. 2022

Paper omitted from online edition due to publisher's regulations

## Article 2

E. S. Røed, M. Bring, F. Tichy, E.-M. Åsjord and L. Hoff, "Electrical power factor for a single crystal tonpilz versus a plate with matching layers", *IEEE Ultrason. Symp.*, Xi'an, China, 2021

Paper omitted from online edition due to publisher's regulations

### Article 3

E. S. Røed, M. Bring, M. Frijlink, A. Henriksen, F. Tichy, E.-M. Åsjord and L. Hoff, "Underwater single crystal piezocomposite transducer with extended usable frequency band", *Ultrasonics*, vol. 125, Sep. 2022, 106794

Paper omitted from online edition due to publisher's regulations

## Article 4

E. S. Røed, M. Bring, A. Henriksen, F. Tichy, E.-M. Åsjord and L. Hoff, "Compact and wideband underwater transducer using single crystal piezocomposite in 32 mode", submitted to *IEEE Trans. Ultrason., Ferroelect., Freq. Contr.*, Sep. 2022

The following acknowledgement will be added:

The authors would like to thank Roy Henriksen, Trine Ressem, Stig Harefallet, Anel Habibovic and other colleagues at Kongsberg. Their fabrication expertise was greatly appreciated.

Paper omitted from online edition due to publisher's regulations

Doctoral dissertation no. 154

2023

**Impact of single crystal properties on underwater  
transducer designs**

Dissertation for the degree of PhD

Ellen Sagaas Røed

ISBN 978-82-7206-746-4(print)

ISBN 978-82-7206-745-7 (online)

usn.no

